

*SELF FORMED Cu - W  
FUNCTIONALLY GRADED MATERIAL  
CREATED VIA POWDER SEGREGATION*

DISSERTATION

Zur Erlangung des grades  
des Doktors der Ingenieurwissenschaften  
der Naturwissenschaftlich-Technischen Fakultät III Chemie, Pharmazie  
und Werkstoffwissenschaften  
der Universität des Saarlandes

Von  
Dragana Janković Ilić

Saarbrücken  
2007

Tag des Kolloquiums: 23.03.2007

Dekan: Prof. Dr. rer. nat. Kaspar Hegetschweiler

Berichterstatter: Prof. Dr. rer. nat. Horst Philipp Beck, Universität des Saarlandes  
Prof. Dr. rer. nat. Rolf Clasen, Universität des Saarlandes  
Prof. Dr.-Ing. Frank Mücklich, Universität des Saarlandes  
Dr. -Ing. Andrés Lasagni, Universität des Saarlandes

---

**Saarbrücker Reihe**  
**Materialwissenschaft und Werkstofftechnik**

---

Band 11

Self Formed Cu-W Functionally Graded Material  
Created via Powder Segregation

Dragana Janković Ilić

Herausgeber:

**Prof.Dr.-Ing. Frank Mücklich**

Prof.Dr.rer.nat. Walter Arnold  
Prof.Dr.rer.nat. Ralf Busch  
Prof.Dr.rer.nat. Rolf Clasen  
Prof.Dr.-Ing. Stefan Diebels  
Prof.Dr.rer.nat. Michael Kröning  
Prof.Dr.-Ing. Frank Mücklich  
Prof.Dr.rer.nat. Wulff Possart  
Prof.Dr.rer.nat. Helmut Schmidt  
Prof.Dr.rer.nat. Horst Vehoff

Shaker Verlag

Aachen 2008



To

Jelena and Nenad

Јелени и Неши

## Acknowledgments

I would like sincerely to acknowledge the help and encouragement of many individuals and institutions during the work on this Ph.D. thesis.

- Prof. Dr. F. Mücklich for the given opportunity for research in an interesting field. His scientific supervision, encouragement and support during the research.
- Prof. Dr. R. Clasen for reviewing the manuscript.
- Dr. J. Fiscina for his constant help during the work. Also, for enthusiastic discussions concerning different aspects of the research, science, nature, and life in general.
- Dr. F. Soldera for constant support and friendship.
- DFG-Graduiertenkolleg, Projekt # III GK-GRK 232 / 2 "Neue Hochleistungswerkstoffe für effiziente Energienutzung" Saarbrücken, under leadership of Prof. Dr. R. Clasen and Prof. Dr. W. Arnold, for the scholarship.
- Vinča Institute of Nuclear Sciences, Belgrade, Serbia, for the given scientific leave to conduct Ph.D studies.
- Dr. M. Mitkov (Department of Materials Science, Vinča Institute of Nuclear Sciences) for opportunity to conduct Ph.D work in Germany, her support and friendship.
- Dr. C. González-Oliver (CONICET-Centro Atómico Bariloche and Instituto Balseiro. 8400S.C.de Bariloche) for his reviewing the manuscript, valuable suggestions and constant support.
- M.Sc D. Kićević, Dr. S. Bosković, Dr. M. T. Jovanović (Department of Materials Science, Vinča Institute of Nuclear Sciences) for encouragement and always optimistic approach to the coming subjects.
- Dipl.-Ing. J. Schmauch and Dr. A. Tschope for their help regarding dilatometric measurements. Dipl.Chem. M. Sauer (INM, Saarbrücken) for help during dilatometric experiments. J. Schwarz and P. Kohl for help in doing many repairs when necessary. Dr. Rabe and Dr. A. Koka (Fraunhofer Institut for Nondestructive Testing, Saarbrücken) for ultrasonic test. Co-workers in workshops in Bild. 43 and 22, particularly, H.J.Jakoby and especially P. Limbach. D. Hohnerlein for his great help with metallurgical specimen preparation, mechanical tests and for their friendship. Dr. U. Schmidt for measurement of electrical resistivity.
- Dr. A. Lasagni for development of the "Aglomerado" software for the quantitative determination of microstructural parameters, help by PVD of tungsten thin layer and for interesting discussion and friendship.
- Dipl.-Ing. C. Gachot is greatly acknowledged for German translation of the abstracts.
- Many thanks go to all colleagues and friends from Functional Materials department for their support and friendly work atmosphere, particularly to: C. Mass, B. Epstein, E. Philip, W. Ott, C. Holzapfel
- Finally, I am greatly indebted to my husband Dr. Nenad Ilić for his scientific help and for encouraging me in the pursuit of my research and study during these years, in addition to his love. Special thanks goes to my daughter, Jelena, for following mama's Ph.D with great interest. I would like also to thank to my parents, my brother and his family and my parents in law for constant encouragement, motivation and love.

## **TABLE OF CONTENTS**

Abstract.....	xi
Summary.....	xii
Introduction.....	xvii
<b>1. LITERATURE REVIEW .....</b>	<b>1</b>
1.1. Functionally graded materials .....	3
1.1.1. Design and processing of functionally graded materials.....	3
1.1.2. Testing and characterization of functionally graded materials .....	4
1.1.3. Modeling of functionally graded materials .....	4
1.1.4. Application of functionally graded materials .....	4
1.1.5. Copper - tungsten functionally graded materials .....	6
1.2. Granular media .....	11
1.2.1. Granular media as an unusual state of matter .....	11
1.2.2. Statics of granular media .....	12
1.2.2.1. Geometry and packing of granular media .....	12
1.2.2.2. Thermodynamics of granular media .....	13
1.2.3. Dynamics of granular media .....	16
1.2.3.1. Relaxation behavior of granular media .....	16
1.2.3.2. Size segregation .....	19
1.3. Solid state sintering .....	32
1.3.1. Driving force for sintering .....	32
1.3.2. Stages of sintering .....	35
1.3.3. Sintering of agglomerates .....	36
1.3.4. Rearrangement process in solid state sintering .....	37
<b>2. EXPERIMENTAL PROCEDURE .....</b>	<b>39</b>
2.1. Tungsten bimodal granular media preparation .....	39
2.2. Vibrational compaction .....	39
2.2.1. Principles of electrodynamic shaker performance .....	41
2.3. Cold pressing .....	42
2.4. Thermal treatment .....	42
2.5. Infiltration .....	42

2.6. Characterization techniques .....	43
2.6.1. Density measurement and flow behavior of tungsten granular media ....	43
2.6.2. Light microscopy and image analysis .....	44
2.6.3. Scanning electron microscopy .....	44
2.6.4. Electrical resistivity measurement .....	44
2.6.5. Elastic modulus measurement .....	44
<b>3. RESULTS .....</b>	<b>46</b>
3.1. Characteristics of tungsten granular media .....	46
3.1.1. Powder morphology .....	46
3.1.2. Flow rate, apparent density and angle of repose .....	46
3.2. Compaction dynamics of tungsten granular media .....	49
3.2.1. Relaxation behaviour of weakly excited tungsten granular media .....	49
3.2.1.1. Effect of ambient humidity on compaction dynamics .....	51
3.2.2. Geometrical segregation .....	52
3.2.2.1. Microstructural characteristics of the geometrical segregation regime .....	52
3.3. Sintering of tungsten granular media .....	54
3.3.1. Sintering kinetics of small monomodal tungsten agglomerates .....	55
3.3.1.1. Microstructural characteristics of sintered small tungsten agglomerates .....	58
3.3.2. Sintering kinetics of large monomodal tungsten agglomerates .....	60
3.3.3. Sintering kinetics of vibrated bimodal tungsten granular media in percolation and diffusion stage .....	62
3.3.4. Sintering kinetics of bimodal tungsten granular media: homogeneous mixture (A1+A2) .....	64
3.3.5. Sintering kinetics of bimodal tungsten granular media in stationary state - graded structure .....	65
3.4. Characteristics of copper - tungsten materials .....	67
3.4.1. Electrical resistivity .....	67
3.4.2. E-modulus .....	68

<b>4. DISCUSSION</b> .....	70
4.1. Characteristics of tungsten granular media .....	70
4.1.1. Powder morphology .....	71
4.1.2. Flow rate, apparent density, and angle of repose .....	71
4.2. Compaction dynamics of tungsten granular media .....	72
4.2.1. Compaction mechanism of bimodal tungsten granular media .....	73
4.2.1.1. Compaction mechanism in weakly excited tungsten granular media .....	75
4.2.2. Geometrical segregation .....	79
4.2.1.1. Microstructural characteristics of the geometrical segregation mechanism .....	82
4.3. Sintering of tungsten granular media .....	83
4.3.1. Sintering kinetics of small monomodal tungsten agglomerates .....	83
4.3.1.1. Microstructural characteristics of sintered small monomodal tungsten agglomerates .....	86
4.3.2. Sintering kinetics of large monomodal tungsten agglomerates .....	87
4.3.3. Effect of agglomerate size on sintering kinetics .....	88
4.3.4. Effect of vibration on sintering kinetics .....	90
4.3.5. Sintering kinetics of vibrated bimodal tungsten granular media in percolation and diffusion stage .....	90
4.3.6. Sintering kinetics of bimodal tungsten granular media – homogeneous mixture .....	92
4.3.7. Sintering kinetics of bimodal W granular media in stationary state (graded structure).....	92
4.3.7.1. Development of a graded profile with temperature .....	93
4.4. Characteristics of copper - tungsten materials .....	94
4.4.1 Electrical resistivity .....	94
4.4.2 Elastic properties .....	97

<b>5. CONCLUSIONS</b> .....	98
5.1 Compaction dynamics of weakly excited bimodal tungsten granular media .....	98
5.1.1 Size segregation .....	99
5.2. Sintering .....	99
5.2.1. Sintering of monomodal granular media .....	99
5.2.2. Sintering of bimodal granular media .....	100
5.3. Properties of graded copper - tungsten materials .....	101
5.3.1. Electrical resistivity .....	101
5.3.2. E-Modulus .....	101
<b>6. FINAL REMARKS AND SUGGESTIONS FOR FURTHER WORK</b> .....	102
<b>7. REFERENCES</b> .....	104

## **ABSTRACT**

The aim of the present work is to develop a technique to produce continuously formed Cu-W functionally graded materials (FGMs) with adequate mechanical and electrical characteristics for application in extreme environmental conditions. For that purpose a novel process based on size segregation of W bimodal granular media (GM), composed of monomodal W agglomerates A1 (45-60 $\mu$ m) and A2 (200-250 $\mu$ m), has been applied. The study of compaction dynamics and related relaxation behavior of selected granular media have demonstrated that, under weak excitation and under controlled ambient condition, vibrated bimodal W GM segregates in a manner that a gradient in packing is self formed. During sintering, such a graded packing structure turns into a W preform with a gradient in porosity. Studied W GM fulfills both critical demands: i.e. size segregation and effective sintering process. The final Cu-W FGM has been produced by subsequent infiltration of molten Cu into W graded preform.

## **KURZZUSAMMENFASSUNG**

Das Ziel der vorliegenden Arbeit besteht in der Entwicklung einer neuen Methode zur kontinuierlichen Herstellung funktioneller Cu-W Gradientenwerkstoffe (FGM) mit besonderen mechanischen und elektrischen Eigenschaften für Anwendungen unter extremen Umgebungsbedingungen. Zu diesem Zweck wurde ein neuer Prozess, der auf der Größensegregation granularer Medien beruht, eingesetzt. Ausgangspunkt waren bimodal verteilte granulare Medien bestehend aus Wolfram, die sich wiederum aus zwei verschiedenen Agglomeraten A1 (45-60  $\mu$ m) und A2 (200-250  $\mu$ m) zusammensetzen.

Die grundlagenorientierte Studie der Kompaktierungsdynamik und dem damit zusammenhängenden Relaxationverhalten der genannten granularen Medien zeigt dass bei schwacher Anregung und unter kontrollierten Umgebungsbedingungen diese granularen Medien segregieren derart, dass sich selbstständig ein Gradient bildet. Während des Sintervorgangs wandelt sich eine solche Struktur in eine Wolfram-Vorform mit einem Porositätsgradienten um. Die untersuchten W-Gradientenwerkstoffe erfüllen zwei wichtige Anforderungen: die Größensegregation und die Sinterfähigkeit. Der finale Cu-W-Gradientenwerkstoff wird über eine nachträgliche Infiltration der zuvor hergestellten W-Vorform mit geschmolzenem Kupfer erzeugt.

## **SUMMARY**

The aim of the present work is to develop a technique to produce continuously formed Cu-W functionally graded materials (FGMs) with adequate mechanical and electrical characteristics for application in extreme environmental conditions. For that purpose a novel process based on size segregation of W bimodal granular media (GM), composed of monomodal W agglomerates A1 (45-60 $\mu$ m) and A2 (200-250 $\mu$ m), has been applied. The study of compaction dynamics and related relaxation behavior of selected granular media have demonstrated that, under weak excitation and under controlled ambient condition, vibrated bimodal W GM segregates in a manner that a gradient in packing is self formed. During sintering, such a graded packing structure turns into a W preform with a gradient in porosity. Studied W GM fulfills both critical demands: i.e. size segregation and effective sintering process. The final Cu-W FGM has been produced by subsequent infiltration of molten Cu into W graded preform.

Compaction dynamics of weakly excited W GM (frequency 600 Hz and acceleration 6 g) shows three distinguished stages. The first quasi linear stage is attributed to percolation. This process is controlled by an individual particle relaxation where inelastic collisions between particles dominate and it is effective for a moderate packing density. Through a transient stage, where critical slow down occurs, the system attains a steady state. The steady state stage is driven by collective relaxation of close packed particle clusters, where interparticle forces are of the primary importance. The compaction dynamics of studied W GM can be well predicted by Kohlrausch-Williams-Watts law.

Size segregation of polymodal GM is a specific case of vibro-compaction, where collective nature is dominated by excitation level, particle size and friction force. In weakly excited GM, in regimes of geometrical segregation and geometrical segregation aided by convection motion, a gradient in packing can be self formed. Each of these regimes correspond to collective motion of the small agglomerates (A1), whereas the larger agglomerates (A2) play the role of an inert phase. It was shown that a gradient of packing represents the most effective random packing model.

Sintering of the constitutive monomodal agglomerates (A1, A2) is strongly inhomogeneous with a statistical nature dependant on initial configuration of selected GM. The low temperature sintering (1400-1700 K) of monomodal W GM is controlled by simultaneous action of rearrangement process and grain boundary diffusion (GBD). A dominance of one of the

processes is determined by initial agglomerate size and initial loose packing structure. Agglomerate / particle contact asymmetry and therefore induced transient / residual stresses cause the rearrangement process with the apparent activation energy of  $E_a \sim 100$  kJ/mol and  $E_a \sim 80$  kJ/mol for the agglomerates A1 and A2, respectively. Agglomerate mobility caused by agglomerate structure and polymodal porosity distribution result in viscose flow like regime in the available free volume of the porous W skeleton, similar to rearrangement in liquid phase sintering. Both mechanisms recognize that enhancement of densification can be achieved by improving the packing factor. Rearrangement process continues until a geometrical factor is exhausted, defined by the random close packing density limit, and makes a condition for GBD to be later operating. Sintering kinetics at higher temperature (1700-1950 K) revealed for both monomodal agglomerates important contribution to sintering coming from the action of GBD.

Sintering kinetics of bimodal W GM is strongly influenced by a packing structure obtained during vibration. The packing structure evolves through three stages: 1) skeleton of smaller particles (percolation stage); 2) skeleton of larger particles (diffusion stage); and 3) graded structure (steady state). The self formed skeleton and graded structures exhibit different sintering behavior. Sintering kinetics of the skeleton type structure resembles the behavior of skeleton-forming powder. The sintering is controlled by a competition between rearrangement and GBD. Sintering of the W graded structure is similar to the sintering of the homogeneous mixture. Due to a improved packing density, the sintering of the graded structure dominantly controlled by GBD. After sintering the graded structure shows an increase in density of 10 % compared to corresponding percolation structure.

The final Cu-W FGMs have been characterized by measurement of electrical resistivity and effective E-Modulus. The content of Cu and W-W contiguity are two features which determine the resistance for current flow and E-modulus of the studied materials. The higher W packing density in graded structure and correspondingly lower Cu content lead to poorer current flow, but higher E-modulus.

## ZUSAMMENFASSUNG

Das Ziel der vorliegenden Arbeit besteht in der Entwicklung einer neuen Methode zur kontinuierlichen Herstellung funktioneller Cu-W Gradientenwerkstoffe (FGM) mit besonderen mechanischen und elektrischen Eigenschaften für Anwendungen unter extremen Umgebungsbedingungen. Zu diesem Zweck wurde ein neuer Prozess, der auf der Größensegregation granularer Medien beruht, eingesetzt. Ausgangspunkt waren bimodal verteilte granulare Medien bestehend aus Wolfram, die sich wiederum aus zwei verschiedenen Agglomeraten A1 (45-60  $\mu\text{m}$ ) und A2 (200-250  $\mu\text{m}$ ) zusammensetzen. Die grundlagenorientierte Studie der Kompaktierungsdynamik und dem damit zusammenhängenden Relaxationverhalten der genannten granularen Medien zeigt dass bei schwacher Anregung und unter kontrollierten Umgebungsbedingungen diese granularen Medien segregieren derart, dass sich selbstständig ein Gradient bildet. Während des Sintervorgangs wandelt sich eine solche Struktur in eine Wolfram-Vorform mit einem Porositätsgradienten um. Die untersuchten W bimodale granulare Medien erfüllen zwei wichtige Anforderungen: die Größensegregation und die Sinterfähigkeit. Der finale Cu-W-Gradientenwerkstoff wird über eine nachträgliche Infiltration der zuvor hergestellten W-Vorform mit geschmolzenem Kupfer erzeugt.

Die Kompaktierungsdynamik für schwach angeregte granulare Medien (Frequenz 600 Hz und Beschleunigung 6 g) zeigt drei unterschiedliche Stadien. Das erste nahezu lineare Stadium kann auf Perkolationsvorgänge zurückgeführt werden. Dieser Prozess wird durch eine individuelle Partikelrelaxation kontrolliert, wobei inelastische Stöße zwischen den Partikeln überwiegen. Daraus ergibt sich eine moderate Packungsdichte. Nach einem Übergangsbereich, in welchem eine kritische Verzögerung (critical slow down) auftritt, gelangt das System in einen stationären Zustand. Der stationäre Zustand wird dabei von einer kollektiven Relaxation dicht gepackter Partikelcluster gesteuert, wobei die Kräfte zwischen den Partikeln von entscheidender Bedeutung sind. Die Kompaktierungsdynamik der untersuchten Wolfram-Gradientenwerkstoffe kann sehr gut mit Hilfe eines erweiterten Exponentialgesetzes (Kohlrausch-Williams-Watts-Gesetz) beschrieben werden. Die Gültigkeit dieses Relaxationsgesetzes für bimodale Systeme wurde experimentell bestätigt.

Größensegregation stellt einen spezifischen Fall der Vibro-Kompaktierung dar, mit einer kollektiven Natur, die durch Anregungsniveau, Partikelgröße und Reibungskräfte gesteuert ist. Bei schwacher Anregung dieser granularen Medien im Regime der geometrischen Segregation und der von einer Konvektionsbewegung unterstützten geometrischen

Segregation bildet sich eine Gradientenpackung völlig selbständig. Jedes der genannten Regime entspricht der kollektiven Bewegung kleineren Agglomerate (A1), während die größeren Agglomerate (A2) eine inerte Phase darstellen. Es zeigt sich, dass das Modell der Gradientenpackung das effizienteste Modell für eine sich zufällig einstellende Packung repräsentiert. Während des Sintervorgangs, wandelt sich die Gradientenpackung in eine Wolfram-Vorform mit einem Porositätsgradienten um.

Das Sinterverhalten der gründende (konstitutiven) monomodalen W Agglomeraten ist stark inhomogen und von statistischer Natur. Diese hängt entscheidend von der gewählten Ausgangskonfiguration der verwendeten granularen Medien ab. Das Sinterverhalten bei geringen Temperaturen (1400-1700 K) wird durch gleichzeitig auftretende Umordnungsprozesse und Korngrenzendiffusion (GBD) kontrolliert. Der dominierende Einfluss einer der beiden Prozesse ist abhängig von der anfänglichen Agglomeratgröße. Die Asymmetrie der Agglomerate / Partikelkontakte und infolge dessen die induzierten Eigenspannungen unterstützen die Umordnungsprozesse. Die Aktivierungsenergie liegt bei  $E_a \sim 100$  kJ/mol für die Agglomerate A1 und bei  $E_a \sim 80$  kJ/mol für die Agglomerate A2. Die Mobilität der Agglomerate in dem zur Verfügung stehenden freien Volumen der porösen Wolfram-Vorform aufgrund der Agglomeratstruktur mit polymodaler Porenverteilung, ruft in Analogie zum Flüssigphasensintern ein viskoses Fließen hervor. Die beiden Transportmechanismen lassen erkennen, dass eine Erhöhung der Verdichtung durch einen verbesserten Packungsfaktor erzielt werden kann. Die Umordnungsprozesse finden solange statt, bis der geometrische Faktor, welcher als obere Grenze für die Packungsdichte definiert ist, aufgebraucht ist. Dieser führt zu einem späteren Einsetzen der Korngrenzendiffusion. Bei höheren Temperaturen (1700-1950 K) wird das Sintern monomodaler Agglomerate lediglich durch die Korngrenzendiffusion bestimmt.

Die Sinterkinetik bimodaler Agglomerate ist stark von der während der Vibration erzeugten Packungsstruktur abhängig. Die Einstellung der Packungsstruktur vollzieht sich in drei Stadien: 1) Bildung eines „Skeletts“ bestehend aus kleineren Agglomeraten (Perkulationsstadium), 2) Entstehung eines Gerüsts aus größeren Agglomeraten (Diffusionsstadium) und 3) Bildung einer Gradientenstruktur (stationärer Zustand). Das sich einstellende Gerüst und die Gradientenstruktur zeigen ein unterschiedliches Sinterverhalten. Die Sinterkinetik der Skelettstruktur ähnelt der eines skelettartigen Pulvers (skeleton-formed powder). Das Sintern wird durch die konkurrierenden Vorgänge in Form von Umordnungsprozessen und Korngrenzendiffusion gesteuert. Das Sinterverhalten der Gradientenstruktur ist mit dem einer homogenen Mischung vergleichbar. Aufgrund einer verbesserten Packungsdichte, wird das Sinterverhalten einer Gradientenstruktur wesentlich

von Korngrenzendiffusion kontrolliert. Die gesinterte Gradientenstruktur zeigt im Vergleich zu der entsprechenden Perkolationstruktur eine um 10 % größere Dichte.

Die hergestellten Cu-W Gradientenwerkstoffe wurden durch Messungen des elektrischen Widerstandes sowie des effektiven Elastizitätsmoduls näher charakterisiert. Es konnte dabei festgestellt werden, dass der Cu-Gehalt und die W-W Kontiguität zwei maßgebliche Faktoren hinsichtlich des elektrischen Widerstandes und des E-Moduls darstellen. Je höher die Packungsdichte des Wolframs in der Gradientenstruktur und entsprechend geringer der Cu-Gehalt ist, desto größer sind der elektrische Widerstand und der effektive E-Modul.

## ***INTRODUCTION***

Demand for energy standing increases, consequently there is great competition for the fuel resources available. In 1990, about 75% of the world' population ( those in the developing countries) were responsible for only 33% of the world's energy consumption. By the year 2020, that 75% is likely to have risen to 85% and the energy consumption to around 55%. The International Energy Agency says the world will need almost 60% more energy in 2030 than 2020, and fossil fuels will still meet most of its needs. But oil industry experts estimate that current reserves will only last for about 40 years.

Nuclear physicist proposed fusion as a way to provide a relatively safe, green alternative to fossil fuels; enabling the production of vast amounts of energy from abundant sources. The future fusion reactor, named The International Thermonuclear Experimental Reactor with an acronym ITER (also means " the way" in Latin) is to be constructed at Cadarache, France and the first plasma operation is expected in 2016. ITER is a tokamak reactor which confines plasma by high magnetic fields of the order of 10 to 12 Tesla operating at over 100 million Celsius degree, and it is estimated t produce 500 MW of fusion power.

The deployment of fusion power as a viable energy source depends to a large extent on the successful development of high performance materials required for the structural nuclear components. The accepted approach in ITER considers Be, W, and Cu-based materials for the application as plasma faced materials in first-wall in the chamber and in the divertor structure. Among them W is the primary candidate fort the divertor baffle area due to its high melting point, high-energy threshold for physical sputtering and its resistance to chemical sputtering. In the accepted ITER design, the divertor has carbon targets and tungsten high heat-flux components, mounted on a copper substrate, and a water-cooled stainless steel structure bolted to rails on the vessel floor [Ite06].

Due to requested ability to withstand a steady power load of up to 210 MW, one of the critical points is the interface quality between the plasma faced materials and the Cu substrate. Different thermal expansion coefficient of Cu-W, pose a serious problem on the coexistence of the two phases. For that reason, different joining techniques have been developed: plasma spray of Cu or Cu/W to the tip of W rods; casting of Cu to the tip of the W rods; direct diffusion bonding of the W rods to the Cu substrate [Yos99]. A possible solution in overcoming the high interfacial stresses involves the Functionally Graded Material (FGM) concept [Koi95, Gas99]. Absence of mutual solubility in solid and liquid states, as well as

very different melting points enable the production of highly dense Cu-W FGMs via infiltration technique. The main issue therein lies in the formation of a porous W skeleton with defined properties and its proper infiltration. Vibro-compaction and powder segregation of bimodal W granular media have been proposed in this work as method to create W graded packing structure in a continuous way.

The importance of this work is the observation that under controlled ambient humidity, weakly excited bimodal W granular medium, selected for the segregation experiment, evolves towards a steady state. The microstructural manifestation of this steady state is a self- formed graded packing with a maximal disordered packing density which after subsequent pressureless sintering and infiltration with Cu turns into a Cu-W FGM. In this work, sintering kinetics of the W graded preform, and elastic and electrical properties of the final material are studied representing an attempt to better understand the structure-properties relationship of such a complex material.

### 1. LITERATURE REVIEW

The subject of the present work is Cu-W functionally graded material (FGM) produced by powder segregation and powder metallurgy techniques (pressurless sintering and infiltration). In order to give an understandable insight into this problematic, the literature review is divided in three main parts.

Firstly, concepts, characteristics, testing and applications of FGMs will be given in short. The concept of FGMs was proposed in 1984 at the National Aerospace Laboratory of Japan by Niino and co-workers [Koi95], as a preparation method for thermal barrier material for space plane application. The original idea of FGMs has been later expanded for a variety of applications (cuttings tools, coatings, packing, optical and biomaterials).

The copper –tungsten system is a very intensively investigated group of FGMs, primarily due to an attractive combination of high thermal stability and low thermal expansion of W, with the high thermal conductivity of Cu. Such a combination of properties allows application of these materials as heat resistant materials, contact materials in plasma environments and contacts in high voltage switches. In the accepted International Thermonuclear Experimental Reactor (ITER) design, a divertor consists of W high heat flux components mounted on a copper substrate and a water-cooled stainless steel structure. It has been recognized that different thermal expansion coefficients of Cu and W pose a serious problem on the coexistence of the two phases. Besides the large difference in thermal expansion coefficients and melting points, the absence of mutual solubility in solid and liquid states is also critical. However, the infiltration technique showed to be suitable for overcoming these problems and enables production of highly dense Cu-W FGMs. The main issue lies in the formation of a porous W skeleton with defined properties and its proper infiltration. Vibro-compaction and powder segregation of bimodal W granular media (GM) have been proposed in this work as methods to create W graded packing structure in a continuous way.

In the second part, statics and dynamics of granular media have been taken into consideration. Granular media is a subject of interest and sometimes of fascination in the field of theoretical physics, but according to the author's knowledge this work is the first attempt to involve GM in a FGM production. Granular media are simply systems made of discrete particles, larger than 100  $\mu\text{m}$ , like sand or powder, often interacting with each other through dissipative contact forces. On the contrary, excited GM exhibits a very complex relaxation behavior toward a nonequilibrium steady state that can involve different phenomena, i.e convection, density waves, anomalous sound propagation, segregation, and

## 1. LITERATURE REVIEW

---

even turbulent behaviors which usually progress in parallel. Phenomenological segregation can be described as upward movement of larger particles when a polymodal granular media system is subjected to vibration. Size segregation inevitably seems to contradict equilibrium statistical mechanics, since the equilibrium position with larger particle on the bottom is more favorable (minimum of potential energy). Additionally, density of the overall packing increases with polydispersivity, and contrary to the space-saving consideration, segregation leads to separation of constitutive particle sizes. Depending on the excitation level different segregation regimes are active and a geometrical segregation regime the system segregates in a such manner that a gradient in particle size can be self formed in a continual way.

The final step in the production of the continuously graded materials involves sintering of such a packing structure. For that reason the third chapter gives a concise overview of the solid state sintering theory. Due to non-uniform size and shape of GM particles and later due to asymmetric necks, sintering is strongly influenced by a rearrangement process.

### 1.1 Functionally Graded Materials

According to Gasik [Gas03]. “A functionally graded material (FGM) is a material with engineered gradients of composition, structure and/or specific properties aiming to become superior over homogeneous material composed of same or similar constituents”.

The first concept of FGMs was proposed in 1984 by Niino and co-workers [Koi95] at the National Aerospace Laboratory of Japan, as a preparation method for thermal barrier materials. The final target of the proposed concept was to produce a material which could endure both the maximum temperature of 2000 K and the temperature difference of 1000 K primarily for the space plane application [Koi95]. The original idea of FGMs has been later expanded for a variety of applications (cuttings tools, coatings, packages, semiconductors, optical and biomaterials). Theoretical prediction of the usefulness of functional composites with a graded structure came already in 1972 from the work of Bever et al. and Shen et al. [Kie03]. However, their work had only limited impact, probably due to the lack of suitable production methods. During the last years, FGMs have been developed from single specimens to industry oriented applications. In fact, several national R&D programs (Japan, China, Germany) have started in this field very recently [Gas05]. The overview of the production routes, properties and applications of FGMs are described in several monographs [Sur98, Miy99] and review articles [Kie03, Neu97].

#### 1.1.1 *Design and processing of functionally graded materials*

The manufacturing of FGMs can be divided in two steps: building of a structure with a gradient, and later transformation of the designed structure into bulk material. The gradation process is usually classified in three main groups: constitutive, homogenizing, and segregating processes. Stepwise build up of a graded material from precursor materials is the basic constitutive process. In homogenizing processes a sharp interface between two materials is converted into a gradient by material transport i.e. diffusion. Segregating processes start with a macroscopically homogeneous material which is converted into graded material by material transport caused by an external field (gravitational or electric field). The primary advantages of the homogenizing and segregating processes is a possibility to produce a continuous gradient. Afterwards, usually drying and sintering (or solidification) follow the gradation step. This consolidation step needs to be adapted for a particular material selection and attention has to be paid also to non uniform shrinkage rate during the sintering of FGMs. Very extensive review of the processing techniques has been given by Kieback et al. [Kie03]. It is emphasized that “conventional” powder metallurgy (PM) remains the most useful method for mass production of FGMs [Wat95, Kaw95, Gas05].

## 1. LITERATURE REVIEW

---

Different coating methods like atmospheric / vacuum plasma spray (APS / VPS), high velocity oxygen fuel (HVOF) may be also listed under PM benefits [Gas05].

### *1.1.2 Testing and characterization of functionally graded materials*

The existence of a designed concentration / structural profile is the most exclusive characteristic of FGMs. In order to define the characteristics of a graded profile, the starting point of FGMs testing is the determination of the chemical composition. Optical microscopy, scanning electron microscopy (SEM), and energy dispersive analysis (EDS) are the most convenient techniques for that purpose. Nevertheless, the state of the art is advancing, and cross-sectional scanning by electron-beam microprobes or (scanning transmission electron microscopy (STEM) can already be considered as classical tools for obtaining concentration profiles.

The second point of interest has been residual stresses of both the “macro” type (due to inhomogeneous cooling of the graded sample) and the “micro” type (due to different expansion of neighboring grains or phases). For stress analysis diffraction techniques, conventional X-rays, high energy synchrotron radiation, or neutron diffraction are used depending on the depth of penetration required. For internal stress in coatings diffraction techniques can be complemented by mechanical curvature measurements [Ils99]. Another widely used subject of characterization is a fracture mechanics analysis and crack propagation [Dag02].

### *1.1.3. Modeling of functionally graded materials*

Analytical method and both finite element method and micromechanical models are most frequently used for modeling of FGMs [Hir95]. The most extensively investigated subjects of modeling are: elastic strain, elastic stress plastic yielding and deformation, creep at elevated temperature and crack propagation [[Ils99, Erd95].

### *1.1.4 Application of functionally graded materials*

The first application which has been envisioned in the National Aerospace Laboratory of Japan was the implementation of FGMs to avoid stress peaks at interfaces in coated panels for the space shuttle in extreme heat flow situation (during re-entry) [Koi95]. Later on, application potentials have been expanded to also components of chemical plants, solar energy generators, heat exchangers and high efficiency combustion systems. Some of the most important applications will be addressed in short.

## 1. LITERATURE REVIEW

---

The concept of FGMs has been successfully applied in thermal barrier coatings (TBC) where requirements are aimed to improve thermal, and oxidation and corrosion resistance. Two important research material systems are: Al<sub>2</sub>O<sub>3</sub> [Kre99] and ZrO<sub>2</sub> [Gas05] exterior protective ceramic layers on Ni-superalloy (NiCrAlY) based substrates. Consequently, coatings were deposited by different techniques involving physical vapor deposition (PVD), chemical vapor deposition (CVD), plasma spraying, arc spraying, pulsed laser deposition (PLD), sol-gel techniques, as well as build up welding [Sch03]. The novel TBC design made by a Finnish – Japanese cooperation has shown to have significantly extended lifetime and improved delamination crack resistivity [Gas05].

In the thermoelectric field, the concept of graded material, such as doped BiTe / PFe, has been implemented for application in sensors and thermo-generators with metal-semiconductor transition. In such “functionally graded thermoelectric materials”, an efficiency improvement of up to 50 to 100% in comparison to homogeneous material could be achieved in certain cases [Mül99, Mül03]. A Solid Oxide Fuel Cell (SOFC) is a system for energy generation, where composition gradients close to the electrodes or in the electrolyte can largely enhance the performance [Ger99].

FGMs can also find application in communication and information techniques. An entirely new FGM, named photonic fractal, composed of epoxy with a titanium-based ceramic particle dispersion, has been developed by Miyamoto et al [Miy05, Kir05]. It was shown that this material can strongly localize electromagnetic waves in a dielectric fractal cube (called menger sponge) with neither reflection nor transmission. The future vision of these authors is to use the proposed concept to obtain a perfect electromagnetic absorber and highly efficient antenna.

Abrasive tools for metal and stone cutting are another important example where gradation of surface layer has improved performance. The main industry interest in hard metal (WC-Co) cutting tools is based on higher cutting speeds, higher tolerance and prolonged expected tool life. The manufacturing of hard metal FGMs by PM requires precise knowledge and control of the sintering processes to avoid specimen distortion. It was shown that new modeling and optimization of sintering regime can result in lower stresses and lower shape distortion (up to 10 time less) after processing [Gas05]. Gasik and co-workers succeeded to gain such improvements by choosing the proper component geometry and starting parameters. A new method named, spark plasma sintering (SPS) facilitates production of WC/Co and WC/Ni systems in an economically and satisfactory way. The SPS is an electrical sintering technique which directly applies an ON-OFF DC pulsed voltage and a large pulsed current from a specially designed pulse generator [Tok05, Kis05].

## 1. LITERATURE REVIEW

---

An important breakthrough of FGMs could be witnessed in the field of biomedical components [Oto95]. Titanium based alloys, Al<sub>2</sub>O<sub>3</sub>, and YTZP are frequently used for orthopedic prosthesis, especially hip prosthesis [Lik05]. In dentistry, for fabrication of crowns and bridges for dental restoration, novel dental resin adhesive material are developed [Fan05]. Candidates for human hard tissue implants (artificial bones) are hydroxyapatite, tricalcium phosphate, and diopside ceramics (CaO, MgO, 2SiO<sub>2</sub>) [Zou05]. Very advanced research has been done in Japan aiming to produce bone fixation device that can release therapeutical agents such as antibiotics, as prevention for bacterial colonization and infection [Ash05].

As a final observation concerning FGMs it can be noted that the proposed materials concept has demonstrated that compositional micro- or macrostructure gradient can not only dismiss undesirable effects such as a stress concentration, but can also generate an unique positive function [Gas05]. Despite the significant results that were achieved, practical implementation of these materials was shown not to be appropriate. The lack of theoretical basis, material design routes and knowledge of how FGMs work, have significantly hindered the commercial implementation. The future perspective lies in more experimental work and testing with tight industry cooperation. That is the most efficient way to demonstrate the feasibility of the FGM concept and to realize this solution in practice.

### 1.1.5. *Copper - tungsten functionally graded materials*

Copper-tungsten (Cu-W) system is a very intensively investigated group of functional gradient materials [Tak90]. The combination of high thermal stability and low thermal expansion of tungsten, with the high thermal conductivity of copper, allows application as heat resistant materials, contact materials in plasma environments, and contacts in high voltage switches. Some application examples of homogenous Cu-W composite materials are high voltage arc contact material, vacuum contact, electrodes for resistance welding and spark erosion, steel rolling leaders, casting dies, heat sinks, microwave carriers, hermetic package basis, ceramic substrate carriers, GaAs and silicon device mounts and laser diode mounts [Mar06].

Physical properties of both constitutive metals are summarized in Table 1.1.

## 1. LITERATURE REVIEW

**Table 1.1** Physical properties of Cu and W.

<b>Characteristic</b>	<b>Cu</b>	<b>W</b>
Atomic number	29	74
Atomic weight, [g/mol]	63.5	183.9
Density [g/cm <sup>3</sup> ]	8.96	19.30
Crystal type	FCC	BCC
Atomic diameter, [nm]	0.256	0.274
Melting Temperature, [°C]	1083	3410
Boiling Temperature, [°C]	2578	5657
Heat capacity, [J/kg °C]	386	138
Heat of fusion, [kJ/mol]	13.0	35.0
Heat of vaporization, [kJ/mol]	307	824
S-V surface energy, [J/m <sup>2</sup> ]	1.75	2.8
Elastic modulus, [GPa]	145	411
Poisson's ratio	0.34	0.28
Yield strength, [MPa]	120	550
Elongation to failure, [%]	45	1
Thermal expansion coefficient, [10 <sup>-6</sup> /°C]	16.6	4.6
Thermal conductivity, [W/(m°C)]	403	172
PLC (power law creep) stress exponent, n	4.8	4.7
PLC constant, [MPa <sup>-n</sup> /s]	7.4·10 <sup>5</sup>	1·10 <sup>8</sup>
PLC activation energy, [KJ/mol]	197	585
VD (volume diffusion) frequency, [m <sup>2</sup> /s]	6·10 <sup>-5</sup>	8·10 <sup>-6</sup>
VD activation energy, [KJ/mol]	213	520
GBD (grain boundary diffusion) frequency, [m <sup>2</sup> /s]	2·10 <sup>-14</sup>	3·10 <sup>-13</sup>
GBD activation energy, [KJ/mol]	107	385
SD (surface diffusion) frequency, [m <sup>2</sup> /s]	2.6	10 <sup>-3</sup>
SD activation energy, [KJ/mol]	205	293
Brittle to ductile transition temperature [°C]		100~400
Recrystallization Temperature, [°C]		1150~1350
Vapor Pressure at 2000°C, [Pa]		1.3·10 <sup>-7</sup>
Cross section for thermal neutrons [10 <sup>-24</sup> cm <sup>2</sup> ]	3.8	18.5
Estimated neutron leakage		1.0

## 1. LITERATURE REVIEW

---

### Copper –Tungsten material for application in a fusion reactor

Fusion power offers the potential for a safe, environmentally attractive and economically competitive energy source for electric power generation. However, the deployment of fusion power as a viable energy source depends to a large extent on the successful development of high performance materials required for nuclear components. The current international program on fusion development is focused on the tokamak design (Fig. 1.1), firstly discovered by Soviet physicists Andrei Sacharow and Igor Jewgenjewitsch around 1950 [Ite06].

Although several combinations of light ions can undergo a fusion reaction, the deuterium-tritium (DT) reaction is currently considered as the most viable fuel for reactor applications. In the DT fusion reaction (Eq. 1.1) 80 % of the energy is released in 14.1 MeV neutrons which leave the plasma and enter the vessel walls. The remaining 20% is given to the 3.5MeV <sup>4</sup>He-particles, which have to be confined for some time to deposit their energy in the plasma, thereby maintaining the plasma temperature and heating the new fuel.



The biggest realized tokamak at the moment is the JET (Joint European Torus) in Culham (Oxford). The JET experiment have demonstrated in 1997 fusion power ~ 12MW and temperature and time equal to 6 x10<sup>20</sup> KeV s/m<sup>3</sup>. In Germany there are two experimental reactors: ASDEX Upgrade at the Max Plank Institute for Plasma Physic in Garching, and TEXTOR at the Research Center Jülich.

The future tokamak has been named The International Thermonuclear Experimental Reactor with an acronym ITER (also means "the way" in Latin) and is to be constructed in Europe, at Cadarache, near Aix-en-Provence, France. It is technically possible to start construction and the first plasma operation is expected in 2016. ITER is a tokamak reactor which confines plasma by high magnetic fields of the order of 10 to 12 Tesla [Ite06]. The ITER is constructed around a hydrogen plasma torus operating at over 100 million °C, and it is estimated to produce 500 MW of fusion power. The great challenge for material science includes selection and production of materials for application as plasma faced material in the first wall in the chamber (Fig 1.1) and in the divertor structure (Fig. 1.2). The ITER divertor exhausts the flow of energy from charged particles produced in the fusion reactions; it also removes helium and other impurities resulting from the reactions, and from interaction of plasma particles with the wall material. A single divertor, consisting of 54 modules (cassettes), is located at the bottom of the vacuum vessel. The divertor itself, has the ability to withstand a steady power load of up to 210 MW.

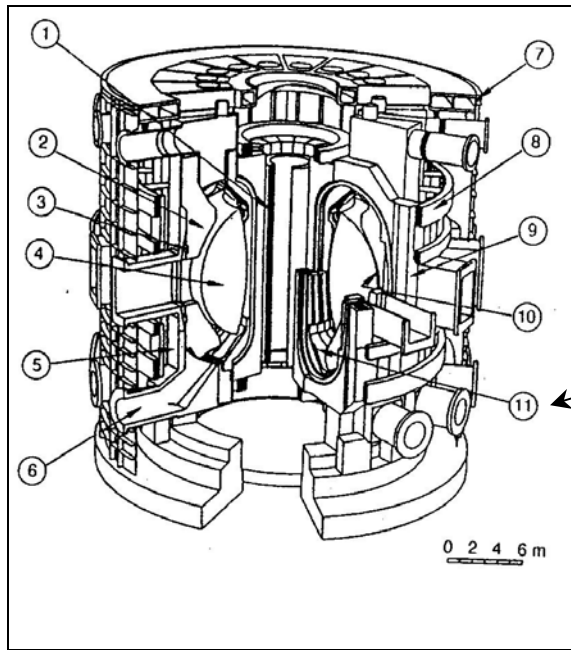


**Fig. 1.1.** Schematic view of a tokamak fusion reactor: 1) central solenoid, 2) shield / blanket, 3) active coil, 4) plasma, 5) vacuum vessel shield, 6) plasma exhaust, 7) cryostat, 8) poloidal field coils, 9) toroidal field coils, 10) first wall, 11) divertor plate

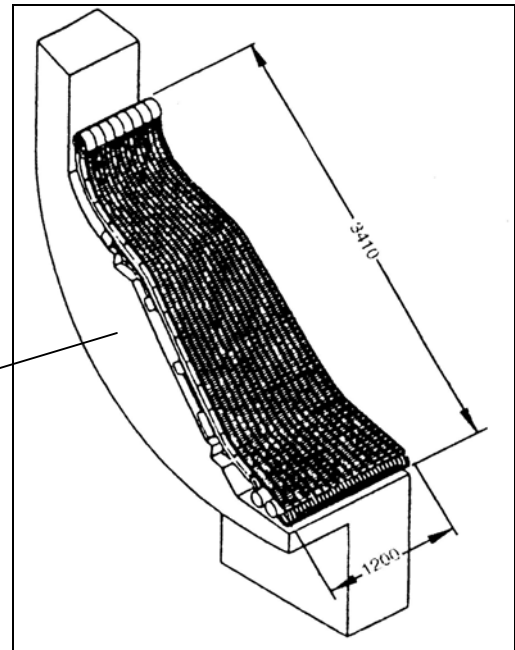


**Fig. 1.2.** Schematic diagram of a divertor.

During plasma disruption event the hot plasma is dumped along the magnetic field lines to the divertor plates in a very short time interval, causing a sudden evaporation of a thin layer of the divertor plate material. In the case of ITER, the flux and average energy of hydrogen ions bombarding divertor plates are estimated to be  $< 10^{24}$  ions/m<sup>2</sup>/s and  $< 100$ eV. However, most of the ablated materials would be re-deposited back onto the surface. This erosion and redeposition process is a major concern in the design of plasma faced components. The erosion of the divertor due to ablation by the incident plasma ions can significantly reduce the life time of the armor. The deposition of heat by neutrons and impinging high energy particles on the divertor is also non-uniform which results in an uneven temperature distribution.

The materials in this reactor area are required to have high melting resistivity, high thermal conductivity, superior mechanical strength at elevated temperature, low chemical erosion and low tritium retention [Ge03]. Berillium, carbon-based material and tungsten are considered as plasma faced materials in the new generation of fusion reactors. Among them, W is the primary candidate for the divertor plate due to its high melting point, its high-energy threshold for physical sputtering and its resistance to chemical sputtering [Lin03]. Tungsten shows the lowest vaporization losses, less than 1/5 of the losses of carbon. The main reason for the low erosion rate of W and its alloys ( W-5wt % Re, W-1 wt % La<sub>2</sub>O<sub>3</sub> ) is low vapor

## 1. LITERATURE REVIEW

---

pressure [Yos99]. Except for the brittle to ductile transition temperature, far above the room temperature, the main drawback dealing with W is high Z impurities in the plasma core, which lead to strong radiation losses, cooling of the plasma and decrease in the fusion rate [Phi98, Smi98]. In the accepted ITER design, the divertor has carbon targets and tungsten high heat flux components mounted on a copper substrate, and a water-cooled stainless steel structure bolted to rails on the vessel floor. The targets can accommodate heat loads of more than 20 MW/m<sup>2</sup> for 20 s, but the realistic peak heat load should be 5 - 10 MW/m<sup>2</sup>.

Different thermal expansion coefficients of Cu-W, pose a serious problem on the coexistence of the two phases. For that reason different joining techniques have been developed: plasma spray of Cu or Cu/W to the tip of W rods; casting of Cu to the tip of the W rods, direct diffusion bonding of the W rods to the Cu substrate [Yos99]. A possible solution in overcoming the high interfacial stresses involves the FGM concept [Gas99, Bok99]. Absence of mutual solubility in solid and liquid states, as well as very different melting points enable the production of highly dense Cu-W FGMs via infiltration technique. The main issue lies in a formation of a porous W skeleton with defined properties and its proper infiltration. A variety of methods have been proposed in order to achieve appropriate tungsten porous preforms: sintering of compact with different W particle size [Koi95, Tak90, Tak93, Lez87], centrifugal powder metallurgy shaping method [Bir99] and the electrochemical treatment of sintered W preforms with variable open porosity [Jed00, Str99, Str97, Jed96].

### 1.2 Granular media

#### 1.2.1 Granular media as an unusual state of matter

Granular media (like sand, powder) are very simple systems made of particles larger than  $100\mu\text{m}$ , often interacting with each other only through dissipative contact forces. GM consist of discrete particles and their interaction is governed by two major concepts:

- excluded volume (one grain cannot occupy the same volume that is occupied by another grain)

- dissipation of energy (governed by the first concept) [Lud99].

Granular media (GM) exhibit behavior that is neither solid like nor liquid like, but a combination of both. For that reason, GM are described of GM as an unusual state of matter. Unique characteristics of such systems can be illustrated in heap formation, a common phenomenon which occurs in technological praxis but also in nature (sand dunes). As opposed to liquid, granular heaps are stationary as long as the slope at the surface is less than the angle of repose ( $\theta_r$ ). No avalanches occur until the slope is higher than the maximum angle of stability ( $\theta_m$ ). However, instead of uniform motion through granular heap, as expected in ordinary fluids, all the motion occurs in a relatively thin boundary layer near the surface [Jae96, D'An01]. The transition region (between  $\theta_r$  and  $\theta_m$ ), shows a complex, bi-stable behavior in which the material can be either stationary (solid like) or flowing (liquid like) depending on how the pile was prepared. Sand piles have served as a macroscopic metaphor for thinking about many complicated microscopic systems that are "marginally stable". Analogies have been made with the flux flow in a superconductor and with relaxation in spin glasses [Jae92]. There is even unusual behavior even for a simple configuration as that given in a container filled with GM up to a height  $h$ . In normal liquid the pressure at the bottom of a filled vessel is proportional to the height of the liquid. In the case of GM the pressure at the bottom of a sufficiently tall structure is independent of the height. The reason for that is that the friction of particles along the wall of container is sufficient to withstand the weight of the extra mass placed on top. For this reason, in an hourglass filled with fine sand, there is an approximately linear relation between filling height and draining time.

Dilatancy phenomena, which can be observed by walking on a beach, is another exclusive feature of GM. Dilatancy is the ability of the system to sustain different degrees of packing. The wet sand around one's foot dries out as weight is put on it (like in liquid). Deformation caused by the pressure of the foot causes the sand to expand. Dilatancy arises from the

## 1. LITERATURE REVIEW

---

need of densely packed material to spread in order to make place for passing grains [Jae92, Nic97].

In addition to phenomena exhibited by liquid the randomness of shape and texture of GM strongly influences their static and dynamic properties [Her95]. GM are highly non-linear and hysteretic. The complexity of GM causes occurrence and relative stability of a large number of metastable configurations.

An essential difference between a classical gas and GM is the dissipation of energy. In a classical, conservative system in equilibrium, energy is conserved. In a dissipative system, the energy loss is quantified by the restitution coefficient  $r$  that describes the ratio of the relative velocities of two particles before and after the collision. A situation where  $r = 1$  corresponds to a perfectly elastic collision. In a dissipative system  $r < 1$ . Since the particles in granular media dissipate energy, the multi-particle system is usually not in equilibrium. This leads to various complex, non-linear phenomena.

Because thermal agitation in a powder takes place on an atomic rather than a particulate scale, external vibration plays an essential role in the behavior of powders. In the absence of external agitation, the grains are frozen into one configuration (jammed) since their thermal energy is insufficient to generate the equivalent of Brownian motion (thermal energy  $\ll$  gravitational energy).

### 1.2.2 Statics of granular media

The statics of GM are subject of extensive theoretical work concentrated predominantly on static packing efficiency and the development of a statistical mechanical theory of powder system under gravity.

#### 1.2.2.1 Geometry and packing of granular media

The properties of GM are strongly affected by randomness in shape and in texture. In general, GM are composed of grains which form disordered structures. As a consequence, in such systems the properties of random packing become important. There are two important limits concerning packing densities. The loosest random packing of uniform spheres which remains mechanically stable is named the random loose packing limit ( $\rho_{RLP}$ ). The  $\rho_{RLP}$  occurs at fractional density  $\Phi = 0.56$  (where gravitation,  $g = 0$ ). The second limit is the random close packing limit ( $\rho_{RCP}$ ), with  $\Phi = 0.64$  [Jae92]. The  $\rho_{RCP}$  gives a framework to analyze GM mechanical stability, load-carrying capability and force distribution under compression. It was

## 1. LITERATURE REVIEW

---

experimentally observed that under applied external pressure exist stress-transmitting paths enclosing virtually stress-free regions [Jae92]. The distribution of force in random networks is related to the rigidity threshold of the entire system. In general this is a non linear problem and nonlinearity enters into creation for the occurrence of a local rupture. For example, if the force locally exceeds a threshold value, a grain may break or permanent rearrangements may occur.

### 1.2.2.2 Thermodynamics of granular media

Granular media represent a case study for the investigation of the concept of temperature in non equilibrium thermodynamics. Two important approaches to this problem are recognized: statistical mechanics - where compactivity is used analogous to temperature [Edw89] and an approach based on elementary excitation such as the Fermi liquid theory in condensed matter physics - where temperature is explicitly related to vibration intensity,  $\Gamma$  [Hay97].

#### Statistical mechanics of granular media

The main issue of defining a full analogy between GM and statistical mechanics of molecular liquids and gasses, lies in finding GM system properties analogous to temperature. In that sense, Ogawa [Jae92] proposed a concept of “granular temperature”, as a measure of random motion. When GM flows, in addition to an average velocity of the grains in the direction of flow, a random velocity generated by collisions induced by the flow itself is the second component of motion. The magnitude of the random velocity components will be approximately proportional to the average shear rate. However, this concept has not led to a full analogy with statistical mechanics.

Edwards and Mehta have proposed an alternative description of GM in complete analogy to statistical mechanics [Edw89,Meh89,Meh90a]. In contrast to the concept of “granular temperature”, which is based on particle motion, compactivity characterizes a static system. The starting point of the proposed theory is the “ergodic hypothesis” of powder meaning that all powder with the same content and occupying the same volume (V) will have the same macroscopic properties. This basic assumption, oriented in formulation a complete analogy with conventional statistical mechanics is presented in the following:

Thermal System			Powder ( GM)
Energy (E)	≡		Volume (V)
Temperature (T)	≡		Compactivity (X)

## 1. LITERATURE REVIEW

---

The compactivity  $X$  has been defined as the analogue of temperature (Eq.1.2)

$$X = \partial V / \partial S \dots \dots \dots (1.2)$$

where:  $S$  is the entropy,  $V$  is the volume actually occupied by the powder.

The  $V_{min}$  corresponds to the random close packed limit with powder in the most packed state (compactivity  $X=0$ ). Whereas  $V_{max}$  is reached when the powder is most fluidized with compactivity  $X = \infty$ . The entropy here has dimensions of volume, and can be formulated in terms of disorder induced by voids. The entropy is defined as the logarithm of the number of configurations [Jae92]:

$$S = \lambda \ln ([ \int \delta(V-W) d(\text{all configurations}) ] \dots \dots \dots (1.3)$$

where:  $W$  - the function which specifies the volume of the system in terms of the position of the individual grains,

$\lambda$  - the constant analog to Boltzman's constant,

$\delta$  - the Dirac delta function.

As a analogue to the free energy ( $F$ ), the effective volume ( $Y$ ) has been defined as :

$$Y = V - X S \dots \dots \dots (1.4)$$

The state of maximum entropy will be that corresponding to the random close packing limit.

### Fermi-like theory of granular media

Hayakawa and Hong formulated the theory of weakly excited GM from the viewpoint of elementary excitations of spinless fermions and the free volume theory [Hay97]. GM entity has been seen as a macroscopic object, robust to thermal disturbance, and at any finite temperature it is effectively in the ground state. Excitation of this ground state may be achieved by subjecting the system to vibration or shaking where the degree of excitation is controlled by the global acceleration amplitude ( $\Gamma = r \omega^2/g$ ).

For a weakly excited system ( $\Gamma \sim 1$ ), potential energy dominates over kinetic energy, and in this situation the most probable particle configuration should be determined by the state of maximization of entropy,  $S$  (i.e. minimum of free energy). According to Pauli's excluded volume principle two grains it is not allowed to occupy the same states and the statistics are given by the Fermi statistics. Therefore, maximization of entropy yields that the density

## 1. LITERATURE REVIEW

---

profile (the average number of occupied cells at a given energy level), must be given by the Fermi distribution. This assumption agrees with several experimental work where the density profile obeys a universal function that is independent of the phase of oscillations [Cle91,Fis05]. The crucial observation in this theory is that for a weakly excited granular system, most excitations occur near the Fermi surface, which may be effectively well represented by the motion of a single particle on the Fermi surface that is in contact with the vibrating plate. Through the analogy to the free volume theory of the liquid state it has been assumed that the dominant process involving particle rearrangement is hopping with the rate dominated by the activation energy [Car91].

The authors complete their thermodynamical formulation by presenting an explicit relation between temperature and acceleration amplitude (Eq1.5):

$$T = (m g / \pi \omega) [3 D g H_0 (\Gamma)]^{1/2} \dots\dots\dots(1.5)$$

where,  $m$  is the mass of grains,  $D$  is the grain diameter,  $H_0(\Gamma)$  is the maximal height achieved by a single ball bouncing on the vibration plate with a intensity of  $\Gamma$ .

Recently, J.Fiscina and M.Caceres [Fis05], motivated by the Hong's approach, proposed a theory based on Fermi-like behavior of weakly vibrated GM, where the concept of temperature is resolved by the generalization of the equipartition of energy. In this work the granular matter gas at the surface has been experimentally investigated. Important contribution coming from this study of the spectrum properties of vibrated GM under gravity, is that in the weakly excited GM regime the dynamics of fluidized particles cannot be described as a simple Brownian particle, as observed in results of G. D 'Anna et al. [D'An03, D'An01]. The authors emphasized that weakly excited beds experience complex cooperative dissipative dynamics. The global temperature at the nonequilibrium steady state was characterized by a Lagrange parameter ( $\beta^{-1}$ ). The relation between global granular temperature and the external excitation frequency is given by Eq.1.6.

$$\beta^{-1} \approx \frac{m h \sqrt{(3 g \delta \omega / d)} A \omega}{\pi}, \quad h = \mu_0 / m g \dots\dots\dots(1.6)$$

where:  $\mu_0$  is the zero-point "chemical potential",  $\delta$  is the accounts for inelastic factor,  $\beta$  is Lagrange multiplier parameter,  $A$  is the amplitude,  $\omega$  is the frequency of plate and  $h$  is the height. Both proposed formulations may open a way to visualize the invisible quantum behaviors of fermions through the manipulation of GM.

### 1.2.3 Dynamics of granular media

The dynamical properties and flow of GM have been an intriguing question studied by many physicists including Faraday, Maxwell, and Reynolds. In general, excited granular media exhibits very complex relaxation behavior toward non-equilibrium steady state. The dynamics of this steady state involve different phenomena (i.e convection,[Cle92], density waves [Hay97], anomalous sound propagation [Liu89], segregation and even turbulent behaviors) which usually progress in parallel. Additionally, density fluctuation has been observed in the bed volume which increases the complexity of phenomena [Kni95].

#### 1.2.3.1 Relaxation behavior of granular media

Important impact to relaxation behavior of GM came from the work of Jaeger's group through investigation of the distribution of avalanches occurring when the slope of a sandpile exceeds the metastable slope given by angle of repose [Jeg89]. It was observed that the relaxation behavior of the angle of repose is strongly affected by the vibration intensity. Under high vibration intensity, the slope of the pile fell to zero in a such way that logarithmic law has been obeyed between angle of repose and vibration time. On the contrary, at smaller intensity, the slope of the pile stays finite, and relaxation is below the value predicted by the logarithmic law. The experimental observations of Jaeger et al. have been confirmed by a simulation from Mehta [Meh90].

The same logarithmic relaxation law has been observed by Knight et al. [Kni95] by analyzing the density relaxation of 2 mm diameter spherical soda-lime glass beads submitted to vertical vibration. Figure 1.3 presents experimental density relaxation curves for different excitation level (from 1.4 g to 5.4 g). Rapid increase in the packing density was observed at a characteristic acceleration  $\Gamma_c \approx 1.8$  and the logarithmic law, known as Chicago's law, fits the whole range of data well. Due to the experimental technique applied (capacitive technique), spatial distribution of density along the column could be followed, and the fluctuation of packing density has been observed at low accelerations.

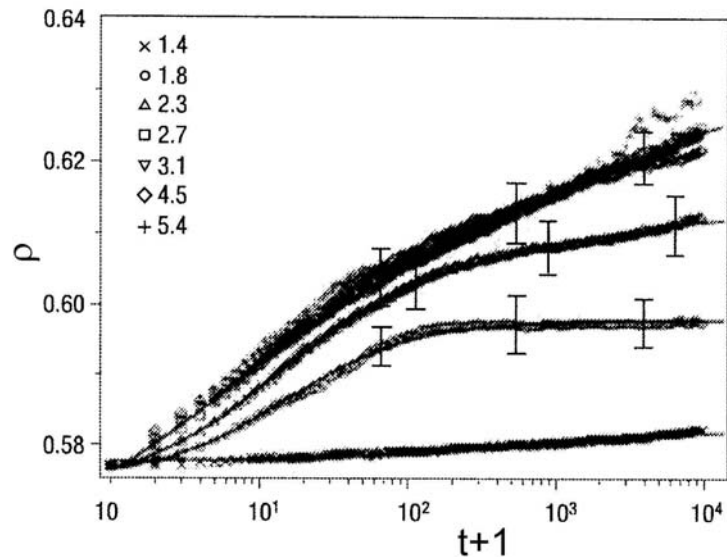


**Fig 1.3.** Packing fraction as a function of the logarithm of the tap number for different vibration amplitudes [Kni95].

Important contribution to understanding the relaxation mechanism came from the work of Mehta et al. [Meh90,Meh90a,Meh91,Bar92]. In their simulation of granular compaction, two relaxation mechanisms dependant on excitation intensity were proposed.

The first one, independent particle motion (single particle relaxation) dominates at high shaking intensities. This regime, named grain-inertial regime is characterized by the breaking of particle-particle contacts and the formation of the new contacts. This simulation has modeled powder under highly kinetic conditions and it is shown to be most efficient at moderate particle density  $\Phi \sim 0,3 - 0,4$ .

The second regime, called quasi-static regime, performs collective motion with a slow deformation of local environments without breaking particle-particle contacts. The collective reorganization regime (collective relaxation) dominates at lower shaking intensities where instantaneous, inelastic, two-particle collision dominates the motion. The quasi-static regime occurs in close-packed collections of particles ( $\Phi > 0.55$ ) and in this case the contact forces between particles are of great importance. For most materials, the precise nature of the contact forces is unclear. The so-called principles of limiting friction and indeterminacy of stress, which are familiar to chemical engineers, say that internal stress in a granular assembly is indeterminate because the friction between two grains in contact can lie anywhere between 0 and a limiting value. Therefore, the application of granular dynamics in the quasi-static regime are restricted by (ad hoc) estimates of contact forces usually constructed from viscous and harmonic elements.

Fig. 1.4 presents results of the simulation ensued from a microscopic approach for different shaking intensities. Two qualitatively different relaxation behaviors are illustrated. At low shaking ( $\epsilon=0.05$ ), comparing Fig. 1.4b and 1.4c, the contact network deforms, while there are few topological changes. By contrast, after more intensive shaking, as seen from comparison of Fig. 1.4(b) and 1.4(d), the network connectivity is substantially altered, i.e. there are several examples of bond creation and annihilation. It has been recognized that the collective relaxation mechanism is an efficient way of minimizing voids.

Most shaking processes takes place in a series of regimes that traverse the spectrum from grain inertial to quasi-static regime. The competition between the two proposed mechanisms will determine the global relaxation of GM. Mehta's model quantitatively estimated a global relaxation dynamic as the sum of two exponential terms corresponding to the two relaxation mechanisms, as described with Eq 1.6.

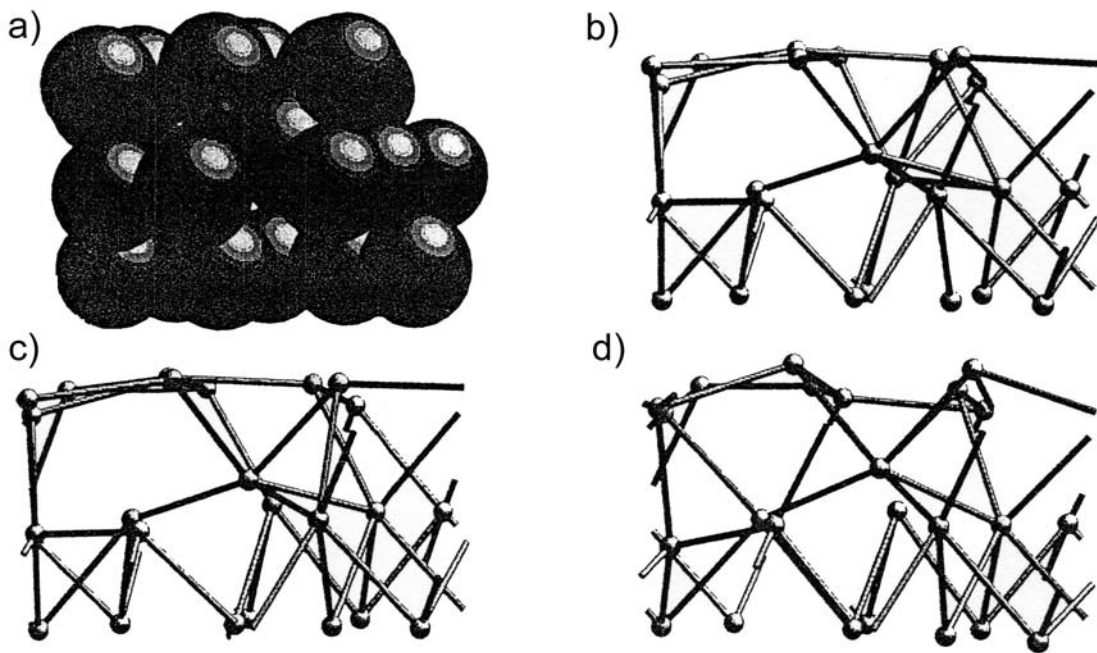


**Fig 1.4.** (a) A random close packing of 24 spheres supported by a hard base, (b) contact network corresponding to the packing in (a), (c) the contact network for the packing which results when a shake of amplitude  $\epsilon=0.05$  is applied (d) the contact network for the packing which results when a shake of amplitude  $\epsilon =1$  is applied to the cluster in (a) [Meh91].

$$\rho(t) = \rho_f - \Delta\rho_{ind} \exp[-t/T_{ind}] - \Delta\rho_{col} \exp[-t/T_{col}] \dots\dots\dots (1.7)$$

where:  $\rho_f$  is the final steady state density,  $\Delta\rho_{ind}$  and  $\Delta\rho_{col}$  are the amplitudes for the two relaxation processes,  $T_{ind}$  and  $T_{col}$  are the relaxation times for single-particle relaxation and cluster relaxation respectively.

### 1.2.3.2 Size segregation

Phenomenological segregation can be described as an upward movement of larger particles, when a polymodal granular media system is subjected to vibration. Segregation is important in many industrial disciplines: pharmaceutical, powder metallurgy, coal and mineral processing. The most obvious industrial problem that arises from this phenomenon is that the particles tend to unmix when free-flowing particles of different size are being mixed. In feeding to packaging machines or tableting processes, segregation causes fluctuations in the size distribution of the particles and in turn leads to variation in bulk density. Rosato emphasized that: "Segregation is an example of a simple, mechanical system displaying nonequilibrium, counterintuitive behavior" [Ros87]. Size segregation inevitably seems to contradict equilibrium statistical mechanics, since the equilibrium position with larger particles on the bottom is more favorable (minimum of potential energy). Additionally, the density of the overall packing increases with polydispersivity and contrary to the space-saving consideration segregation leads to separation of constitutive particle sizes [Meh90]. In the literature, segregation is commonly known as the Brazil Nut Effect (BNE). The term "Brazil Nut Effect" stems from the fact that in a container consisting of a mixture of different sized nuts, the largest nuts, often the Brazil nuts, always seem to rise to the top. More often than we may think, we do encounter granular segregation. For instance, when a pack of muesli is shaken, the larger particles like nuts and currant end up on top of the smaller ones.

The origin of segregation is still an open problem. The scientific community argue and debate whether large particles are lifted up via inertial differential motion, or via long-range friction, or via some other process yet to be discovered. In the literature, BNE has been mainly attributed to the following phenomena: 1) shifting and percolation [Wil76, Ros87], 2) geometrical reorganization [Ros87, Dur93], 3) global convection [Gal92, Elp97], 4) condensation driven segregation [Hon01, Qui00], 5) inertial driven segregation [Jen02, Shi98]. Recent theoretical investigations show the existence of reverse BNE (RBNE), where large particles are settled on the bottom of the container [Hon01, Shi01]. There is controversy regarding experimental verification of the theory of the reverse BNE (RBNE). In some experimental work no RBNE has been observed [Can02] but, on the another hand experimental results of Breu et al. confirm that the theory by Hong et al. is able to predict occurrence of the reverse BNE correctly [Bre02].

## 1. LITERATURE REVIEW

---

### Mechanism of segregation

In the 1970s, segregation was a subject of consideration in engineering field. The first review paper concerning segregation of particle materials was written by Williams [Wil76]. In his experimental work, the author demonstrated that, under vibration, single large particles placed underneath the smaller-size particles, will rise to the top. The observed size segregation was explained through a pressure increase in the region below the larger particles. This pressure increase improves the compaction of materials and stops the particles from moving downwards. Very extensive experimental investigation was performed by Ahmad and Smalley [Ahm73]. A frequency from 50-150 Hz and acceleration of 1-10 g was selected in order to verify critical parameters. It was shown that a large sphere with an initial position in the middle of the container base segregates more quickly than those closer to the wall. Also, at constant acceleration, segregation was reduced with increase in frequency. On the contrary, at a constant frequency, segregation rate increases as acceleration increases. Particle size ratio and density influence segregation in manner that larger particle size ratio enhances segregation, and lighter particles segregate more quickly than heavier particles of the same size, under identical vibratory conditions. The important cognition coming from the experimental evidence is that higher frequency and lower acceleration are useful in controlling segregation.

Segregation has been intensively studied by theoretical physicists and various numerical simulations have been carried out to determine the origin of this phenomenon. For that purpose a system is usually modeled as one large sphere (intruder) in a bed of smaller spheres. In some models a 50-50 binary mixture of larger and smaller spheres has been considered. The most important models, usually classified as percolation, geometrical reorganization and convection, will be introduced in following text.

### Percolation driven segregation

One of the earliest computer simulation of segregation driven by percolation was developed by Haff and Werker [Haf86]. The 2D simulation was analogous to the direct molecular dynamics computations used for studies of transport properties in gases and liquids. The author suggested that in the presence of sufficient friction, the large particle was able to roll up over the adjacent smaller particles and in this way make its way to the top.

Rosato et al. have used an adaptation of the Monte Carlo method in 2D (Monte Carlo shaking algorithm) in order to study the dynamics of size segregation driven by percolation [Ros87, Ros86]. In this approach, shaking of hard spheres is modeled by involving energy

## 1. LITERATURE REVIEW

---

dissipation. The effect of interparticle collision and particle-wall collision has been modeled as random movements of the particles with respect to one another.

In shaking simulation, the container was firstly filled by simply falling under gravity. Simulation was conducted in both a system of one large intruder in a smaller size bed, and in a binary 50-50 mixture of smaller and larger particles. Typical experimental conditions were: ratio between potential ( $E_p = m g h$ ) and thermal energy ( $E_t = k_B T$ ) approximately  $10^6$ , which essentially means  $T=0$ . In both experimental cases, the upward motion of larger particles was observed. The segregation was explained through relative motion between particles solely by geometric effects where the creation of voids of smaller particles beneath the large one has been emphasized as the critical parameter. The intruder causes a protuberance in a bed of smaller particles, and new formed voids filled by smaller particles are essential to upward motion. In order to create large voids for the intruder to move downward, several particles must move simultaneously. Clearly, this is a rather unlikely event, thus the intruder experiences a net upward motion. The shaking amplitude and particle size ratio have been identified to be two of the primary factors influencing segregation. It was concluded that for each fixed size ratio, an increase in the shaking amplitude resulted in faster segregation. Secondly, segregation proceeds more quickly for the larger size ratio due to the decrease in the randomness of the motion of larger particles. Also, it was observed that segregation is independent from density.

An important contribution of Rosato's group comes from, the observation that for amplitude of vibration in order of smaller particle size (in 50-50 mixture), segregation of larger particles obeyed a linear law with time. This linearity demonstrates that segregation the rate is strongly dependent on the local structure. Hence, the process can be described primarily by local geometrical effects, i.e. volume per particle.

A similar numerical approach has been applied by Jullien et al. [Jul92] known as the piling algorithm. This model also explores some topological properties of a disturbance created by an intruder (large particle) in a field of smaller particles. The importance of the piling model is related to the existence of a size threshold number for segregation, defined for particle size ratio of  $\Phi = d_l / d_s = 2.8$ . Existence of such threshold limits was criticized by Mehta [Bar93], since this result is in conflict with well-established experimental work [Wil76, Bri85], where segregation is observed in systems with particle size ratios below 2.8. The segregation threshold limit depends in a complex way on excitation level, fluctuation of system densities, regime of segregation, and morphology of the grain; so, at present, the threshold limit cannot be used as a general parameter

### Geometrical reorganization

Duran's research group proposed an arching model in order to explain the origin of size segregation [Dur93]. Starting from 2D experimental observations and using topological arguments, authors searched for the set of stable positions for upward motion of the intruder. Experimental conditions used in the study were: low excited GM (slightly above the acceleration of gravity) and two different particle size ratios  $\Phi$  ( $\Phi = 2$  and  $\Phi = 16$ ). It was shown that the dynamics of a system are strongly linked to the particle size ratio. Two different initial geometrical configurations were formed in assembly of large disk in smaller disk beds depending in particle size ratio. For  $\Phi=16$ , the large disk causes a perturbation in the arrangement of smaller disk beds in the form of triangular domain with an opening angle of  $60^\circ$ , as shown in Fig.1.5 a and b. On the contrary, for the smaller  $\Phi$ , smaller discs are supported by the underlying network, as presented in Fig. 1.5. c and d.

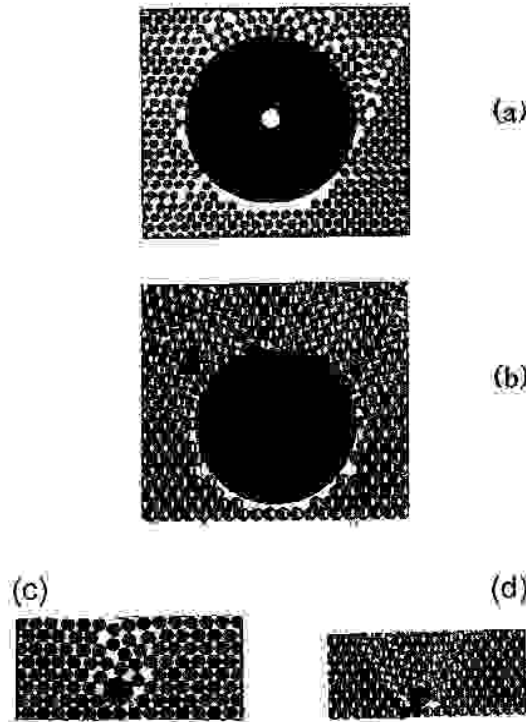


**Fig. 1.5.** Various configurations of one large disk in an assembly of monodisperse smaller disks. Photographs in real experiment were as shown in (a) and (c), The results of computer simulation are shown in (b) and (d). For the case of  $\Phi= 16$ , the arching effect is clearly observed (a and b). On the contrary, the smaller disk is supported by underlying network when  $\Phi= 2$  (c,d) [Dur93].

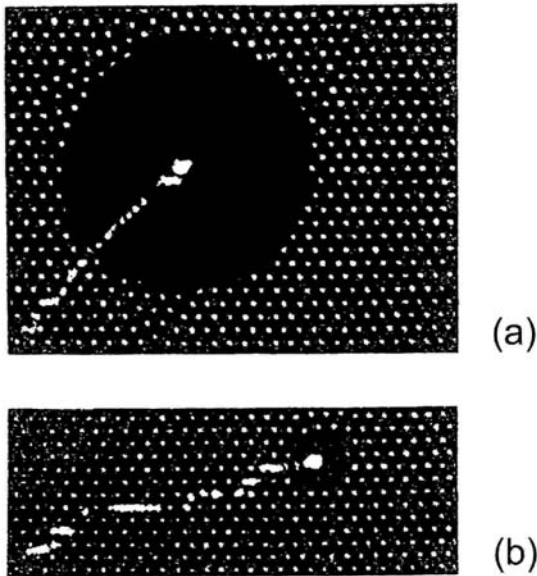


**Fig. 1.6.** Experimental observation of the continuous upward motion of a large disk ( $\Phi = 16$ ) (a) and of the intermittent ascent of a smaller disk ( $\Phi = 2$ ) (b) [Dur93].

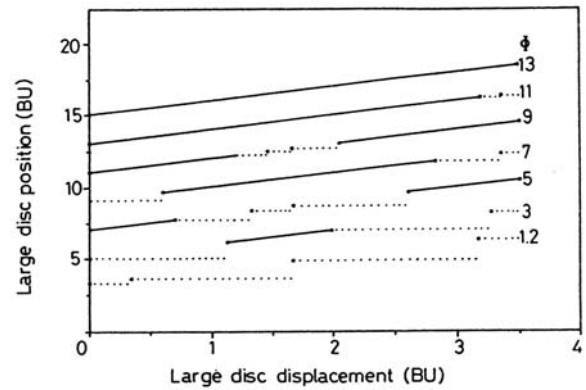


**Fig. 1.7.** Ascent diagrams of various diameter ratio  $\Phi$ . The solid lines represent stable configurations whereas dashed lines depict unstable ones [Dur93].

Several important consequences may be deduced from the arching effect model. Firstly, the model revealed that the presence of a hole beneath the larger particle is essential to its upward motion. The larger intruder moved upward continuously via arching effect, whereas the smaller intruder may only climb up intermittently (Fig. 1.6). Figure 1.7 depicts a stable and unstable configuration for the ascent of an intruder in particle beds for various diameter ratios ( $\Phi$ ). The upward motion of the smaller intruder ( $\Phi=2$ ), which is not always supported by vaults, can only be obtained by inducing large upward steps. In that way, the intruder covers the distance corresponding to a plateau. Secondly, critical diameter ratio ( $\Phi$ ) for continuous ascent has been calculated to be of the order of 2.78. A third important result coming from this study is the relationship between amplitude of vibration and diameter ratio. It has been observed for the larger intruder ( $\Phi=16$ ) to move up at lower amplitude, whereas smaller ones ( $\Phi=2$ ) require a higher amplitude. Through experimental work Duran et al. have verified the results of their simulations [Dur94].

### Convection driven segregation

Convection flow of granular media is an extensively investigated phenomenon concerning size segregation. One of the earliest and most famous studies of convection was conducted by Faraday in 1831 [Far31]. Faraday observed a motion of grains towards the center near the base of the vibrated heap. The grains rise upward through the middle of the heap and move back down the sides. The effect was explained by the influence of surrounding air.

## 1. LITERATURE REVIEW

Faraday's work has motivated a variety of theoretical approaches to convection, mainly based on the particle dynamic model (PDM) of two dimensional grains under vibration. Elperin and Goldstein gave important contribution to the simulation of the segregation process [Elp.97]. In their simulation, the effect of vessel geometry visualized through aspect ratios ( $G = \text{container diameter} / \text{bed height}$ ) and effect of coefficient of friction forces on segregation dynamics have been investigated. In Fig. 1.8 the effect of different aspect ratios on the convection onset has been presented.

In the simulation with aspect ratio  $G=0.25$  (Fig.1.8a), the convection onset is presented only in upper parts, while lower parts of the packing remained static. In the aspect ratio of 2 (Fig 1.8b) the convection rolls were attached to the container walls, which indicates a contribution of the wall-particle friction to the origin of the convection. The most intensive convection was detected at aspect ratio,  $G=0.8$  ( Fig 1.8b), where the convection rolls spread over almost the whole packing content.

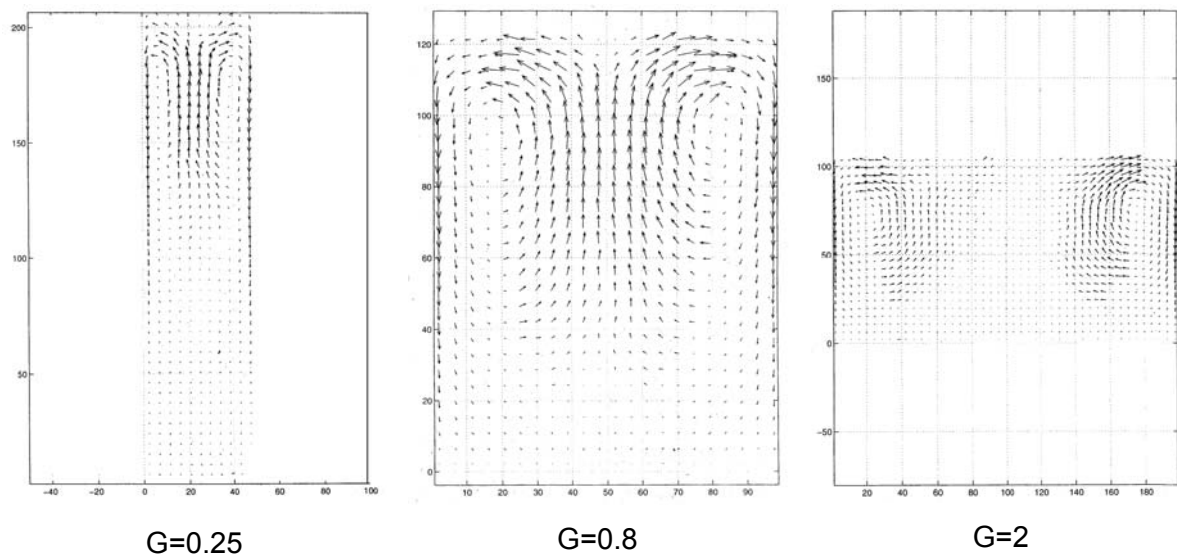


**Fig. 1.8** Flow patterns in a container with different aspect ratios:  $G=0,25$  (a);  $G=0.8$  (b),  $G=2$  (c). In simulation based on particle dynamic method (PMD) 600 grains have been used [Elp97].

In the conducted simulation size segregation has been considered by immersing large grains at the lower part of a container filled with small grains. In the experimental system with the aspect ratio  $G= 0.25$  two different segregation regimes have been observed. Firstly, when the large grains were located at the lower container position, slow segregation with the rate of  $v= 0.6$  cm/s took place. This regime is attributed to geometrical segregation, dominantly caused by relative particle motion and in the final stage, large grains concentrate on the surface. Much faster segregation has been observed with large particle in the upper

## 1. LITERATURE REVIEW

---

container position where convection rolls are detected. In this second regime, driven by convection flow, segregation rate was significantly higher ( $v=5$  cm/s) and the large grains are placed near the centers of different rolls and do not mix (Fig.1.9).

The influence of the friction coefficient ( $\mu$ ) on convection, as well as on interaction between the two observed mechanisms (convection driven segregation and geometrical segregation) has also been studied. The results revealed that the transition point between two segregation regimes is strongly related to the friction coefficient. In Fig.1.10 at  $\mu = 0.2$ , a strong change in segregation rate occurs. The convection was observed only when friction was significantly higher ( $\mu > 0.4$ ) and only with grain-grain friction forces no convection was noticed. For that reason, it was proposed that convection motion is driven by grain-wall friction. However, under real experimental conditions with polished and oxidized  $Al_2O_3$  particles, segregation has not been observed in the case of frictionless particles [Dur94] contradicting numerical observations of Elperin [Elp97].

Another important theoretical contribution to the study of convection flow came from the work of Galas et al. where the first numerical evidence for the occurrence of convection cells due to inhomogeneities in the vibration amplitude has been presented [Gal92]. Also, convection-cell generation in relation to the existence of walls was analyzed. The start point of the investigation was molecular dynamic simulation (MDS) of inelastic particle in a 2D system, with an additional shear friction. Two forces act on the system: on the one hand, gravitation pulls each particle downwards; on the other hand, the bottom of the container is subjected to a vibrating motion described by:

$$Z_0(t) = A(x)\sin ( 2\pi f t).....(1.8)$$

where  $f$  is the frequency and the amplitude ( $A$ ) can have an explicit spatial modulation of the form:

$$A(x)=A_0[1-B\cos(2 \pi x/L)].....(1.9)$$

Simulation clearly shows that the particles flow upward in the center where the amplitude of vibration is larger and form two convection cells. Similar to Elperin et al. [Elp97], Gallas [Gal92] involved the friction coefficient  $\mu$  in analysis. In the case of no shear friction the vertical walls do not transfer any vibration motion from the container, representing a steric hindrance to the flow. In this situation, a flow parallel to the bottom plate will spontaneously

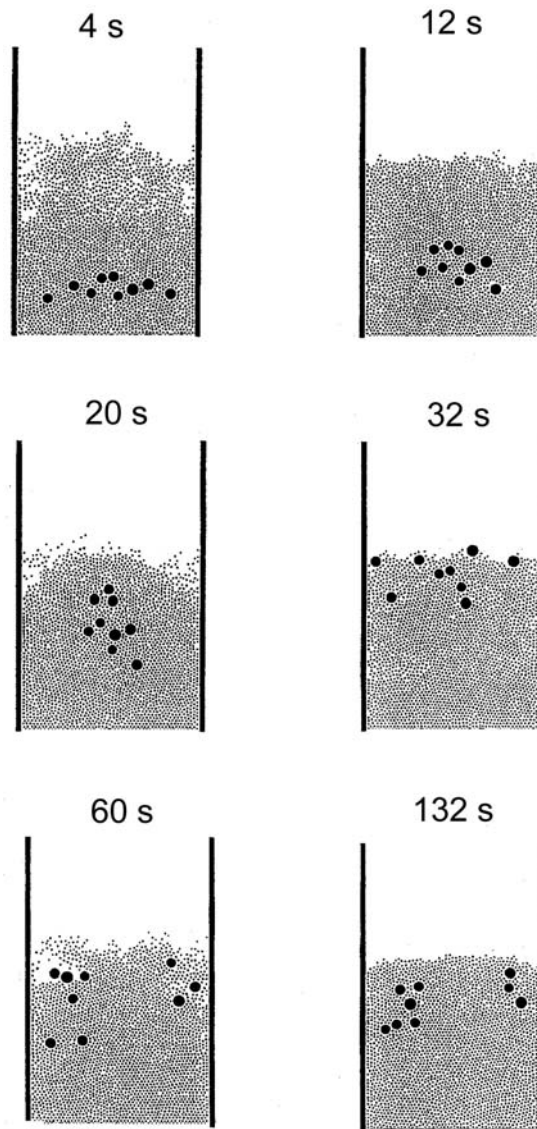


**Fig 1.9** Flow path of larger particles in regime of convection driven segregation [Elp97].

appear. The driving force for the upward flow in this case therefore is the horizontal flow along the bottom. When shear friction with wall is present a different mechanism appears. While the particles are pushed up and start to levitate, strong pressure (due to still high compressed packing) is exerted on the walls giving strong shear friction. Afterwards, when particles fall back (packing is much looser in respect to wall) the shear frictions are much less efficient. Therefore the upward motion of the particles with respect to the wall is slowed down strongly resulting in a net drag down along the wall.

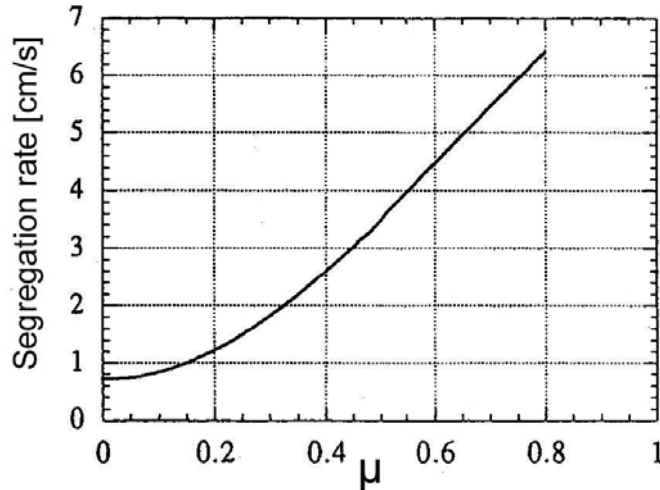


**FIG. 1.10** Segregation rate versus friction coefficient,  $\mu$  [Elp97].

The first experimental study of the convection cell phenomena in a two-dimensional box with 3 mm glass beads have been undertaken by Hsiao et al. [Hsi00]. Using image processing technology and particle tracking methods, the velocity fields of the convective granular beds were measured and analyzed. The two critical parameters were defined as: dimensionless acceleration amplitude  $\Gamma$  (Eq.1.10) and dimensionless velocity amplitude  $Vb$  (Eq.1.11):

$$\Gamma = a / g \dots\dots\dots(1.10)$$

$$Vb = r \omega / \sqrt{g d} \dots\dots\dots(1.11)$$

where  $d$  is the particle diameter,  $g$  is gravity,  $r$  is the oscillation amplitude and  $\omega$  is the radial frequency.

The vertical and horizontal velocity distributions were measured under different conditions in the range of  $Vb$  (1.21- 2.42) and for two accelerations  $\Gamma=3$  and 6. In almost all of the experimental conditions the existence of two symmetric convection rolls have been observed. Granular media move upward in the central part and move downward along the side walls of the container. It was shown that convection flow rate increases with the bed velocity in a power law relation:  $J \propto Vb^{2.02}$ . Also, the greater the acceleration, the stronger the convection cell is. Interesting phenomena occur at low excitation conditions ( $Vb = 1.21, \Gamma = 3$ ) where convection has been detected only on the surface, although the velocity scale was not large.

## 1. LITERATURE REVIEW

---

### Reverse Brazil Nut Problem (RBNE)

Contrary to the common observation of BNE, there are studies where it has been noticed that a large particle, depending on its density, could also sink to the bottom of the container leading to Reverse Brazil Nuts Problem (RBNE) [Shi98]. The work of Shinbrot [Shi98] demonstrated that in an highly excited shaking regime large heavy grains will rise but equally large, lighter grains, sink in the granular bed. The process seems to be independent of type of shaker, driving wave form, container material, and container form, but it depends strongly on vibration amplitude. The central observation underlining this model is that inertia causes heavy object to lift off the bed, permitting smaller particles to infiltrate beneath. The motion of light object, by contrast, can fluctuate wildly, preventing formation of a void space for this infiltration. For intruder density less than about 50% of bed density ( $\rho_b$ ), the intruder moves to the bottom of the container, where it remains indefinitely. For intruder with density between 1.2-1.7 of  $\rho_b$ , on the other hand, the intruder rests on the surface of the bed.

Another experimental observation of reverse BNE has been recognized by Breu et al. In the studied system of 10mm polyurethane [ $\rho=1.2 \text{ g/cm}^3$ ] and 4mm glass [ $\rho=2.5 \text{ g/cm}^3$ ] beads [Bre03] depending on acceleration the following scenario is proposed.

- 1) For acceleration,  $\Gamma < 0.8g$  - particles stay in rest.
- 2) In the range of  $0.8g < \Gamma < 1g$  - large particles rotate around initial position.
- 3) For acceleration  $\Gamma > 1g$  - large particles rearrange themselves, ending in hexagonal close-packed structure.
- 4) For acceleration  $\Gamma > 3.5g$  - smaller particles tend to move upward. In the final stage, smaller particles are placed on the top, behaving like a granular gas and RBNE is established.

It is demonstrated that transition through regimes (1-3) did not depend on the driving frequency, but only on the acceleration. On the other hand, transition from BNE to RBNE depends on both acceleration and frequency. It has been proposed that transition of the two effects could be predicted by Eq.1.12.

$$d_l / d_s \approx (\rho_l / \rho_s)^{-1} \dots \dots \dots (1.12)$$

where: subscript l indicates larger particles and s, smaller particles.

The Brazil Nut Effect has been observed for particle size ratio larger than density ratio

## 1. LITERATURE REVIEW

---

$(d_l / d_s > (\rho_l / \rho_s)^{-1})$ . In mentioned experimental work, a variety of materials were investigated (glass, Al, bronze, steel, polypropylene, polyurethane, synthetic resin, wood), and for 82% of the test combinations the prediction of Eq 1.12 was correct. The prediction failed when one particle type was Al or polyurethane, it was concluded that, for these materials, the condition of hard sphere was not met

Recently Hong et al. [Qui00,Hon01] have proposed a conceptually new approach named condensation drive segregation. The proposed model explained that both effects, the rise or descent of large particles, may occur. The starting point in Hongs's observation, confirmed by MD simulation, is the existence of a critical temperature,  $T_c$ , below which a monodisperse system of hard spheres undergoes a condensation transition in the presence of gravity. For a fully fluidized granular system where all particles are in motion, the ideas of the kinetic theory of gases can be applied. It then is possible to define a granular temperature in analogy to a gas, using the mean kinetic energy. If the system is in contact with a thermal reservoir at temperature  $T$ , the dimensionless thickness of the fluidized layer,  $\Delta h$  in D dimension can be estimated by equating the kinetic energy of one grain to the potential energy equivalent (1)

$$m\langle v \rangle^2/2 = DT/2 \sim mgd\Delta h \dots\dots\dots(1.13)$$

which yields to

$$\Delta h \sim DT/(2mgd) \dots\dots\dots (1.14)$$

At the point  $T_c$ , at which the system is fully fluidized, the setting  $\Delta h$  is replaced by  $\mu$ , layer thickness in units of diameter  $d$ . The critical temperature for condensation has been defined by equation [Eq.1.15].

$$T_c = m g d / \mu_0 \dots\dots\dots(1.15)$$

where  $\mu_0$  is a constant that depends on the spatial dimension and the underlying packing structure.

When  $T > T_c$ , the system is fully fluidized and dimensionless thickness of the solid vanishes ( $h_{\text{solid}} = 0$ ). On the other hand, for  $T < T_c$ , a fraction of particles with  $h_{\text{solid}} \neq 0$  has been condensed at the bottom. The solid phase refers to a hard sphere state where each particle fluctuates around a fixed point, without exchanging its center of mass position with neighboring particles.

Extending analysis to a binary mixture of spheres (A, B, having masses:  $m_A, m_B$  and diameters  $d_A, d_B$ ), the authors have found a ratio of critical temperatures (Eq. 1.16)

## 1. LITERATURE REVIEW

---

$$T_c(A) / T_c(B) = m_A d_A / m_B d_B \dots\dots\dots (1.16)$$

If the system is quenched at a temperature  $T$  between the two critical temperatures  $T_c(A)$  and  $T_c(B)$ , ( $T_c(B) < T < T_c(A)$ ), then hard spheres of type B are above the condensation temperature, while the hard spheres of type A are below it. As a consequence, particles of type A will try to condense, while B particles remain fluidized. Hence, A particle will tend to segregate to the bottom. The underlying assumption of this event is that particles of type A interact only with themselves, while seeing particles B as inert (“phantom”) particles, and vice versa ( Fig. 1.11).

The ratio between particle masses and diameters has been recognized as the critical parameter that controls competition between condensation and percolation. At critical parameter ( $T_c(A) / T_c(B) > 1$ ), condensation of large particles takes place, whereas small particles could percolate through a condensed phase, forcing the large particles above them. Since the critical temperature depends on the ratio between particle mass and diameter (Eq. 1.16) an inversion of the segregation should be achieved by simply altering the values of  $m$  and  $d$ , as illustrated in Fig. 1.12.

Hong’s numerical observation is, however, subject of controversial discussion in the physics community. There are experimental works which confirm the existence of RBNE [Shi01, Shi98, Bre03]. However, other experiments have been conducted where no RBNE was observed [Can02]. An important contribution coming from the outlined model is the proposal of a more general framework for understanding the segregation process. The range of application is beyond that of convection, classical percolation, geometrical reorganization, or arching models, since all those models are limited to special situations.

Jenkins et al. [Jen02] used the kinetic theory for a binary mixture and the crucial role of interaction between particles was considered. They also considered, like Hong [Qui00, Hon01] a thermal binary mixture of grains under gravity in attempting to predict the ascent of the large particles. In this analysis it has been postulated that segregation is driven by a competition between the inertia of the particles (through the ratio of their masses) and their geometries. It has been noted that when both species are dilute, such segregation is predicted for particles that differ in mass, no matter what their radii may be. The used criteria for segregation are relatively close to those of Hong et al. [Qui00, Hon01], even though the proposed mechanisms are very different. The main difference is in the fact that Hong’s model

neglected interactions between the two species, while Jenkins et al. [Jen02] considered those interactions crucial to segregation mechanisms.

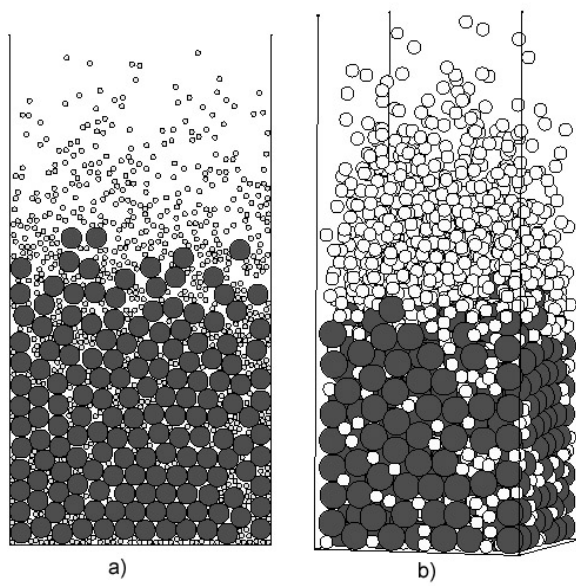


**Fig. 1.11** Reverse BNE a) 2D scheme with mass ratio  $m_A/m_B=4$  and diameter ratio  $d_A/d_B=8$  (a), and b) 3D scheme where  $m_A/m_B=6$ ,  $d_A/d_B=2$ .

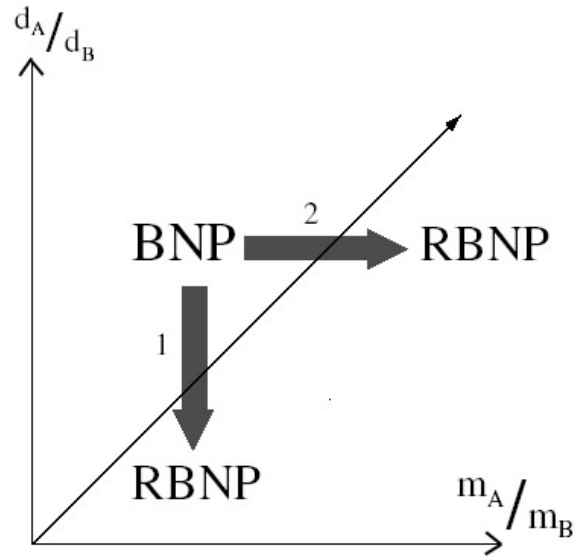


**Fig. 1.12** The schematic picture for the crossover from the Brazil Nut Effect (BNE) to the reverse Brazil Nut Effect).

### 1.3 Solid state sintering

Sintering can be described as a thermally activated material transport, in powder or in a porous compact, that leads to density increase. This process is followed by a reduction of the specific surface predominantly caused by: particle contact (neck) growth, shrinkage of pore volume and change of pore geometry [Thü93].

Frenkel and Kuczynski pioneered the theoretical modelling of sintering using simplified geometries (sphere-plate, two wires) [Fre45, Kuz49]. The primary objective of a theoretical approach to sintering is understanding the mechanisms of material transport and their respective contribution to the neck growth. Kuczynski's model [Kuz49] describes the neck growth and particle centre to centre approach in quantitative terms as a relation between sintering time and temperature (exponential law). This idea has been brought to a high level of practical significance by Johnson's analysis [Joh69]. In Johnson's analysis proposed quantitative solutions are limited to a model system consisting of two spherical particles of equal size.

#### 1.3.1. Driving force for sintering

The driving force for sintering is the excess surface energy in the system. The reduction in excess surface free energy is translated into a driving force acting at the atomic level by means of the curvature differences which necessarily occur in different parts of the 3-D compacts. Variations in the local surface curvature of particles manifest themselves as a gradient in local pressure and, therefore, gradients in chemical potential and concentration of lattice vacancies.

The surface energy of solids is much more complex than the surface energy of liquids. Solid surface tension in general is anisotropic, with the result that the minimum surface energy is not represented by a sphere, but may include facets, sharp edges and sharp corners (Wulff theorem on the reorganization of polar surfaces). However, sintering models are based on the assumption of isotropic surface tension and diffusion coefficients. Particularly in non-metallic systems (like carbides or nitrides), where surface tension tends to be anisotropic, this approach should be taken with great caution. On the other hand, for some simple metals, the assumption of isotropic surface tension and diffusion coefficient seems to be acceptable [Joh80].

The pressure under an isotropic liquid surface is given by the Laplace equation (Eq.1.17)

# 1. LITERATURE REVIEW

$$P = P_o + \gamma (1/r_1 + 1/r_2) \dots \dots \dots (1.17)$$

where:  $P_o$  is the pressure external to the surface, and  $r_1, r_2$  are the principal radii of curvature.

The Laplace equation can be applied to solid surfaces at temperatures sufficiently high for the surface to be essentially disordered and liquid like in character. As an example of application of Laplace equation for solid surfaces, the situation representing the initial stage of sintering has been used (Fig. 1.13). Initial atomic bonding in the surface and in the neck region is highly disrupted. Along the surface away from the neck the curvature is constant, with both  $r_1, r_2$  equal to the sphere radius,  $D/2$ . From Laplace's law, the stress is equal to:

$$\sigma = 4\gamma / D \dots \dots \dots (1.18)$$

Using a circle approximation to the neck shape with a radius of  $p$ , where  $p$  is approximately equal to  $X^2 / 4D$ ,  $X$  being the neck diameter, the curvature at the neck gives the stress as follows

$$\sigma = \gamma / (2/X - 4D/X^2) \dots \dots \dots (1.19)$$

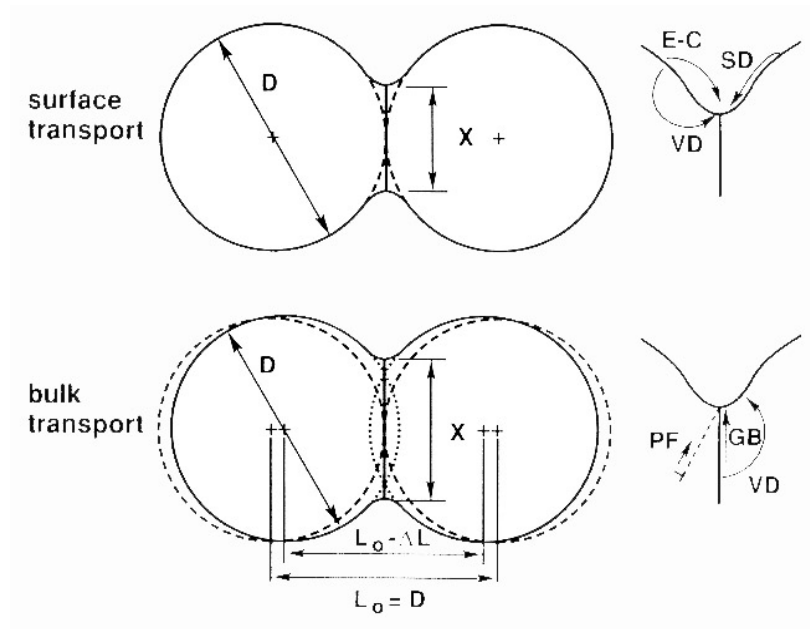


**Fig. 1.13.** Model of two spheres with two classes of sintering mechanisms: 1) surface transport mechanism (SD - surface diffusion, E-C - evaporation-condensation, VD - volume diffusion); 2) bulk transport mechanism (PF - plastic flow, GB - grain boundary diffusion, VD - volume diffusion). Particle diameter is  $D$ , and  $X$  corresponds to neck radius [Ger94].

## 1. LITERATURE REVIEW

---

Comparing Eq.1.18 and Eq.1.19 it can be revealed that there is a large stress gradient in the neck region. For a small neck radius, the gradient can be quite large.

The change in total surface energy (E) can be written as:

$$dE = \gamma \cdot dA \dots\dots\dots(1.20)$$

where :  $\gamma$  is the surface tension and A is the area

If the volume element  $dV$ , is moved from a region with  $r_1$  to  $r_2$ , by modifying Eq. 1.20, the change in surface energy is :

$$\frac{dE}{dV} = \sigma \dots\dots\dots(1.21)$$

with  $\sigma = \gamma (1 / r_1 + 1 / r_2)$

The volume under a concave surface (such as the neck regions), will be under tensile stress ( $\sigma < 0$ ), while the volume under a convex particle surface will be under compressive stress ( $\sigma > 0$ ).

The pressure in solid phase governs the chemical potential of the atoms and the defect concentration. In that way, the variation in curvature gives a material flux [Her50, Her51].

The chemical potential of the material is related to the stress in the system by Eq. 1.22 :

$$\mu = \mu_0 + \sigma \Omega \dots\dots\dots(1.22)$$

where  $\mu_0$  is the chemical potential under a flat surface and  $\Omega$  is the atomic volume. The change in chemical potential can be related to the curvature in the system as

$$\mu - \mu_0 = \gamma \Omega (1/r_1 + 1/r_2) \dots\dots\dots(1.23)$$

The chemical potential can also be written as a function of the vacancy concentration (Eq.1.24) and as a function of vapour pressure (Eq.1.26) [Bar51]

$$\mu = \mu_0 + kT \ln (c / c_0) \dots\dots\dots(1.24)$$

$$\mu = \mu_0 + kT \ln (P / P_0) \dots\dots\dots(1.25)$$

where  $c_0$  and  $P_0$  are vacancy concentration and vapour pressure due to a flat surface. By combining Eq. 1.23 with Eqs. 1.24, 1.25, the direct relationship between vacancy

## 1. LITERATURE REVIEW

---

concentration and surface curvature is obtained through the Gibbs-Thompson equation (Eq.1.26 ),

$$\ln (c / c_0) = \frac{\gamma \Omega}{kT} (1 / r_1 + 1 / r_2) \dots \dots \dots (1.26)$$

The Kelvin equation (Eq.1.27) correlates directly vapour pressure with surface curvature,

$$\ln (P / P_0) = \frac{\gamma \Omega}{kT} (1 / r_1 + 1 / r_2) \dots \dots \dots (1.27)$$

Under the influence of these gradients in stress (Eq. 1.21), chemical potential (Eq.1.26 ), and vapour pressure (Eq. 1.27), material migrates into the neck region between two spheres. Several mechanisms contribute to the migration and determine how mass flows in response to driving forces. The two classes of transport mechanisms are: surface transport and bulk transport as sketched on the two sphere geometry in Fig 1.13. Surface transport involves neck growth without a change in particle spacing (no shrinkage or densification) due to mass flow originating and terminating at the particle surface. In contrast, bulk transport controlled sintering processes cause a global shrinkage. The mass originates at the particle interior with deposition at the neck. Bulk transport mechanism include volume diffusion, grain boundary diffusion, plastic flow and viscous flow.

### 1.3.2 Stages of sintering

It is convenient to think that sintering occurs in four sequential stages. If loose particles are brought into contact, adhesion occurs due to predominant, weak Van der Waals forces. The adhesion stage occurs spontaneously with the formation of an incipient sinter bond. Unbalanced neck geometry results in particle rotation and rearrangement. Consequently, if possible, the particles will rotate and repack to obtain a higher packing density and lower energy grain boundaries [Ger96].

The growth of the sinter bond from an initial loose particle contact is considered as the initial stage of sintering. In this stage the neck size is sufficiently small, prompting neighbouring necks to grow independent of one another, and individual particles are still distinguishable. The initial stage ends when neck size ratio reaches to approximately  $X/D = 0.3$ . Analysis of the initial stage of sintering has been a popular theoretical topic, with the major first contribution provided by Frenkel [Fre45], Kuczinsky [Kuc49], Kingery and Berg [Kin55], Rockland [Roc67], Coble [Cob58], Young and Cutler [You70] and Johnson [64,69].

The intermediate stage is the most important for densification and determining the properties of the sintered compact. In the intermediate stage, the necks are large and lose identity, and attention shifts to the pore structure surrounding the necks. For sintering rate calculation, the pore geometry is assumed to be cylindrical, located on the edges of tetrakaidecahedral grains. The pore space is fully interconnected in three dimensions. There are several intermediate-stage models, as reviewed by Beere [Bee76].

When the pores become spherical and isolated, the final stage of sintering has been reached. Compared with the initial and intermediate stages, final stage is a slow process where simultaneous coarsening events could impede densification. The basic model for final-stage sintering proposed by Coble [Cob61,Cob61a], assumed spherical pores and tetrakaidecahedral grains.

The classification of sintering into stages is useful for modelling of the processes. The difficulty of model application lies in the specification of the appropriate flux field and boundary conditions. This is due, in part, to the complex geometry involved and also due to multiple, simultaneously active mechanisms.

### 1.3.3 Sintering of agglomerates

Agglomerates and other inhomogeneities are detrimental in achieving high final density during the sintering process. Recently, due to enormous interest in sintering and production of nanomaterials, the effect of agglomeration was reexamined by different research groups [Kno00, Ryu02, The93, Lee95, Bou94, Che97].

Lange and Evans extensively studied the sinterability of agglomerated powder [Lan89, Kel89, Lan83, Lan83a, Lan84, Lan86] and the effect of inhomogeneities on sintering kinetics [Eva82, Hsu86]. Lange observed that agglomerates are made of smaller, more dense packing units, called domains and less dense surrounding. Using these two types of packing, three classes of pores can be visualized [Lan84]:

- Pores of lower coordination number inside domains
- Pores of higher coordination between domains
- Pores with still higher coordination between agglomerates.

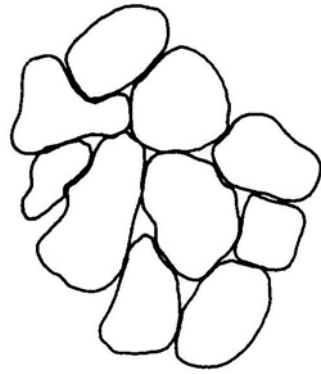


**Fig. 1.14** Schematic view of agglomerate structure, with domains as packing units.

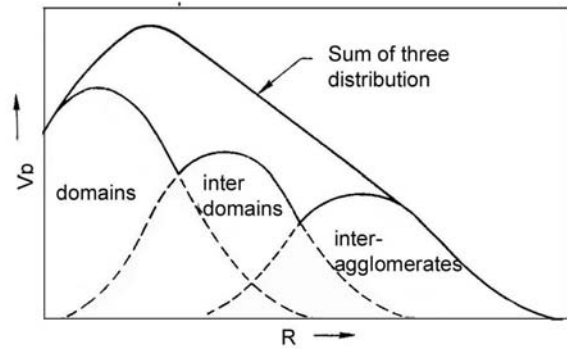


**Fig. 1.15** Schematic view of pore coordination distribution in agglomerated powder, indicating three classes of pores.

It is well established from Kingery's analysis [Kin67] that only pores with coordination number ( $n$ ) lower than critical coordination number ( $n_c$ ), have the thermodynamical potential to disappear during sintering. Otherwise, pores with  $n > n_c$  will even grow. The critical coordination number defines the transition from a convex ( $n > n_c$ ) to a concave ( $n < n_c$ ) surface. As a consequence of such a complex structure, exists strong asymmetric contact bonding inside agglomerates as well as between them, leading to asymmetric neck building when sintering proceeds. The asymmetric neck building causes a new non-diffusional material transport through particle rearrangement.

#### 1.3.4 Rearrangement process in solid phase sintering

It is well established that sintering of crystalline solids is essentially a diffusion process. In explaining shrinkage results, the center to center approach is preferentially used in the sintering theory. However, a metallographic and fractographic study conducted by Dudrova et al. shows that during heating-up and the initial stage of isothermal hold, shrinkage is dominantly caused by individual motion of particles (particle redistribution) [Dud84, Sch92]. The analysis of formation, character and growth of contact points recognized four contacts types: type I - point-shaped, type II - line-shaped, type III - plane bordered grouping of facets and type IV - bordered grouping of facets with well developed diffusional connections. Contacts of type I through III are observed during the heating-up phase and the fracture surface is mainly reduced to a point or a line segment. Otherwise, in later sintering stages, contacts of type IV dominate which lead to the center-to-center approach. Sintering in loosely packed areas also shows less shrinkage than the shrinkage calculated from the center-to-center approach [Exn73]. This behavior has been explained through opening of pores due to the rearrangement process that is intimately related to the rotational or gliding movement of particles relative to each other [Exn73, Sch92]. Particles rotate to form low energy grain

## 1. LITERATURE REVIEW

boundaries. There are two reasons for this deviation from the ideal center-to-center approach: 1) torque stresses in the neck region due to the formation of asymmetric necks and 2) shear and torque stresses due to the different shrinkage rates of pairs of particles in an irregular arrangement.

Asymmetric necks may form due to asymmetric contact geometry, anisotropy of surface energy, and asymmetric packing of particles. The effects of asymmetric arrangement were studied experimentally, as well as theoretically, by Exner and Petzow [Exn73, Pet76], by means of the three particle model (Fig. 1.16). That model showed that during sintering angle between particles changes. An experiment carried out on a three particle model made up of uniformly sized 50  $\mu\text{m}$  copper spheres, showed that the angle is changed of the order of several degrees [Pet76, Exn79]. Presently, there is no quantitative treatment available for the dependence of the angle of rotation as a function of sintering conditions and initial angle.

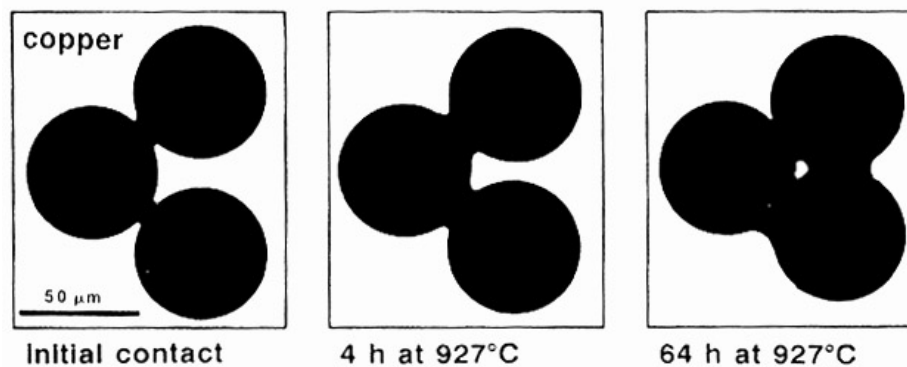


**Fig. 1.16** Evidence of particle rotation and delayed new contact formation during neck growth during the sintering of copper spheres at 927 °C for times up to 64h [Pet76].

In addition to the rearrangement caused by asymmetric neck growth, internal forces can be created by different shrinkage rate of different necks [Mit77, Jon86, Eva82, Hsu86]. A neck with smaller curvature will tend to grow faster and the particle centers will tend to draw nearer than those of particles with larger necks in between. Higher stresses exhibited by the large curvature of small necks induce an additional compressive force and a torsional stress situation in the grain boundary (GB) of larger necks. In real powder compacts, this situation will occur quite frequently due to the following four effects: 1) constraints from network formation, 2) difference in particle size, 3) difference in grain boundary structure, and 4) formation of contacts during sintering. The effects of particle shape and anisotropic surface energy will vary statistically in a powder compact.

## 2. EXPERIMENTAL PROCEDURE

### 2.1 Tungsten bimodal granular media preparation

For this study two W powders with a particle sizes 1-5 $\mu$ m (powder P1) and 45-75 $\mu$ m (powder P2) have been selected. All elemental material used in this work is purchased from Alfa Aesar. The critical step was to produce W agglomerates of a desired size in order to control the segregation process which is induced by vertical vibration. For that purpose polyvinylbutiral (BM18, with molecular weight 135 000-140 000) has been used as binder and iso-propylalcohol as solvent, and they were mixed with the W powders to produce agglomerate cakes. The obtained agglomerate cakes were further crushed in an agate mortar. After carefully sieving of the crushed material two agglomerate fractions have been obtained: agglomerates A1 with agglomerate size 40-60 $\mu$ m from powder P1, and agglomerates A2 with agglomerate size 200-250 $\mu$ m from powder P2. Bimodal W GM has been composed from the same weight of the elemental monomodal agglomerates A1 and A2. The homogeneous mixture (A1+A2) used for the sintering study, was obtained by mixing of equal weights of the elemental powders in a rotary mill for 24 h. Mixing has been conducted in a way that 1/3 of the container volume was filled with the powder.

### 2.2 Vibrational compaction

Agglomerate assemblies (A1 and A2) with equal weights ( $m \sim 1.7$ g) have been placed in stainless steel die, with polished walls in order to minimize friction forces coming from particle-wall interactions, and have then been subjected to vertical vibration in an electromagnetic shaker Tira Vib52120. The shaker was vertically driven by sinusoidal signals generated by a Labwork SC121 oscillator and a Tira 19/7 power amplifier. The relevant characteristics of the shaker are :

Sinusoidal force	- 200 N
Frequency range	- 2-7000 Hz
Max. displacement	- 15 mm
Max. acceleration	- 100g (g – gravitational acceleration)
Max. velocity	- 1,5 m/s
Weight of experimental sample	- 200 g

Vibrational frequency and acceleration have been controlled through PCD a (power control device) accelerometer. This piezoelectric sensor was placed on the plate. Principally, the accelerometer generates an electrical output signal that is proportional to an induced force. The measurement signal from the sensor is then fed into a vibration controller, which adjusts the input

## 2. EXPERIMENTAL PART

parameters that drive the shaker. This is known as a closed-loop feed back control system. The vibro-compaction process has been monitored through a change of GM bed height. For that purpose, a laser emitter based on triangulation method with a spot of  $70\ \mu\text{m}$  and a linear image sensor (CCD-like array), which enables a high speed measurement with  $100\ \mu\text{sec}$  sampling, was applied. The linear image sensing method measures the peak position values for the light spots and suppress the perturbation of secondary peaks, which makes possible a resolution of  $1\ \mu\text{m}$ . The experimental set up was placed in a closed chamber and connected to the vibrational plate. The humidity in the chamber was controlled by a humidity generator with a Peltier element. A schematic of the experimental set up and its real appearance are shown in Fig. 2.1.

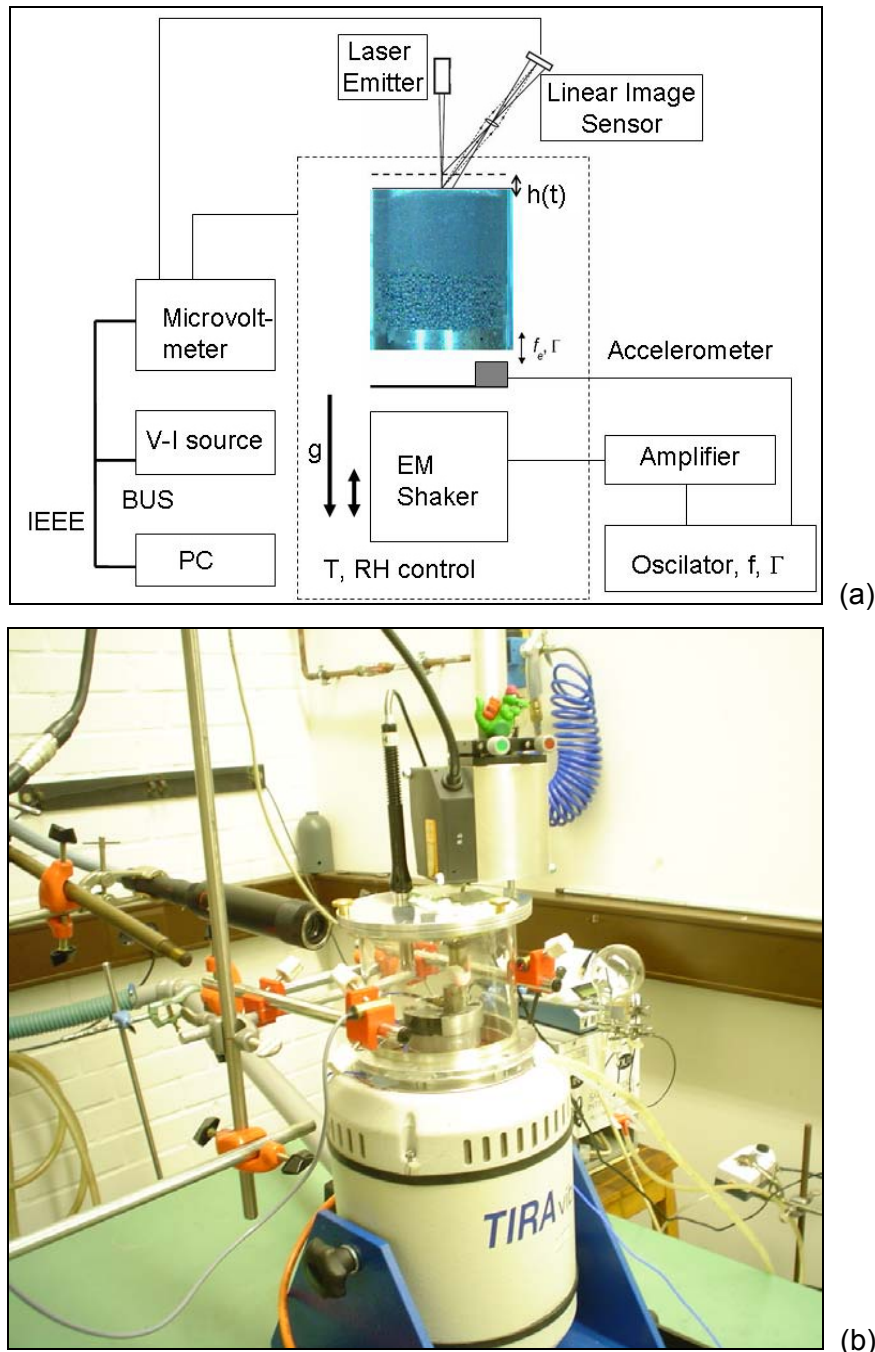


**Fig. 2.1** Schematic illustration (a) and real appearance of the experimental set up (b).

## 2. EXPERIMENTAL PART

The compaction behavior of weakly excited bimodal W GM (A1+A2) used for production of Cu-W FGMs, was investigated at a frequency of 600 Hz, with an acceleration of 6g, at room temperature (20-24 °C), and under a absolute ambient humidity from 6 to 10 g/m<sup>3</sup>.

### 2.2.1 Principles of electrodynamic shaker performance

An electrodynamic shaker resembles, in its structure, a common loudspeaker, but is heavier and far more robust. The shaker devices, if they are used within their specified force and motion limits, are quite linear in their behavior. Fig. 2.2 depicts the structure of the shaker device.

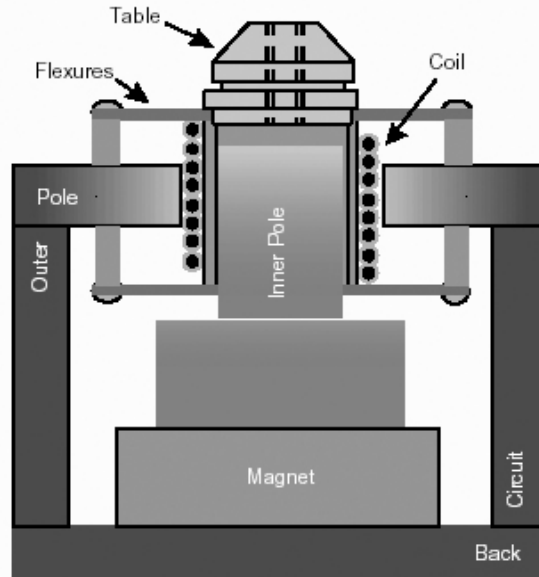


Fig. 2.2 Schematic view of the electromagnetic shaker.

In the central part of the shaker is a coil of wire, suspended in a fixed radial magnetic field. When current is passed through the coil, an axial force is produced. A permeable (ferrous) inner pole piece transmits flux from one end of an axially magnetized permanent magnet (the north face). A permeable “back structure” conducts flux from the opposite pole of the magnet to a permeable disk with a hole in its center, surrounding the inner pole piece. In this manner, a radial flux field, in the air gap between the round face of the north-polarized inner pole and the round hole in the south-polarized outer pole piece, is created. The force provided by the device is proportional to the magnetic flux passing through the coil (B), to the current flowing through the coil (I) and to the length of the wire (L), as described by Eq. 2.1.

$$F = I \cdot L \times B \dots\dots\dots(2.1)$$

## 2. EXPERIMENTAL PART

---

The coil, coil form, and table structure combination is called the armature assembly. The test object is rigidly mounted to the armature assembly. The armature must be accurately centered in the narrow gap between the inner and outer poles. In that way the coil is allowed to move axially while being restrained from all other motions.

### 2.3. Cold pressing

The next step in the FGM processing route is cold pressing of vibrated agglomerates A1 and A2. Uniaxial cold compacting at a pressure of 40 bar for 2 minutes has been conducted and cylindrical compacts with diameter  $\varnothing$  8 mm and  $\varnothing$  10 mm have been produced.

### 2.4. Thermal treatment

A two step thermal treatment has been employed in order to produce a W porous preform:

1) Firstly, samples were heated to 1373 K at a very slow heating rate (0.45 K/min) in a dynamic nitrogen atmosphere in order to eliminate the binder, which burns up at 723 K. The nitrogen used was of technical quality with a purity of 99.8 Vol.%. A low content of oxygen in applied atmosphere prompt oxidation of the binder polymer.

2) The second step is sintering, conducted in a dilatometer in order to the study kinetics of sintering. Two different dilatometers were used in this study. The horizontal type (Bähr DL-803), with a maximal temperature of 1773 K, and vertical type (Linsys), with the maximal temperature of 1973 K. The experiments were carried out in a dynamic atmosphere of gas mixture containing 5 Vol. %  $H_2$ +95 Vol. %  $N_2$  (density =0.88 kg/m<sup>3</sup> and  $O_2$  concentration was lower than 20 ppm). The temperature program was controlled using a thermocouple (Pt/Rh-10Pt, Type S) located next to the sample. The sample dilatation was measured via a linear variable displacement transducer (LVDT). The operating principle of LVDT is that during sintering the sample length change causes the LVDT core to move and an output signal proportional to the displacement is recorded. High temperature sintering of the W preforms was carried out in a furnace with a W heating element with a maximal working temperature of 2373 K.

### 2.5 Infiltration

After sintering, a rigid and porous W skeleton was obtained, which would subsequently be infiltrated with molten Cu of high purity (oxygen free). The infiltration was conducted in two

## 2. EXPERIMENTAL PART

---

steps under a dynamic reduction atmosphere (5 Vol. % H<sub>2</sub>+95 Vol. % N<sub>2</sub>) at 1523 K for 3 h. At first, samples were heated to 1123 K at a heating rate of 4 K/min for 1 h. In that way the reduction of W<sub>3</sub>O<sub>2</sub> could take place. Later, heating continued to 1523K at a heating rate of 8 K/min followed by a 3h hold.

### 2.6 Characterization techniques

The W-W granular media was characterized by measurements of density and flow behavior (apparent density, flow rate and angle of repose). Microstructures of the produced material (W porous preform as well as the final Cu-W FGM) were studied using light microscopy (LM) and scanning electron microscopy (SEM). Quantitative Image Analysis was applied in order to determine microstructural parameters like phase content, porosity, particle size and pore size. Finally, properties of the produced Cu-W materials were characterized through measurements of electrical resistivity and E- modulus.

#### 2.6.1 Density measurement and flow behavior of tungsten granular media

The density of the powder was determined via a Helium pycnometer (Quantachrome Corp. Ultrapycnometer 1000, Vers. 2.2). The volume was averaged from 10 measurements with a method accuracy of 1%. Apparent density and flow rate were measured by an adapted Hall flowmeter. The flow rate is expressed as the time needed for a 25 g of powder to flow through the Hall flowmeter with a funnel with upper diameter 5 cm and lower diameter 8 mm. The precision falls between 1- 5%. The angle of repose ( $\alpha$ ), calculated as an average value of 10 measurements, was determined from the ratio of height (h) to radius (d) of a powder pile ( $\tan \alpha=h/d$ ) passed through the funnel. Density of samples was determined by the Archimedes immersing method where the sample was immersed in diethylphtalate (C<sub>12</sub>H<sub>14</sub>O<sub>4</sub>, Merck-Schuchardt, 99%,  $\rho =1.118 \text{ g/cm}^3$ ) for 24h.

#### 2.6.2 Light microscopy and image analysis

Light microscopy, performed with an Olympus BX 50 light microscope with magnification from 50 to 1000 times, in a bright field imaging technique was used as a first step to characterize the microstructure. Samples were prepared by moulding, followed by progressive mechanical grinding and polishing on SiC paper and diamond polishing paste. Image C software was used to analyze and quantify the microstructure. Contiguity was calculated taking at least 100 randomly chosen intercept lines. Concentration profile was

## 2. EXPERIMENTAL PART

---

also evaluated by the custom made image analysis software Agglomerado [Las03] in order to follow the temporal evolution of segregation and corresponding change in microstructure.

### 2.6.3 Scanning electron microscopy

Specimens were also studied using a CamScan FE (Field Emission gun) scanning electron microscope, operating between 5 and 25 kV. Secondary electron (SE) imaging mode for topography and powder morphology studies, was used to characterize the microstructural features.

### 2.6.4 Electrical resistivity measurement

Electrical resistivity was determined by a four-probe test method in the temperature range from 293 to 973 K in a dynamic N<sub>2</sub> atmosphere. The measurements were taken using direct current (DC). The contact points were prepared by adhesion with a thin layer of high conductivity silver paste. The temperature was controlled using a thermocouple located next to the sample (Pt/Rh-10Pt, Typ S). A schematic view of the measurement is shown in Fig. 2.3.

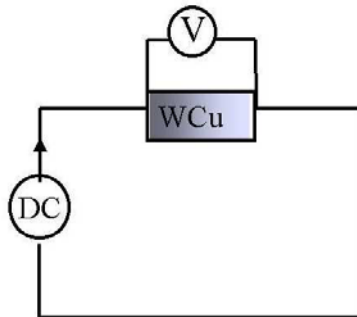


**Fig. 2.3** Schematic view of four-probe test method

The samples had final cross section dimensions of 0,5 x 2,1 mm<sup>2</sup>, and a length of 8,5 mm. In order to improve the contact points on the polished W rich sample side, a thin layer (~200µm) of W was deposited by physical vapor deposition (PVD) technique.

### 2.6.5 Elastic modulus measurement

Pulse echo ultrasonic test was conducted for the E-modulus determination. Experiments carried out at a frequency of 5 MHz. A piezoelectric quartz plate transducer, following the method, was placed on one face of the specimen with the plane parallel faces normal to the ultrasonic wave propagation direction. The quartz plate was bonded adhesively to the

## 2. EXPERIMENTAL PART

---

sample through a thin layer of honey. A position dependant elastic constant was investigated through the B-scan method. By moving the transducer along the sample surface, it was possible to evaluate a large number of single measurements (“shots”). The measurement was conducted in water as a medium and at 80 MHz.

Finally, ultrasonic wave velocities in longitudinal and transversal directions, elasticity (E), shear (G) and bulk (K) module and Poisson’s coefficient ( $\nu$ ) were calculated according to the following relations [Fle89]:

$$G = \rho \cdot C_{\text{trans}}^2 \dots\dots\dots(2.2)$$

$$K = \rho \cdot (C_{\text{long}}^2 - 4 \cdot C_{\text{trans}}^2 / 3) \dots\dots\dots(2.3)$$

$$\nu = \frac{1}{2} [1 - 2 \cdot (C_{\text{trans}} / C_{\text{long}})^2] / [1 - (C_{\text{trans}} / C_{\text{long}})^2] \dots\dots\dots(2.4)$$

$$E = 9KG / (3K+G) \dots\dots\dots(2.5)$$

where  $C_{\text{long}}$  and  $C_{\text{trans}}$  are acoustic wave velocities in longitudinal and transversal directions.

## 3. RESULTS

### 3.1 Characteristics of tungsten granular media

Tungsten GM have been investigated by means of morphology, flow characteristics, compaction dynamics and relaxation law studies. When polymodal GM is subjected to vibration, size segregation occurs and leads to demixing of GM. Depending on vibration intensity and obtained packing density of vibrated GM, different regimes of compaction occur, which are manifested by diverse interior packing structures.

#### 3.1.1 Powder morphology

Granular media investigated in this work is composed of bimodal W agglomerates A1 and A2. Agglomerates A1 have a size of 40-60 $\mu\text{m}$  and they are composed of powder P1 with an initial particle size of 1-5 $\mu\text{m}$ . On the other side agglomerates A2 have a size of 200-250  $\mu\text{m}$  and they are composed of powder P2 with a initial particle size 45-70  $\mu\text{m}$ . Morphology of the W powders and their agglomerates is shown on SEM micrographs (Figs. 3.1a-f). Powder P1 is individually grown with a mixture of nearly spherical and cubic particles (Fig. 3.1a). The morphology of powder P1 can be attributed to a W powder production route ( $\text{H}_2$  reduction of W-oxides), characterized by lower reduction temperatures (600-800 $^\circ\text{C}$ ) and lower dew points [Las98]. Through adhesion with polymer, well bonded aggregates of uniform size and shape have been obtained (Agglomerates A1, Figs. 3.1c and e). Powder P2 is composed of well-faceted W crystals welded together into strings of elementary particles showing a tendency for crystal intergrowth (Fig. 3.1b). The higher reduction temperatures ( $\sim 1000$   $^\circ\text{C}$ ) and high dew point facilitate a production of larger particle sizes (up to 100 $\mu\text{m}$ )[Las96]. The adhesion between polymer and P2 particles is not as effective as in the case of powder P1. The agglomerates A2 exhibit a non uniform sponge - like structure (Fig.3.1d and f).

#### 3.1.2 Flow rate, apparent density and angle of repose

In addition to powder and agglomerate morphology, flow rate, apparent density and angle of repose have also been studied. These characteristics, as a measure of the friction forces, determine the packing and the flow behaviour of W GM.

##### Flow rate

Flow time depends, in a complex manner, on the internal friction between particles and the friction between particles and funnel walls. For this reason, the test method used (modified Halls flow-meter) is applicable to comparative characteristics of free flowing powders. The

### 3. RESULTS

flow characteristics and the particle / agglomerate densities are shown in Tab 3.1. It can be seen that the flow behaviour is dominantly influenced by particle size. The highest flow rate is observed for agglomerates A2, with the largest particle size, and the lowest flow rate is seen in the initial powder P1.

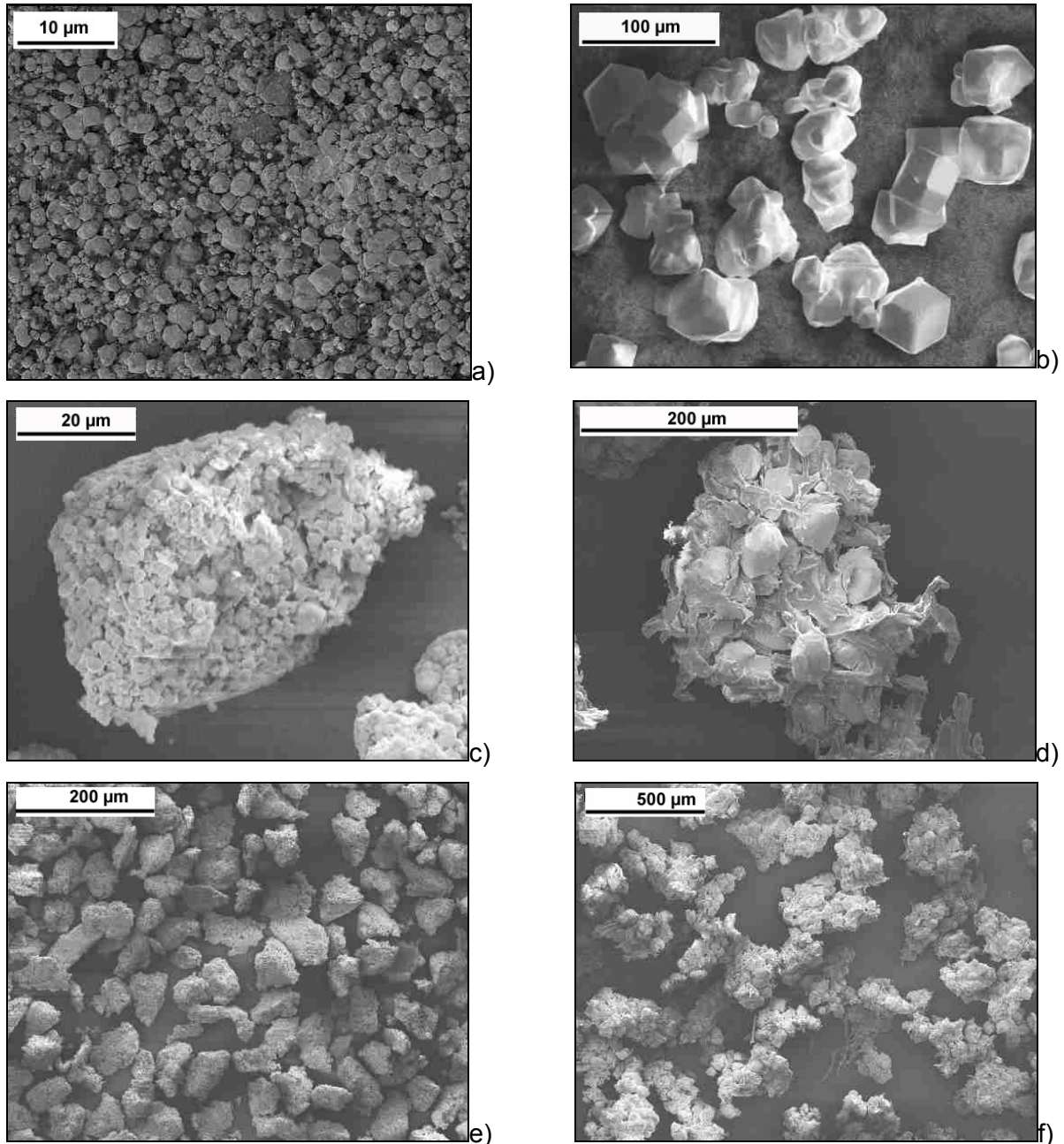


**Fig. 3.1** SEM micrographs of: a) powder P1 (1-5μm), b) powder P2 (45-70 μm), c) single agglomerate A1 composed of powder P1, d) single agglomerate A2 composed of powder P2, e) group of agglomerates A1, and f) group of agglomerates A2.

#### Apparent density

Another indicator of interparticle friction forces is apparent density, i.e. density in loose state without agitation. Tab 3.1 presents the results of the apparent density measurements for two

### 3. RESULTS

different ambient relative humidities (Hr), i.e, 25% and 16 % at room temperature (295 K). The apparent density mainly increases as particle size increases. The measurement of the apparent density appears to be very sensitive to the variation of the ambient humidity. Apparent density mainly decreases as ambient humidity decreases. The strongest dependence was obtained for agglomerates A2.

**Table 3.1** Densities and flow characteristics of powders (P1 and P2) and their agglomerates (A1 and A2) at two different ambient relative humidities (Hr) at a temperature of T=22 °C.

Powders / Agglomerates	Pycnometer density [g/cm <sup>3</sup> ]	Apparent density [g/cm <sup>3</sup> ] Hr = 25%	Apparent density [g/cm <sup>3</sup> ] Hr = 16%	Flow rate [g/s] Hr = 25%
Powder P1 (1-5µm)	19.21	4.75	3.45	3.43
Powder P2 (45-75µm )	19.06	8.54	8.5	4.8
Agglomerates A1 45-60µm (Powder P1)	13.19	4.26	4.41	4.8
Agglomerates A2 200-250µm (Powder P2)	16.92	6.12	3.51	7.38

#### Angle of repose

Figure 3.2 shows the angle of repose as a function of particle / agglomerate size. It is evident that the angle of repose decreases as particle size increases. A large experimental error in the case of agglomerates A2 has been observed. For these agglomerates the upper and lower values of the measured angle of repose were 27.28° and 9.90°, respectively.

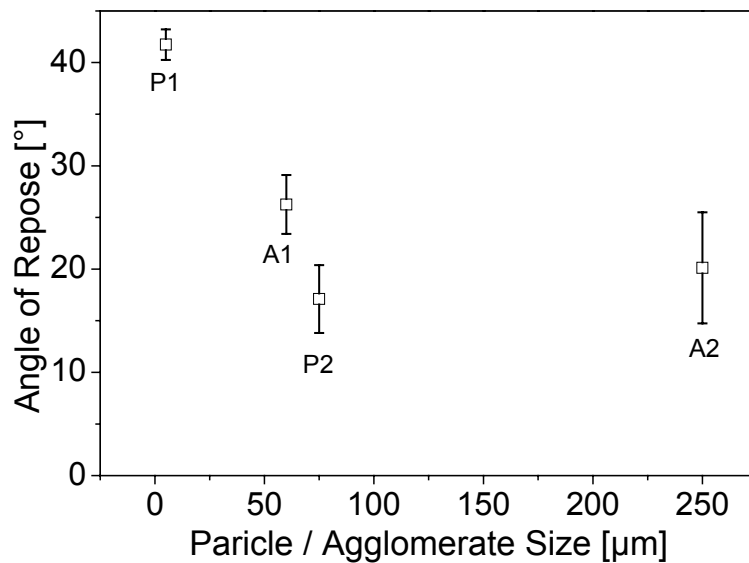


**Fig. 3.2** Dependence of the angle of repose on particle size of W powders (P1 and P2) and their agglomerates (A1 and A2).

**3.2. Compaction dynamics of tungsten granular media**

Compaction dynamics of GM are dominantly controlled by the excitation level. Depending on the intensity of excitation, different regimes of compaction are active, and compaction process can be finished by total or by partial segregation. In this work, compaction dynamics and the accompanying size segregation phenomenon in W-W GM have been investigated. It was observed that weakly excited GMs segregate in the manner that a gradient in a packing was self formed.

*3.2.1 Relaxation behaviour of weakly excited tungsten granular media*

The particle packing fraction  $\rho(t)$  of the studied bimodal W GM was estimated with Eq. (3.1)

$$\rho(t) \sim 1 / l(t) \dots\dots\dots (3.1)$$

where  $l(t)$  is the time dependant bed height.

According to macroscopic observation of the initial bed height, it was assumed that a reasonable approximation of the initial particle packing fraction is 0.22. Table 3.2. shows the packing fraction limits calculated under the experimental conditions used in the current study and theoretical limits for a bimodal spherical system with a large difference in particle sizes [Ger89]. The random close and random loose packing limits of studied W GM are attributed to the initial and final packing densities by analogy to theoretical approach.

**Table 3.2.** Random loose ( $\rho_{RLP}$ ) and random close ( $\rho_{RCP}$ ) packing limits for spherical and for studied W-agglomerate systems.

System	$\rho_{RLP}$ initial	$\rho_{RCP}$ final	$\rho_{RCP} / \rho_{RLP}$
Bimodal spherical system with a large difference in particle sizes - theoretical values	0.55	0.87	1.57
Irregular W agglomerates - experimental values	0.22	0.35	1.59

The results on compaction of the weakly excited bimodal W granular media (frequency  $\nu = 600\text{Hz}$  and acceleration,  $a = 6g$ ), i.e. agglomerates with irregular shapes and narrow size distribution, are shown in Fig. 3.3. Both linear (Fig. 3.3a) and logarithmic scales of time (Fig. 3.3b) are plotted for a better insight and three different stages can be observed. The first stage (percolation stage) corresponds to a rapid process of compaction ( $t \sim 2000s$ ). The

### 3. RESULTS

second stage (intermediate stage) is characterized by a slow dynamic and later on by density fluctuations ( $t \sim 6500s$ ). The final stage (geometrical reorganisation / geometrical segregation) corresponds to non equilibrium steady state behaviour ( $t \sim 7200s$ ).

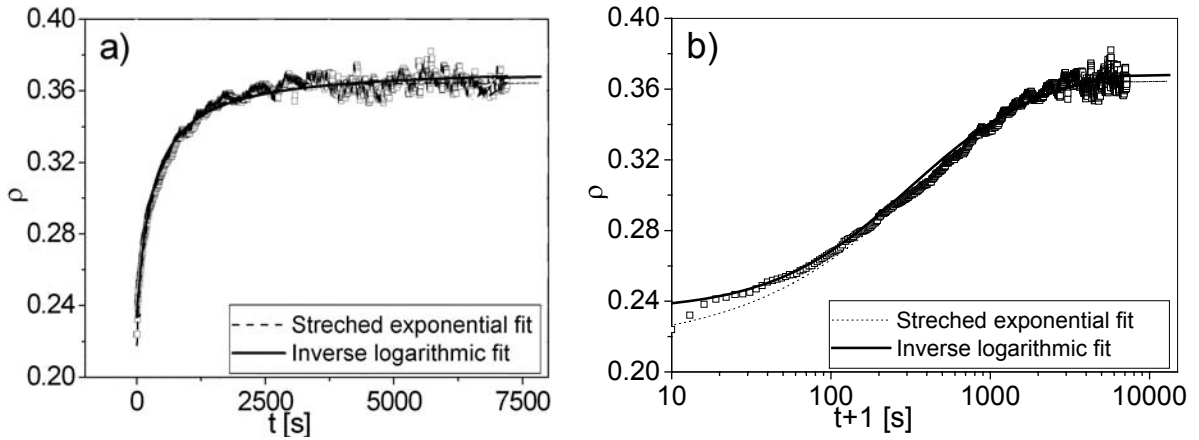


**Fig. 3.3.** Evolution of the bimodal W-W GM packing fraction ( $\rho$ ) as a function of vibration time. Vibration time is presented in: linear (a) and logarithmic scale (b). The solid line is the inverse logarithmic fit (Chicago fit) (Eq. 3.2) and the dashed line is the stretched exponential fit (Eq.3.3). The sample has been vibrated at frequency,  $\nu = 600\text{Hz}$  and acceleration,  $a = 6g$ .

The experimental results on  $W$  granular media are fitted with two relaxation laws according to two approaches from compaction dynamics studies. In one approach suggested by Knight et al. [Kni95], the relaxation behaviour of 2 mm glass GM could be well predicted by the inverse-logarithmic law (so-called Chicago fit) shown in Eq. 3.2:

$$\rho(t) = \rho_f - \frac{\rho_o - \rho_f}{1+B \ln(1+t/\tau)} \quad \dots\dots\dots(3.2)$$

The four fitting parameters in Eq. 3.2 are:

- $\rho_f$  - the final packing fraction
- $\rho_o$  - the initial packing fraction
- $\tau$  - the characteristic time
- $B$  - the fitting parameter

The only control parameter for the dynamic has been found to be the ratio  $\Gamma = a/g$ .

In another approach, Philipp et al. [Phi02, Phi03] proposed that relaxation behavior can be well described by the Kohlrausch-Williams-Watts law (KWW's law) – the stretched exponential law, defined by Eq. (3.3).

### 3. RESULTS

$$\rho(t) = \rho_f - (\rho_f - \rho_o) \exp [-(t/\tau)^\beta] \dots\dots\dots(3.3)$$

Adjustable parameters  $\tau$ ,  $\beta$  correspond to the relaxation time and the stretching of the exponential, respectively, another fitting parameters are the same as defined in Eq. 3.2.

After fittings with both mentioned laws it was observed that the KWW's law fits experimental results well. On the contrary, Knight's model predicts slow increase of density with time even when the steady state was clearly observed.

#### 3.2.1.1 Effect of ambient humidity on compaction dynamics

The results concerning the effect of ambient humidity on tungsten GM relaxation behavior are given in Fig. 3.4. Figure 3.4 plots density relaxation as a function of vibration time for three different values of relative ambient humidities: Hr = 28, 34, 40 - 45 % at 293 - 295K that corresponds to an absolute humidities Ha = (6.1 – 6.4); (7 - 7.4); (8 - 10g/m<sup>3</sup>) respectively. Compaction under the lower relative humidities (28 and 34 %) was faster and, as judged by the density decrease, total segregation is reached. For these samples fitting by the KWW's law gave values for  $\tau \sim 100$  s and  $\tau \sim 400$  s, respectively. These times indicate much higher compaction rates than that under higher humidity condition (40 - 45 %) for which  $\tau \sim 2000$  s.

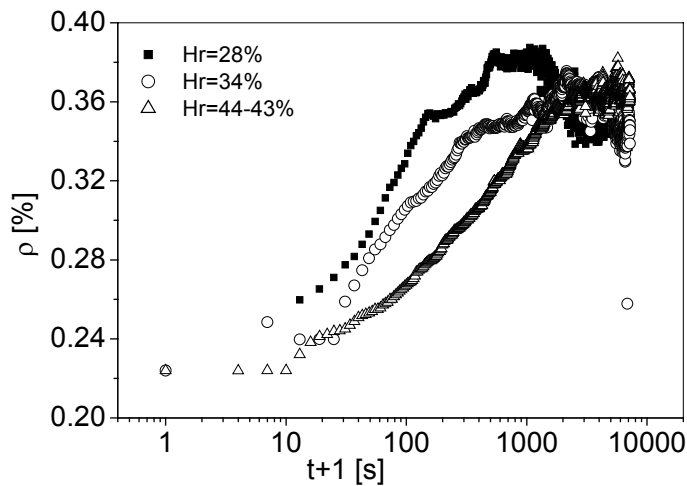


**Fig. 3.4** Density relaxation of bimodal W-W GM vibrated at frequency,  $\nu = 600\text{Hz}$  and acceleration,  $a = 6g$ , under different ambient humidity (Hr) at room temperature (20-22 °C).

#### 3.2.2 Geometrical segregation

Size segregation is a specific case of vibro-compaction of polymodal GM. Geometrical segregation was observed in a weakly excited W GM (frequency of 600 Hz and acceleration 6g) and a steady state with a graded packing (Fig.3.3a) could be formed. This steady has been characterised by an improvement in the packing density and the maximal packing density of disordered structure has been obtained (the random close packing limit -  $\rho_{RCp}$ ). In this regime the surface of weakly excited W GM remains flat and no surface instabilities has been observed. The geometrical segregation has been followed through the investigation of structures formed during vibration which are afterwards sintered and infiltrated with molten Cu.

##### 3.2.2.1 Microstructural characteristics of geometrical segregation regime

The temporal evolution of W skeletons sintered at 1723 K, for 3h, and subsequently infiltrated by molten Cu at 1523 K are shown in Fig. 3.5. The left hand side in the microstructural pictures shows the bottom of container, where larger agglomerates were initially placed. Corresponding concentration profiles have been presented in the right hand side (Fig. 3.5 b, d, f, and h). The microstructure and concentration profile after 40 min. of vibration are shown in Fig. 3.5 (a, b). Observed structure corresponds to the percolation stage. The end of the percolation and start of the intermediate stage (after 60 min of vibration time) is presented in Fig. 3.5 (c, d). It is evident that smaller particles are interconnected and located in the whole container volume (Fig. 3.6a). Smaller agglomerates spread on the whole cross section, and the position change of larger agglomerates is observed. After 100 min. the layer of smaller agglomerates at the bottom of container is formed while in the upper layer larger agglomerates are interconnected in form of a skeleton structure (Fig. 3.6 b). Finally, after 120 min. of vibration the skeleton structure turns into the more complex graded structure. Under experimental condition applied, observed microstructural evolution shows the possibility of self-formation of the graded packing (later graded structure) in a controlled manner.

### 3. RESULTS

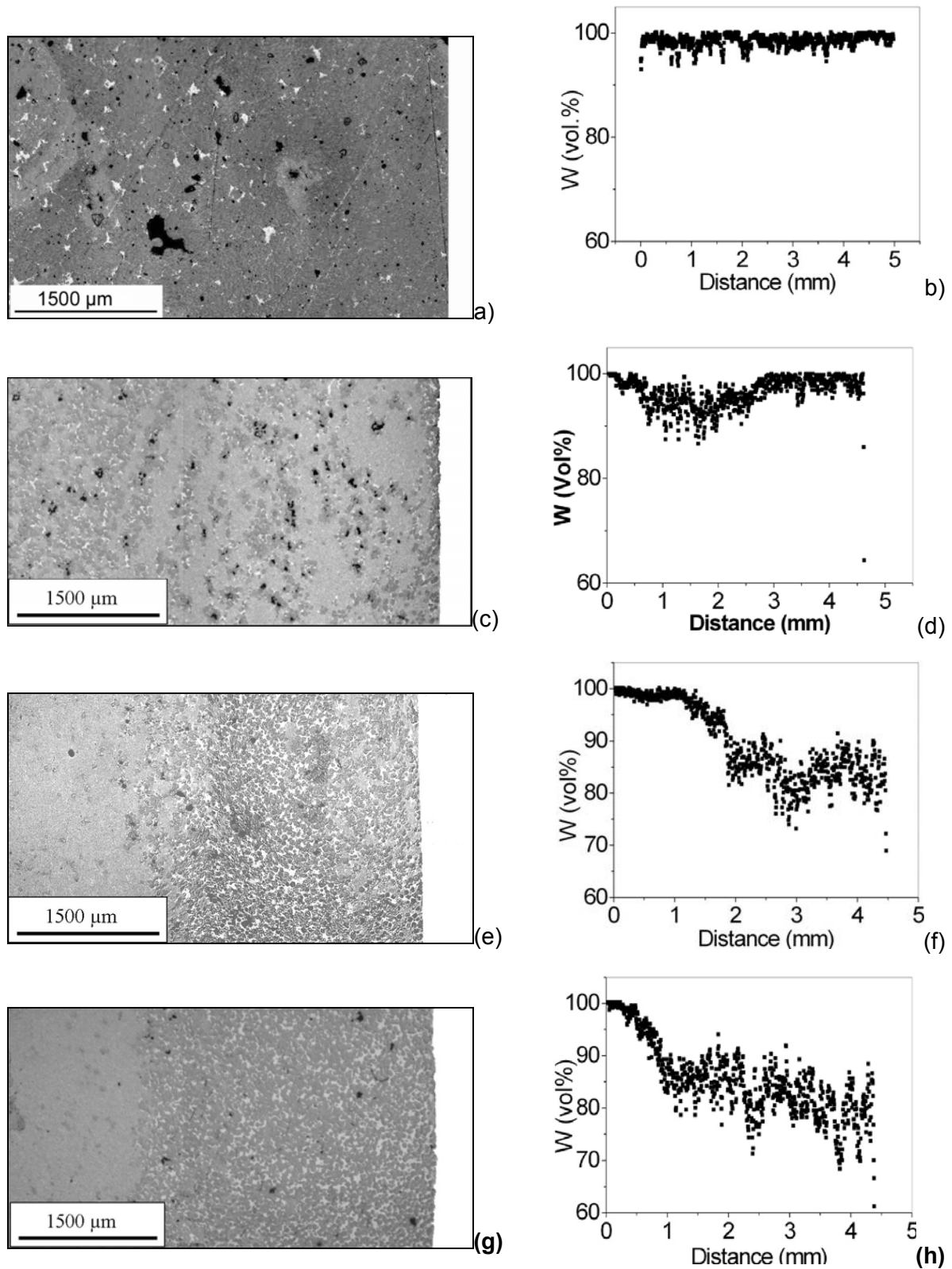


**Fig 3.5** Temporal evolution of microstructure of self-formed W structures vibrated, for: a) 40 min., b) 60 min., c) 100 min., d) 120 min., at 600 Hz, 6 g, and under an absolute humidity from 8 to 10  $\text{g}/\text{m}^3$ . Corresponding concentration profiles are presented on the right hand side (b, d, f, and h respectively). Microstructures represent W performs (at about 5mm in length) sintered at 1723 K for 3 h and subsequently infiltrated by Cu.

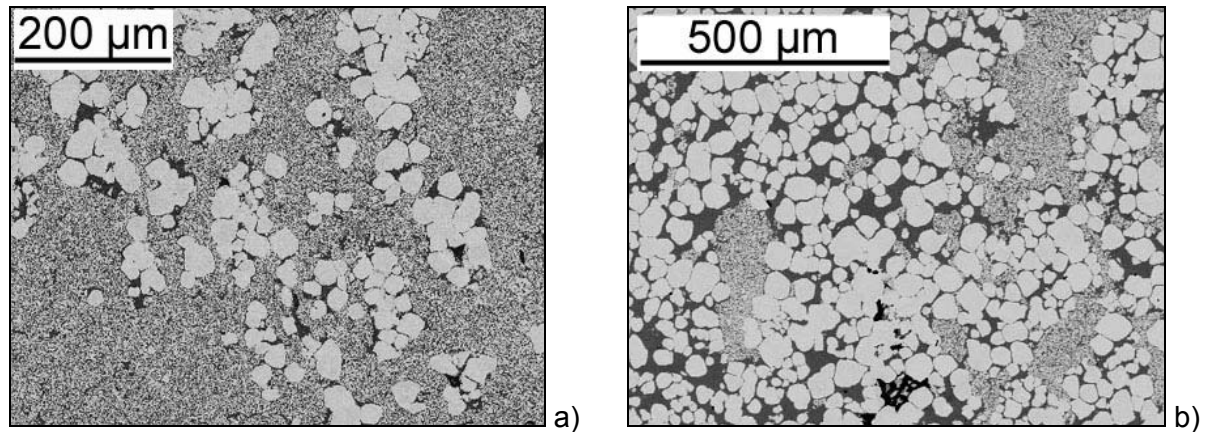


**Fig. 3.6** Local microstructure with: (a) skeleton of smaller agglomerates formed in the percolation stage (after 60 min of vibration) and (b) skeleton of larger agglomerates formed in the intermediate stage (after 100 min of vibration).

### 3.3 Sintering of tungsten granular media

Sintering of monomodal W agglomerates has been firstly considered. Tungsten preforms composed from monomodal agglomerates A1 and A2 have shown a non uniform and complex sintering behaviour, mainly influenced by agglomerate sizes and agglomerate structures. The effect of agglomerate size on sintering kinetics has been additionally analysed through the sintering of fine agglomerates A0 composed from powder P1. The related results are discussed in section 4.3.3. Furthermore, the sintering studies of various W preforms (skeleton and graded structure) obtained during vibration of the bimodal W GM (agglomerates A1 + A2) were carried out. It was observed that sintering is non uniform and strongly related to the spatial agglomerate distributions. Additionally, sintering of homogeneous mixture composed of agglomerates A1 and A2 has been studied, and similarity with the sintering behaviour of graded structure has been observed. The sintering kinetics of various W preforms has been studied by applying the Young and Cutler's model for grain boundary diffusion (GBD) in the initial stage of sintering and the apparent activation energies have been calculated. Simultaneously with GBD a particle rearrangement process is operative. The rearrangement process is influenced by asymmetry of contact points and non uniform sintering rates predominantly caused by agglomerate structures and global bimodal GM structures. The internal stresses, induced in that way, cause particles to rearrange themselves. Kingery's model for rearrangement in liquid phase sintering (LPS) has been applied as the first approximation in order to follow sintering kinetics of the rearrangement process in solid state sintering. Such spatial-reorganizations in the solid state sintering of W GM can be additionally described through a viscose flow of surrounding less dense regions and by a densification provided by diffusional creep.

### 3. RESULTS

#### 3.3.1. Sintering kinetics of small monomodal tungsten agglomerates

The results of two characteristic dilatometric runs of small monomodal W agglomerates (A1) are presented in Fig. 3.7. The agglomerate preparation route, ambient humidities, and the way of filling the die prior to vibration, are some factors that distinguish one sample from the other. Figure 3.7a shows the relation shrinkage vs. temperature, while the shrinkage rate vs. temperature, is presented in Fig. 3.7b. Dilatometric runs have been conducted up to final temperatures 1870 K and 1970 K. The sintering curves reveal the existence of two densification processes, visualised through densification peaks (Fig 3.7b). The first peak occurs at lower temperature (between 1390-1800 K). The new process occurs at temperature above 1800 K. In order to study the low temperature sintering kinetics of tungsten, the Young and Cutler's model for grain boundary diffusion (GBD) in the initial stage has been applied (Eq.3.4 through 3.6).

$$(\Delta L / L_0)^{2.06} d (\Delta L / L_0) / dt = 0.7\gamma\Omega bD_B / kTa^4 \dots\dots\dots(3.4)$$

For sintering with constant heating rates (CHR) equation (3.4) modifies ( $T=c \cdot t$ ) to

$$T(\Delta L / L_0)^{2.06} d (\Delta L / L_0) / dT = 0.7\gamma\Omega bD_B / kca^4 \dots\dots\dots(3.5)$$

where:

- |                      |  |
|----------------------|--|
| $\Delta L = L_0 - L$ | - the change in length of the specimen   |
| $L_0$                | - the initial length of the specimen   |
| $\gamma$             | - the surface energy   |
| $\Omega$             | - the vacancy volume   |
| $bD_B$               | - the grain-boundary diffusion coefficient<br>( $b$ is the effective grain-boundary width) |
| $k$                  | - the Boltzmann constant   |
| $T$                  | - absolute temperature   |
| $A$                  | - the radius of the particles in the specimen  |
| $t$                  | - the sintering time   |
| $a$                  | - the radius of the particles  |
| $c$                  | - the heating rate used for the dilatometric run   |

The absolute shrinkage value  $(\Delta L / L_0)$  is defined as a positive value  $\Delta L / L_0 = [L_0 - L(T)] / L_0$ , where  $L_0$  is the initial height of the pallet and  $L(T)$  is the instantaneous height of the sample at temperature  $T$ . The rate of linear shrinkage is given by  $d(\Delta L / L_0) / dT$ . The parameter  $D_B$  is exponentially dependent on temperature and is defined by Eq.3.6,

$$D_B = D_0 \exp^{-E_a/RT} \dots\dots\dots(3.6)$$

### 3. RESULTS

where:  $D_0$  is the pre-exponential factor,  $E_a$  is the activation energy, and  $R$  is the universal gas constant.

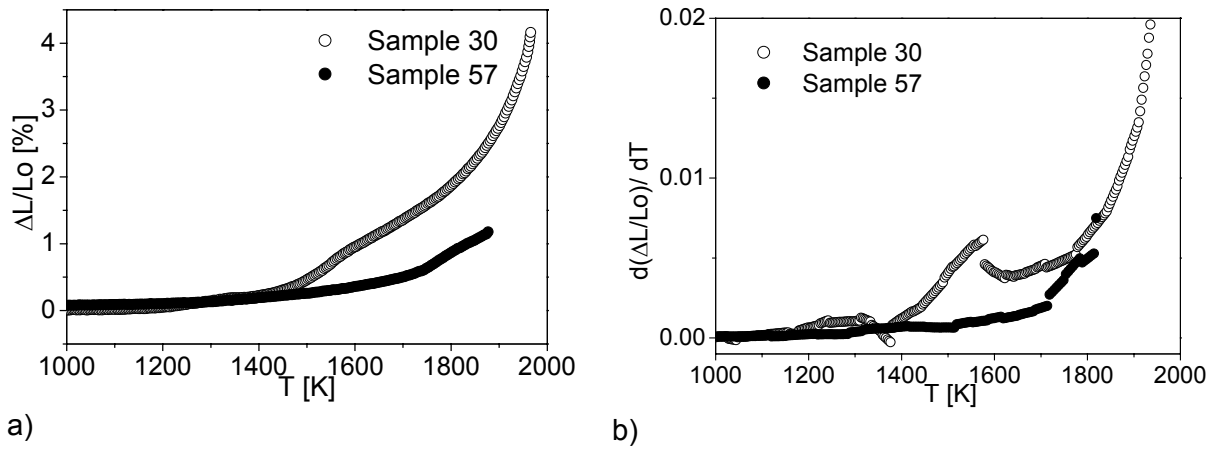


**Fig. 3.7** Dilatometric studies of agglomerates A1 (45-60µm) represented by: (a) shrinkage and (b) shrinkage rate as a function of temperature.

The experimental data are plotted according to Eq. (3.5) as  $\ln[ T \Delta L/Lo]^{2.06} d(\Delta L/Lo)/dT$  vs.  $1/T$ , and from the slope of the plot an apparent activation energy is calculated. Fig. 3.8 illustrates the fitting of the experimental data with proposed model, and it has been observed that there are regimes where a linear relationship has been obeyed. In the temperature range from 1400 to 1580 K for sample 30 and in the temperature range from 1700 to 1800 K for the sample 57, the similar activation energies for GBD have been calculated (480 kJ/mol). Above 1850 K and up to 1960 K a process with the higher activation energy of ~ 800 kJ/mol take place (Sample 30).

Additionally to sintering under constant heating rate (CHR), isothermal sintering at 1723K for 3h, has been conducted. For the kinetics study in the isothermal regime, the well known and frequently applied power-law shrinkage relationship dating back to Kingery and Berg [Kin55] has been applied in the form given by Eq. 3.7:

$$\Delta L / Lo = c t^n \dots\dots\dots(3.7)$$

where:

- $\Delta L / Lo$  – the relative linear shrinkage,
- $c, n$  – the constants,
- $t$  – the sintering time.

Depending of operative mass transport the exponent  $n$  has a following value:

$n = 1$  for viscous flow;  $n = 1/3$  for grain boundary diffusion;  $n = 2/5$  for volume diffusion.

### 3. RESULTS

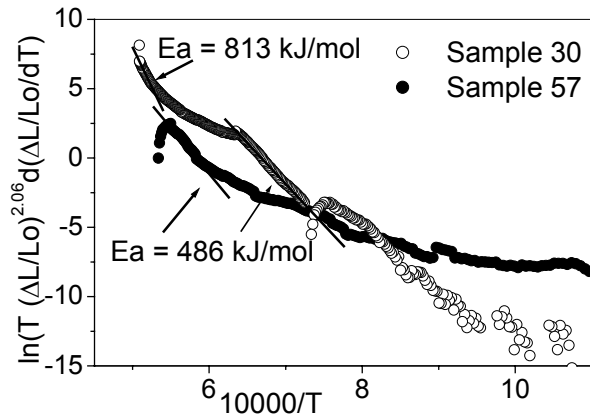


**Fig 3.8** GBD model for initial stage of sintering applied for agglomerates A1 (45-60μm).

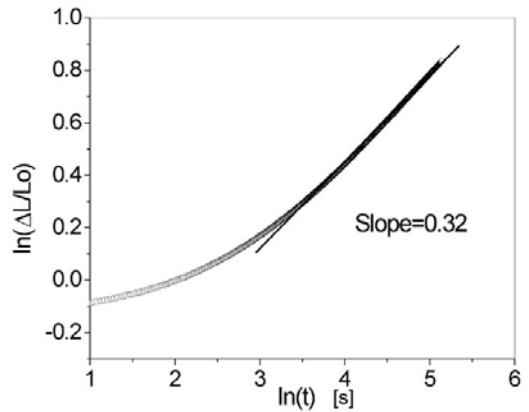


**Fig. 3.9** Power law dependence for sintering of agglomerates A1 (45-60μm) with an 3h isothermal hold at 1723 K.

Linear relationship between shrinkage and time has been detected and the value for power  $n$ ,  $n = 0.32$  has been calculated (Fig. 3.9). Additionally, corresponding microstructure presented in Fig. 3. 12 reveals the evidence of significant sintering signs like necking and particle rounding.

On the other hand there are regions where Young and Cutler’s model does not fit correctly the experimental data (Fig. 3.8). It was assumed that simultaneously to GBD diffusion the rearrangement of particle is operative. As the first approximation in order to model this process, Kingery’s model [Kin59] for rearrangement in liquid phase (Eq.3.8) has been proposed.

$$\ln(d[\Delta l(T) / l_0] / dT) = \ln(\gamma / 2Sc\eta_0) - E_a / RT \dots\dots\dots(3.8)$$

where  $T$  is the absolute temperature,  $\gamma$ - the interfacial energy,  $S$ - the grain radius,  $c$ - the heating rate;  $\eta_0$ -the pre-exponential factor and  $E_a$ - the activation energy for viscous flow [ $\eta = \eta_0 \exp (E_a / RT)$ ], of the assumed liquid phase.

Linear dependence between the logarithm of the shrinkage rate and the inverse temperature ( $1/T(K)$ ) has been obtained (Fig. 3.10), and from the slope an apparent activation energy has been calculated (Tab.3.3). For both characteristic sintering behaviors Kingery’s law, in the wide temperature ranges, fits satisfactory well the experimental data.

**Table 3.3** Apparent activation energy for rearrangement process for agglomerates A1

Sample	Ea (kJ/mol)	T range (K)
57	105	1490-1575
30	100	1610-1705

### 3. RESULTS

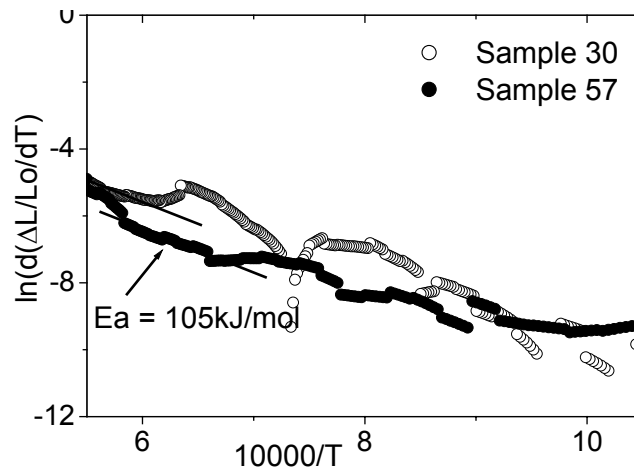


**Fig. 3.10** Kingery's model for liquid phase sintering (LPS) applied for rearrangement process in agglomerates A1 (45-60µm).

#### 3.3.1.1. Microstructural characteristics of sintered small tungsten agglomerates

Table 3.4 summarizes microstructural parameters obtained by image analysis, as well as densities of samples sintered at different temperatures. The microstructure of the sample sintered at 1373 K is presented in Fig. 3.11. It reveals an interconnected porosity network with large pores between the more densified regions (domains). The interior of one agglomerate, sintered at 1723 K for 3h is illustrated in Fig. 3.12. At 1973 K the microstructure changes significantly (Fig. 3.13) with clear signs of sintering within the domains (Fig. 3.13b), in spite of the fact that no important macroscopic densification occurs (Tab. 3.4). Development of microstructure at higher sintering temperature has been investigated and microstructure of samples sintered at 2123 K for 1 h and 3 h, are shown in Fig. 3.14. a. The microstructure of the sample sintered at 2123 K for 1 h, reveals highly dense domains (3.14 a), with smaller inter-domain pores, and still large interagglomerate pores. Significant reduction of inter-domains porosity occurs when sintering continues for 3h at 2123 K (3.14 b), which can be monitored through reduction of number of pores and increase in bulk density (Tab.3.4).

**Table 3.4** Porosity characteristics of W performs sintered at different temperatures obtained by quantitative image analysis.

Sintering temperature and time	Pores surface area (%)	Number of pores	Averaged pore Diameter (µm)	Density (%)
1373 K, 10 h	67.30	26 910	2.66	54
1973 K, 1 h	69.17	21 057	2.61	54
2123 K, 1 h	24.76	10 112	2.37	78.3
2123 K, 3 h	23.58	8 137	2.36	83.4

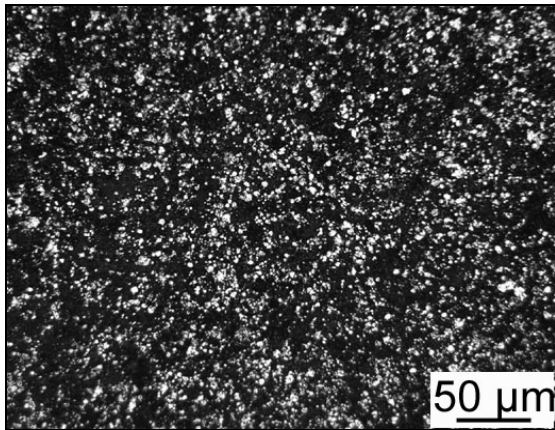


**Fig. 3.11** Microstructure of agglomerates A1 (45-60 $\mu\text{m}$ ), sintered at 1373 K for 10 h, showing the interconnected porosity network with large pores between agglomerates.

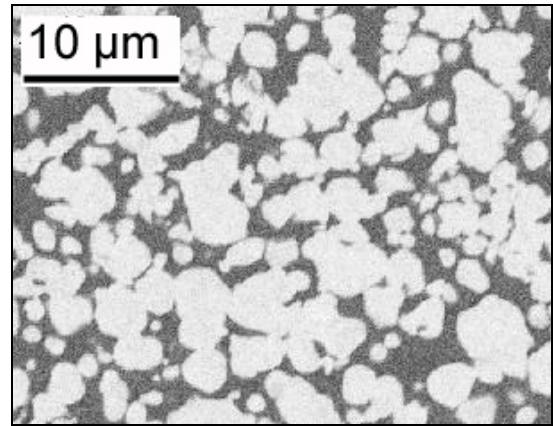
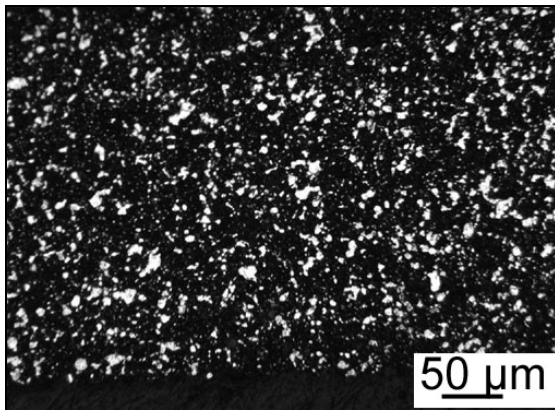
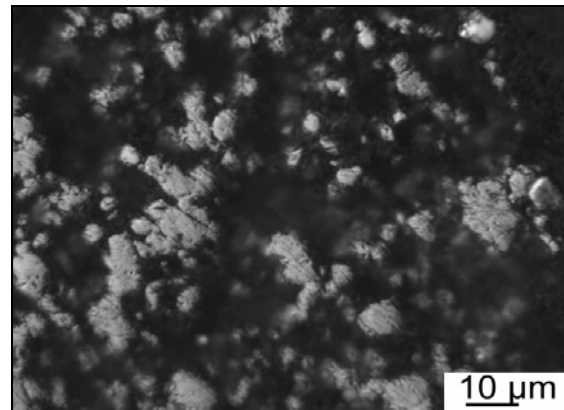


**Fig. 3.12** Microstructure of the interior of one agglomerate in A1, sintered at 1723 K for 3 h, showing sintering signs like necking and particle rounding.

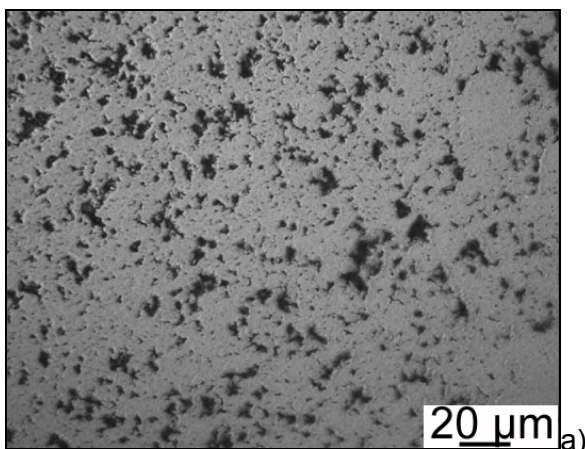


a)

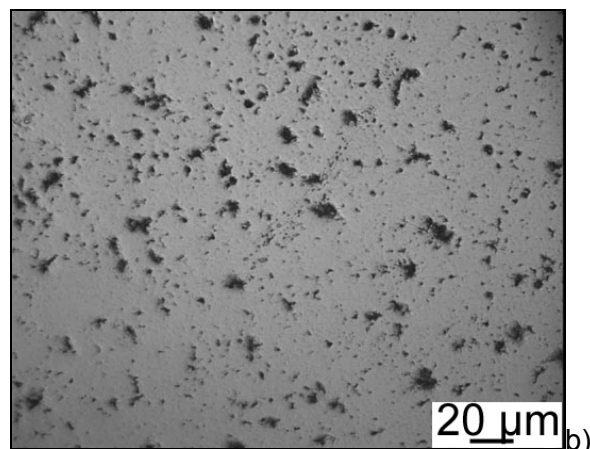


b)

**Fig. 3.13** Microstructure of agglomerates A1 sintered at 1973K. The low (a) and high magnification pictures (b) revealing more dense regions (domains).



a)



b)

**Fig. 3.14** Microstructure of agglomerates A1 sintered at 2123 K for: (a) 1 h and (b) for 3 h. Sintering progress mainly through GBD, and elimination of interdomain porosity takes place. After 3h densification of domains is accomplished.

### 3. RESULTS

#### 3.3.2 Sintering kinetics of large monomodal tungsten agglomerates

Results on sintering study of agglomerates A2 are illustrated in Fig. 3.15, as shrinkage (Fig. 3.15a) and shrinkage rate vs. temperature (Fig. 3.15b). Depending on sintering temperature, similar to the sintering of monomodal agglomerate A1, two densification processes have been observed. The first process (the first peak in Fig 3.15 b) is generally active for temperature lower than 1800K, and the second process takes place above mentioned temperature.

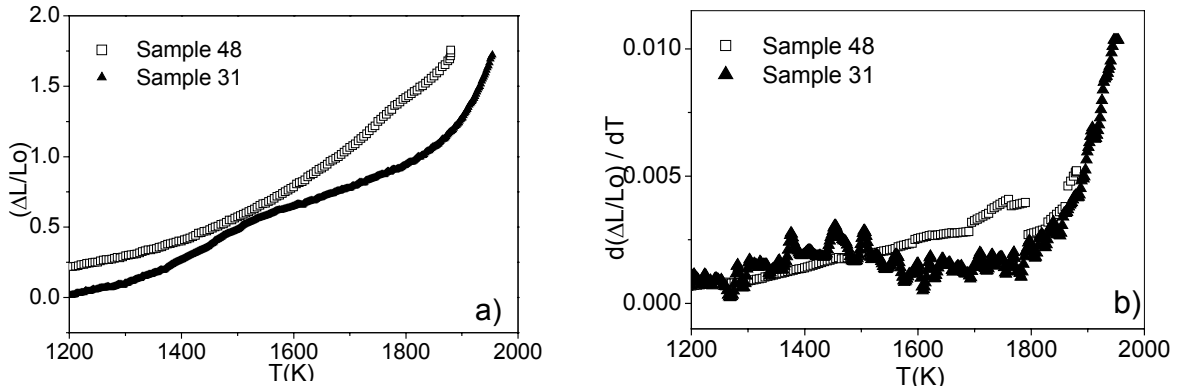


**Fig. 3.15** Dilatometric studies of agglomerates A2 (200-250 $\mu$ m) represented by (a) shrinkage and (b) shrinkage rate vs. temperature.

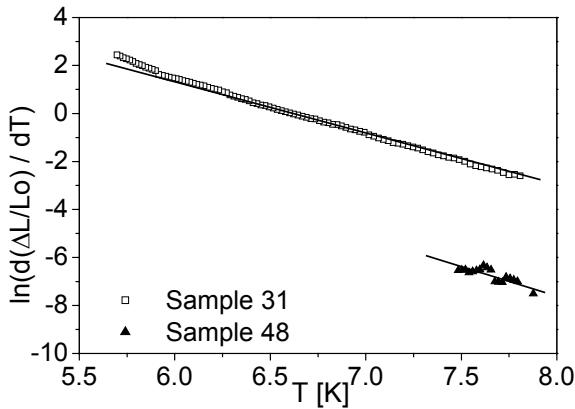


**Fig. 3.16** Kingery's model for rearrangement process in LPS applied for sintering behaviour of agglomerates A2 (200-250 $\mu$ m).

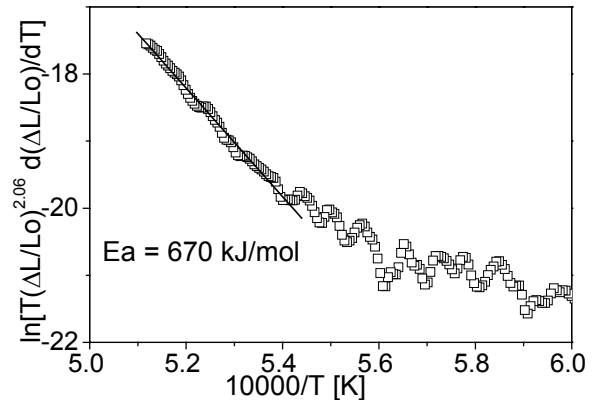


**Fig. 3.17** Young and Cutler's model for GBD applied for agglomerates A2 (200-250 $\mu$ m sample 31) in the temperature range of 1814 - 1940K.

The lower temperature sintering data, fitted by Kingery's model for rearrangement in liquid phase sintering (LPS) are presented in Fig. 3.16, and for the sample 48 Kingery's law covers a wide range of temperature and shrinkage of  $\sim 1\%$  occurs. For the sample 31 Kingery's law fits well experimental data in a narrower temperature range. Table 3.5 summarizes the results of the calculated apparent activation energies for the rearrangement process for both samples (sample 31 and 48) and it may be noted a good reproducibility of the  $E_a$  values.

### 3. RESULTS

**Table 3.5** Calculated apparent activation energy for rearrangement process of large agglomerates A2

Sample	T [K]	Kingery's model / Ea [kJ/mol]
31	1200-1385	82
48	1285-1664	70

As the microstructure of the sample sintered at 1723 K (Fig. 3.18a) reveals no sintering artifacts and since the isothermal sintering has not shown linear relationship according to the power law (Eq.3.7), it is assumed that the controlling process is the rearrangement. The second process in both of samples is connected with GBD and takes place above 1815 K. Applying Young and Cutler's model for GBD in the initial stage of sintering for this temperature range the activation energy of 670 kJ/mol has been calculated (Fig. 3.17).

In order to follow microstructural and density development samples have been sintered at 2123 K for 1 and 3 h. The microstructures of the sample sintered at 2123 K for 1 h and 3 h show clear sintering signs of the initial stage in densification (necking and particle rounding (Fig.3.18b and c)).

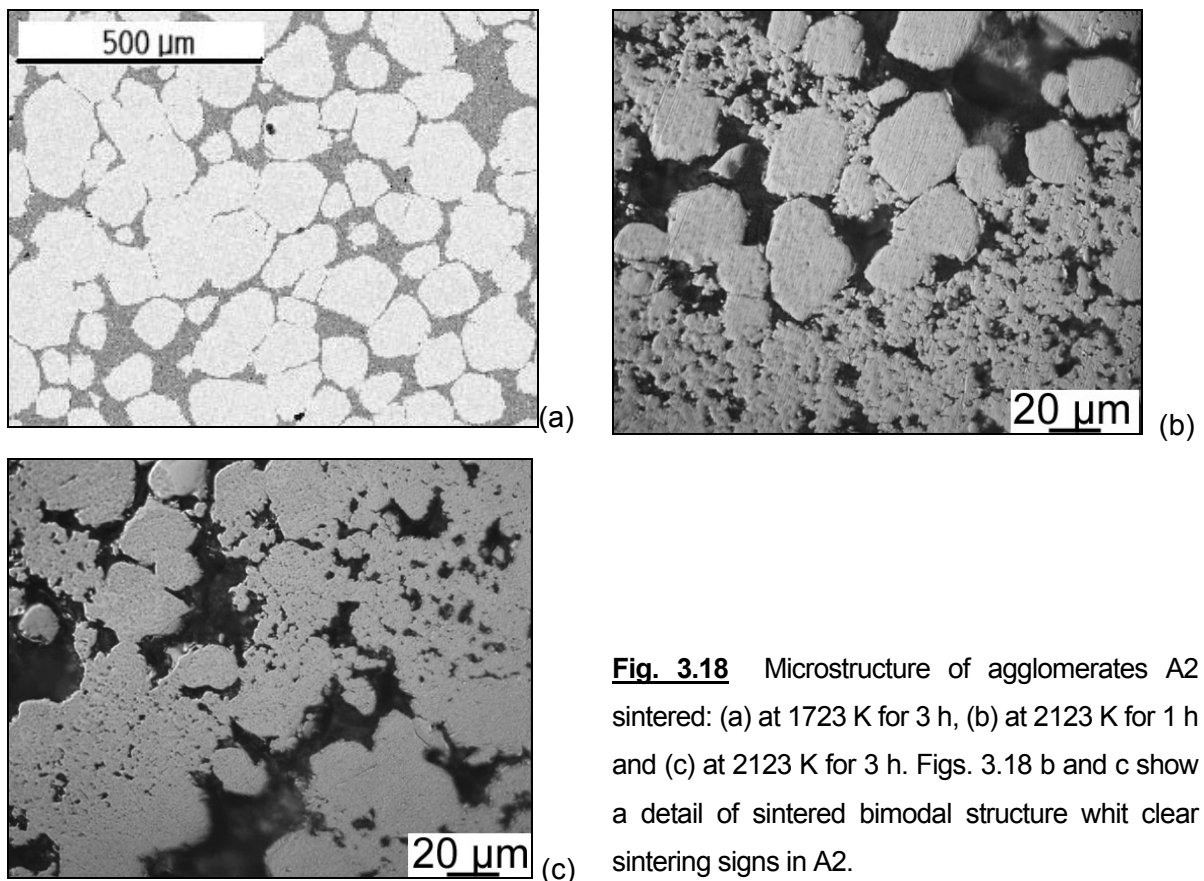


**Fig. 3.18** Microstructure of agglomerates A2 sintered: (a) at 1723 K for 3 h, (b) at 2123 K for 1 h and (c) at 2123 K for 3 h. Figs. 3.18 b and c show a detail of sintered bimodal structure with clear sintering signs in A2.

#### 3.3.3 Sintering kinetics of vibrated bimodal tungsten granular media in percolation and diffusion stages

Shrinkage curves for the skeleton type structures (percolation and diffusion stage) are shown in Fig. 3.19(a). Shrinkage rates as a function of sintering temperature for both structures are shown in Fig. 3.19 (b). In both structures two distinguished densification processes occur, which can be visualized through densification peaks (Fig. 3.19 b). The first peak occurs in the temperature range from 1400 K to 1780 K and the second peak is connected with the main diffusion process and occurs above 1800 K.

The sintering behavior of both stages is strongly influenced by the structure of their skeletons. In the percolation stage smaller agglomerates (A1) are connected and form a skeleton (see Fig. 3.5a and c). In this stage the sintering resembles the sintering behavior of the skeleton - forming component (agglomerates A1) with the activation energy for the rearrangement process of  $E_a \sim 100$  kJ/mol. As vibration proceeds the skeleton structure of larger agglomerates occurs (diffusion stage) (see Fig. 3.6 a) and the sintering of such a structure is similar to the sintering of agglomerates A2 with the activation energy for the rearrangement process of  $E_a \sim 80$  kJ/mol. Table 3.6 summarizes apparent activation energies of the rearrangement process as well as for GBD.

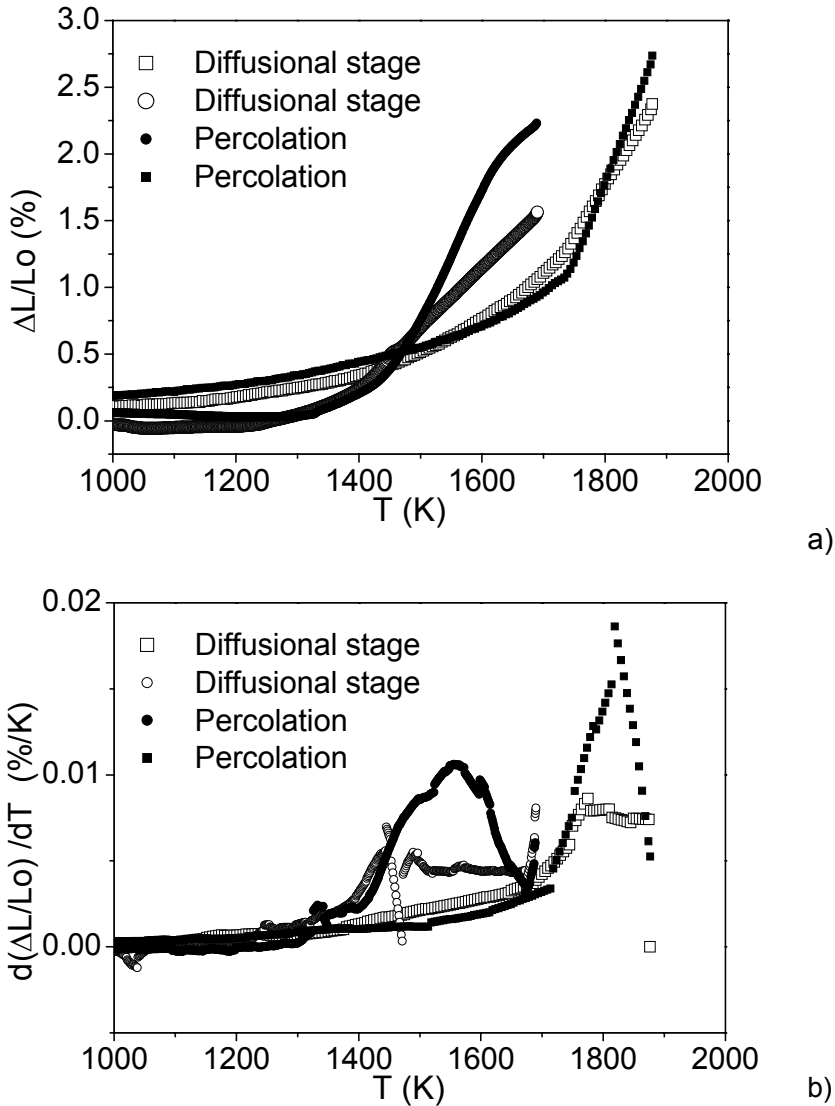


**Fig. 3.19** Dilatometric studies of structure formed in the percolation and diffusion stage presented as: (a) shrinkage and (b) shrinkage rate vs. sintering temperature. Two characteristic sintering behaviors of bimodal system are represented. It should be noted that the differences between them are assigned to variations proper to the individual preparation details (relative humidity and specific powder manipulation).

**Table 3.6** Shrinkage, apparent activation energies for the rearrangement process determined after Kingery's model and for GBD determined after Young and Cutler's model.

Stage	Shrinkage [%]	Ea, Kingery' model [kJ/mol]	Ea, Young and Cutler's model [kJ/mol]
Percolation*	2.6	100 (1504-1785K)	730 (1320-1450K)
Diffusion*	2.2	80 (1300-1720K)	700 (1725-1790)

\* data correspond to characteristic sintering behavior, not to particular.

### 3. RESULTS

#### 3.3.4. Sintering kinetics of bimodal tungsten granular media: homogeneous mixture (A1+A2)

The investigation of sintering behavior of bimodal agglomerates (A1+A2) is continued with an analysis of sintering kinetics of homogeneous mixture composed from agglomerates A1 and A2. In order to study the sintering behavior, three dilatometric runs on the same sample, but up to different temperatures, have been effected (Fig.3.20). The first run was conducted up to 1273 K, the second run at 1723 K with a 3 h hold, and the third run at 1823 K, with a 2 h isothermal hold.

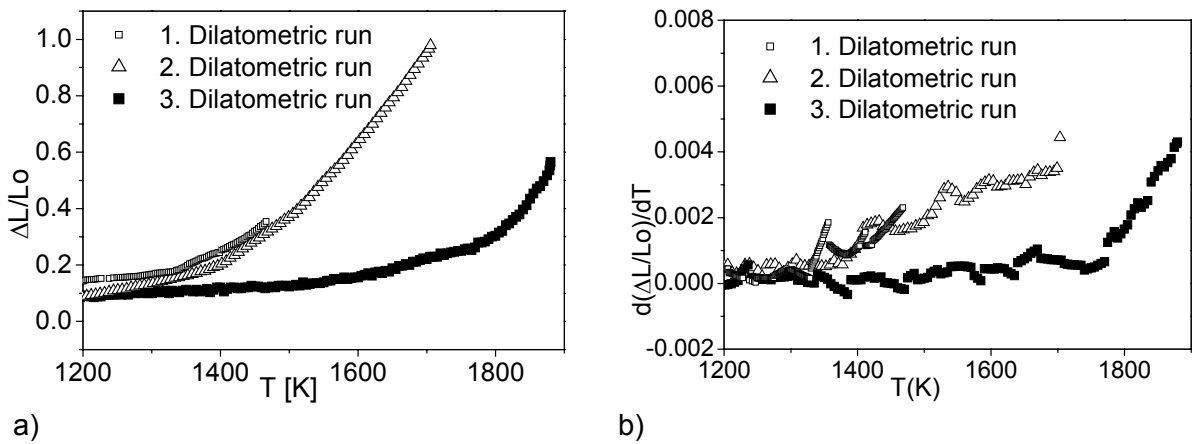


**Fig. 3.20** Dilatometric studies of homogeneous mixture (A1+A2) as: (a) shrinkage and (b) shrinkage rate as a function of sintering temperature.

Repeated measurements revealed the existence of two processes. The first one is active up to around 1770 K. Above this temperature shrinkage rate increases significantly, indicating a new densification process. In all cases the lower temperature densification peak was not observed. Table 3.7 summarizes the results for shrinkage and calculated activation energies for the rearrangement process and for GBD. The microstructure of homogeneous mixture sintered at 1823 K for 2h with the nearly homogeneous distribution of large (A2) and small (A1) agglomerates is shown in Fig. 3.21.

**Table 3.7** Apparent activation energies for operating mass transport process during the sintering of homogeneous mixture (agglomerates A1+A2)

No. of experiment	T (K)	Rearrangement (kJ/mol)	GBD (kJ/mol)	Maximal shrinkage (%)
1. dilatometric run	1250-1464	182	—	0.5
2. dilatometric run	1111-1700	80	—	0.98
3. dilatometric run	1771-1880	338	825	1.54

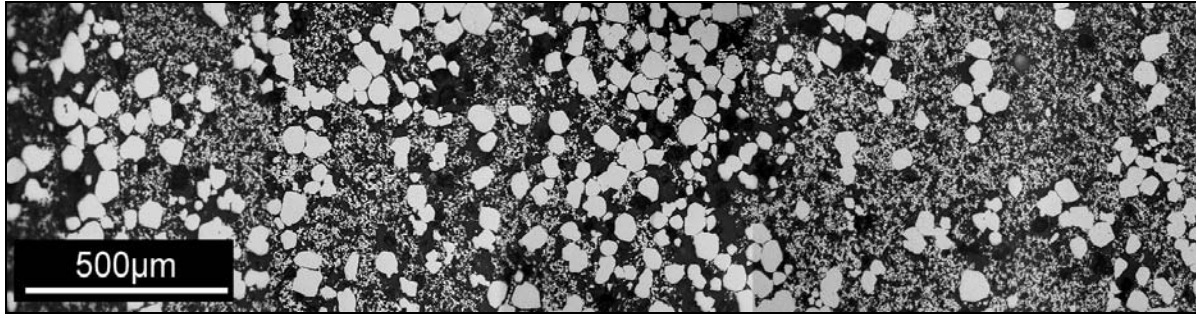


**Fig. 3.21** Microstructure of homogeneous mixture (A1 + A2) sintered at 1873 K for 2 h. with nearly homogeneous distribution of agglomerates A1 and A2.

### 3.3.5 Sintering kinetics of bimodal tungsten granular media in stationary state - graded structure

The compaction curves (see Fig. 3.3a) show that under the geometrical segregation stationary stage is formed. In this stage a graded packing is self formed. Sintering of such a graded material was conducted and quite good reproducibility was observed. Fig. 3.22 depicts the sintering behavior of such a structure, as an example of 5 dilatometric runs. Similar to the homogeneous mixture, and on the contrary to the percolation and diffusion stages, during the sintering of the graded structure the low temperature densification peak is not detected. By applying Kingery's model for the rearrangement and Young and Cutler's model for GBD in the temperature range between 1600–1880K the apparent activation energies of  $E_a = 280$  and  $413$  kJ/mol have been calculated, respectively. Figure 3.23 presents the temperature development of microstructures and corresponding concentration profiles of self-formed W skeletons after 2h of vibration. With increasing temperature and sintering time, the concentration profile spreads in the range of a higher gradient. For the low temperature sintered W skeleton (at 1723K), the concentration gradient is between 100-85 vol. % of W (Fig.3.23a and b), whereas at high sintering temperature (2123K) profile expands in the range between 100-15 vol. % of W (Fig.3.23e and f).

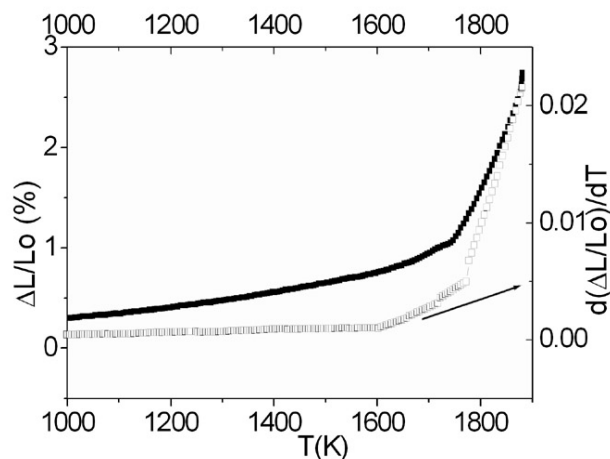


**Fig. 3.22** Sintering behavior of graded structure as: (a) shrinkage and (b) shrinkage rate vs. sintering temperature.

### 3. RESULTS

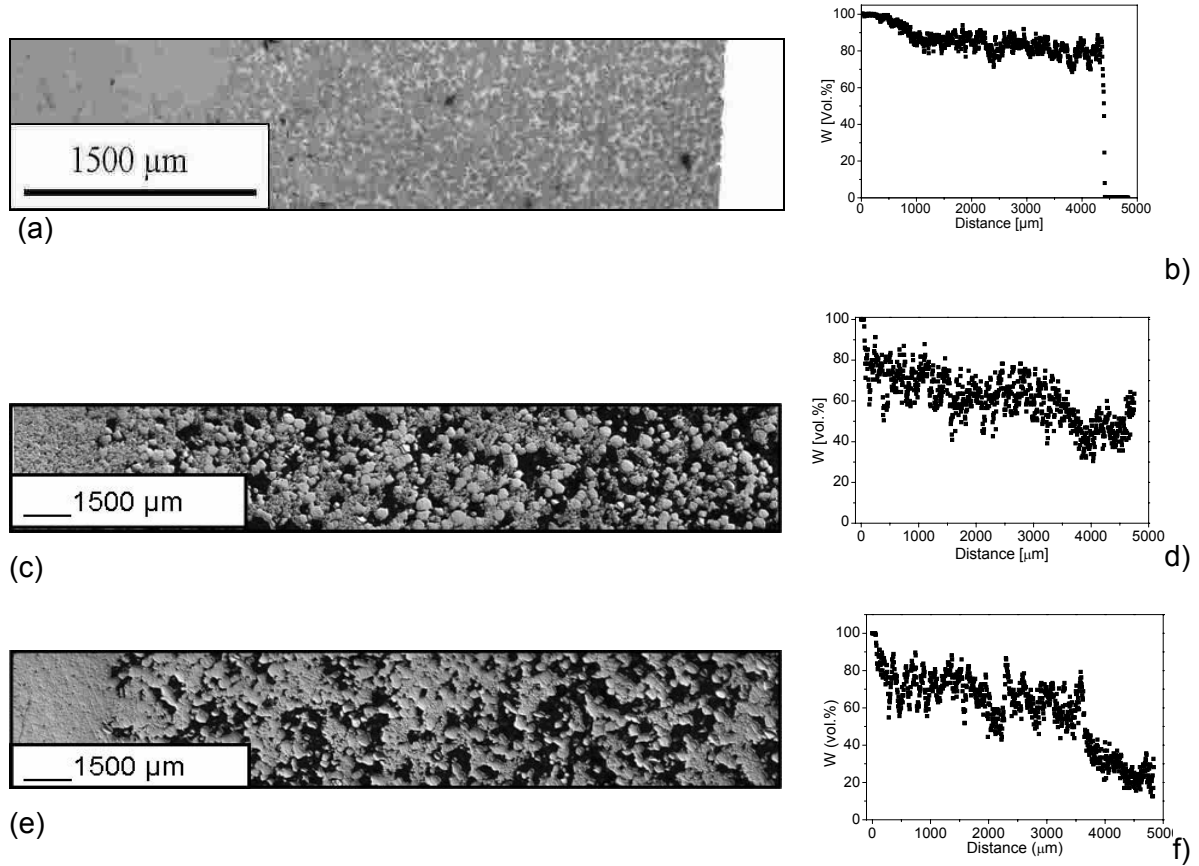


**Fig. 3.23** Microstructure of W-Cu graded material: (a) W skeleton sintered at 1723 K, 3 h and (b) corresponding concentration profile. Microstructure of W skeleton sintered at 2123 K for (c) 1h and for (e) 3h and corresponding concentration profiles (d) and (f) respectively (black pores, light grey W, and white Cu).

Pore size distribution as a function of sintering time at 2123 K has been determined by an image analysis. The pores have been classified in the following way: the large pores - with the maximal dimension  $>50\mu\text{m}$  and convexity  $>0.2$ , and the small pores - with a maximal dimension  $<50\mu\text{m}$  and convexity  $<0.2$ . Table 3.8 summarizes the results obtained by the image analysis. Significant densification (5%), dominantly through the densification of smaller pores, occurs when sintering time increases from 1 to 3 h. This process could be monitored through the reduction of smaller pores and increase in percentage of the larger pores.

**Table 3.8** Density and porosity characteristics of the sample sintered on 2123 K for 1 and 3 h

Experimental condition	Density (%)	Porosity (%) in dense W layer	Large pores (%)	Small pores (%)
$T_{\text{sint}}=2123\text{K}, 1\text{h}$	68	1.4	84	16
$T_{\text{sint}}=2123\text{K}, 3\text{h}$	72	0.3	88	12

### 3.4 Characteristics of copper-tungsten materials

The W-Cu materials are used as contact materials in extreme environmental conditions such as high thermal and neutron flux. Therefore, superior thermal and electrical conductive properties of Cu should be supported by W mechanical stability and wear resistance. That was the reason to investigate electrical and elastic properties of the produced material.

#### 3.4.1 Electrical resistivity

In the current work electrical resistivity ( $\rho$ ) has been selected to compare the electrical properties of the produced Cu-W materials. The electrical resistivity has been measured in the Cu-W materials obtained by infiltration of a self-formed W preform (skeleton and graded types). Figure 3.24 reveals dependence between electrical resistivity and W – W contiguity with vibration time. As vibration time increases W - W contiguity and electrical resistivity also increase. The lowest resistivity has been obtained for shorter vibration duration of 60 min, where the smaller particles are interconnected in a form of skeleton. In the structure with skeleton of large agglomerates (100 min. of vibration) W-W contiguity is higher and the effective resistivity is also higher. In comparison to the skeleton type structures, the graded structure were shown to have higher electrical resistivity.

The temperature dependence of the electrical resistivity of the various specimens produced in this study has been studied from room temperature to 973 K. Figure 3.25 depicts that resistivity increases nearly linearly with temperature. The electrical resistivity of composite structures is between the values for pure Cu and W.

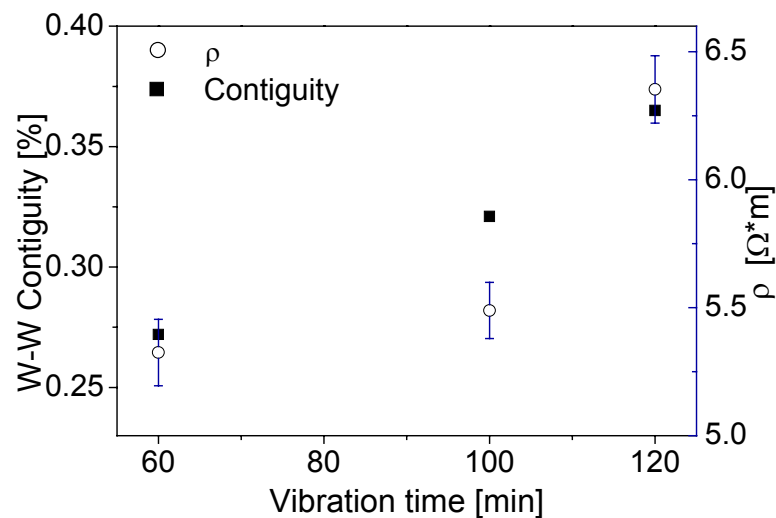


**Fig. 3.24** Electrical resistivity of Cu-W materials and W-W contiguity of W phase as a function of vibration duration.

### 3. RESULTS

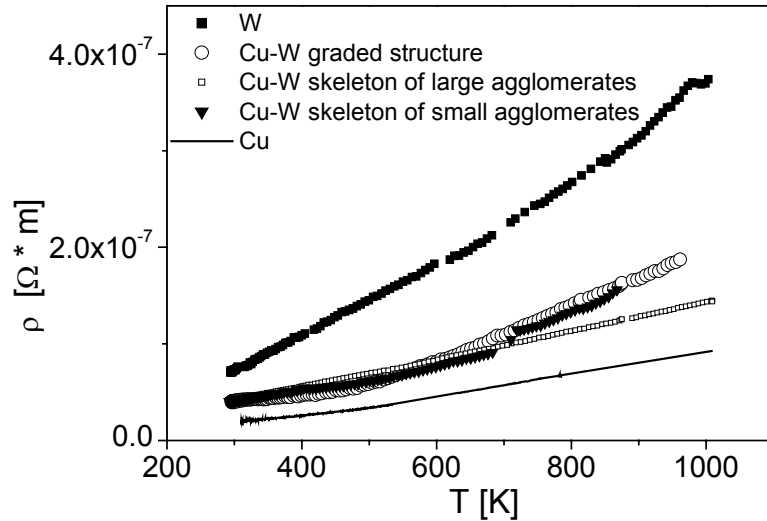


**Fig. 3.25** Temperature dependence of electrical resistivity for pure W, Cu and Cu-W materials.

#### 3.4.2 E-modulus

In order to characterize obtained Cu-W materials effective Young's modulus of elasticity and position dependent E-modulus have been experimentally determined. In Fig. 26 position dependant E-modulus profile, investigated by B-scan ultrasonic method is presented. The profile of E-modulus is analogue to the concentration profile (see Fig. 3.5 (d,f and h)) and it is sensitive to the microstructural effects (porosity and interfaces). Clear agreement with the concentration profile is presented for the sample vibrated for 60 min. (Fig. 3.26a). Samples vibrated for longer time (100 and 120 min) exhibit higher value of E-modulus compared to the samples vibrated for 60 min. Table 3.9 summarizes relevant microstructure properties, experimentally determined Young's modulus and effective electrical resistivity.

**Table 3.9** Microstructural characteristics, E-modulus and electrical resistivity for Cu-W composite material.

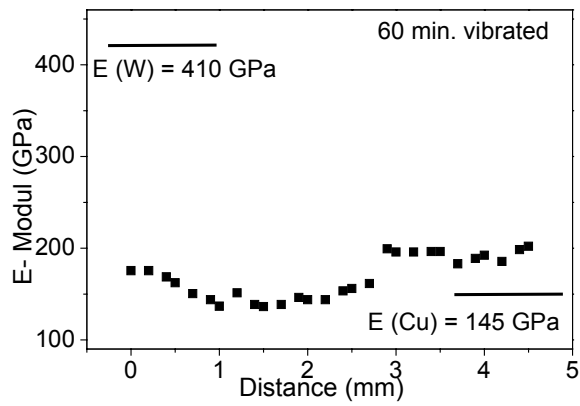
Vib. time [min]	$\rho_t$ [%] (1723 K)	Porosity [%]	Contiguity [%]	wt [%] $C_{inf}$	E - modulus [GPa] (1723 K)	E - modulus [GPa] (2073 K)	$\rho \times 10^{-8}$ [ $\Omega m$ ]
60	50.0	1.85	27.2	37.2	175	241.46	4.635
100	58.3	0.39	32.1	35.2	173	257.27	4.764
120	59.3	0.5	36.5	32.3	229	284.46	5.647

\* E modulus measurement accuracy was 2.66 GPa, on samples sintered at two temperatures: 1723 K and 2073 K

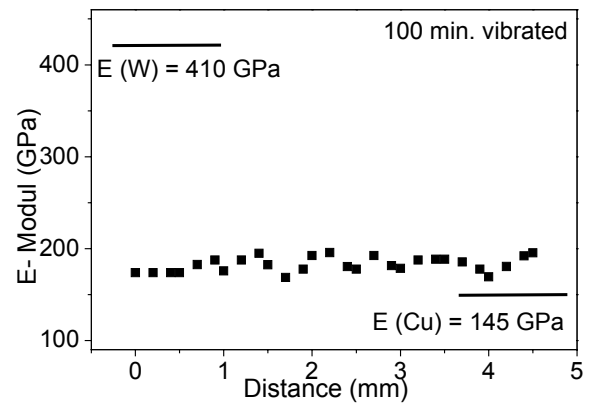
\*\* Contiguity measurement accuracy was 2.73%.

\*\*\* Electrical resistivity measurement accuracy was  $0.12 \times 10^{-8} \Omega m$ .

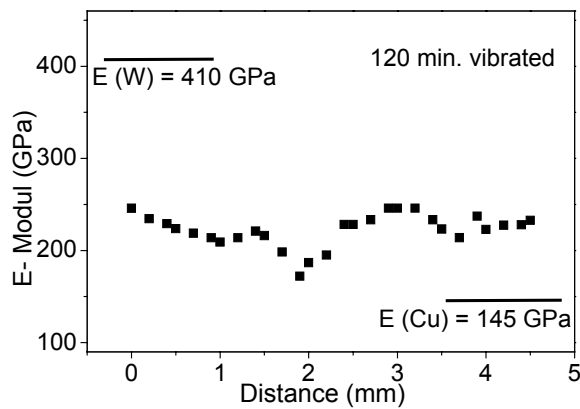
### 3. RESULTS



a)



b)



c)

**Fig. 3.26** E-modulus profile obtained by B-scan ultrasonic method of the Cu-W materials made of bimodal W GM vibrated for different times: ((a) 60 min, (b) 100 min and (c) 120 min), and infiltrated with molten Cu. (W preforms presintered at 1723 K were subsequently infiltrated with Cu at 1473 K).

### 4. DISCUSSION

Discussion of results is divided into four parts. The first part considers the characteristics of the applied W granular media. The second part analyzes compaction dynamics and size segregation as one of the phenomena accompanying the vibration of polymodal GM. Subjected to vertical vibration, selected tungsten GM manifests two different packing structures: skeleton and graded type. In order to study the sintering behavior of these self formed W structures, sintering kinetics of monomodal and bimodal W GM have been considered in the third part. Finally, the fourth part deals with the correlation between microstructural parameters and some properties of the produced Cu-W materials (electrical resistivity and elastic modulus).

#### 4.1. Characteristics of tungsten granular media

Granular media has usually been defined as a simple collection of discrete particles ( $>100\mu\text{m}$ ) kept together through the action of gravity, with repulsive contact forces between particles, and with many different metastable states which can determine the static condition of the system. A static packing of grains is indefinitely trapped in a local minimum of the total potential energy and only through an external perturbation the system is able to leave this metastable configuration. When submitted to an external mechanical perturbation, the system instantaneously acquires extra mechanical energy and relaxes itself through a variety of metastable configurations. Finally, it can possibly reach a non equilibrium steady state. The non equilibrium steady state occurs when the energy lost through collisions is equal to the amount of energy added externally. For an equilibrium state statistical mechanics provide a well established theory where, by usage of functions of state, it is possible to determine the most probable state. However, in non-equilibrium thermodynamics it is the entropy that takes the central position. When the evolution towards a stationary state is facilitated, a non-equilibrium system organizes itself to maximize the non-equilibrium entropy (configurational maximum principle) [Hay97, Fis05].

Due to its simplicity, GM is used as a metaphor for the complex behaviour of glass transition in spin glasses [Jae89], [Kni95],[Ric05] and motion of flux lines in type II superconductors [Jae96], but also as a tool in the macroscopic visualising of Fermions [Hay97,Quo00, Fis05].

In this study, weakly excited W GM has been used to produce continuous graded materials [Müc97, Müc99]. Two important criteria have to be met in order to produce material using the advantages of size segregation. First of all, particle size difference should be large enough to provoke size segregation. Secondly, initial particles should have reasonably high surface

## 4. DISCUSSION

---

energies in order to perform effective sintering (driven by solid state mechanisms). Agglomerates A1 (agglomerate size 40-60 $\mu\text{m}$ , initial particle size, (P1) 1-5 $\mu\text{m}$ ) and agglomerates A2 (agglomerate size 200-250 $\mu\text{m}$ , initial particle size, (P2) 45-75 $\mu\text{m}$ ) is a selection of W GM which has shown to have a potential to fulfill both of critical demands.

### 4.1.1 Powder morphology

The experimental procedure has revealed that agglomeration with PVB as a binder has been successfully adapted for the production of the W bimodal powder assemblies. Agglomerates A1 exhibit the superior bonding quality with more uniform size and shape. On the contrary, agglomerates A2 have a non uniform sponge-like structure indicating the less effective agglomeration process.

### 4.1.2 Flow rate, apparent density, and angle of repose

#### Flow rate

The flow rate of W GM is mainly determined by interparticle friction forces and by friction between particles and funnel walls. The friction between particles is influenced by several factors such as: particle size and shape, surface area, surface roughness, and surface chemistry [Ger94]. Agglomerates A2 show the better flow behaviour (see Tab 3.1) that is attributed to the largest agglomerate size and consequently the lower surface area. The same flow rates for powder P2 and agglomerates A1 (Tab.3.1) demonstrate that the effect of particle / agglomerates sizes dominate over the effects of surface chemistry changes caused by the agglomeration process itself.

#### Apparent density

The apparent density of W particles / agglomerates is sensitive to the variation in ambient humidity and, for this reason, the apparent density can be used as an indicator of the interparticle forces. Generally, the apparent density decreases as the ambient humidity decreases (Tab.3.1). Agglomerates A2 exhibit strong sensitivity to humidity variation and significant decrease of the apparent density has been observed when the relative humidity changes from 25 % to 16 %. This behaviour can be visualised in the sense that, depending on ambient humidity, particles in powder can be covered with thin water layers of different thicknesses. Such bonds, named pendular bonds [Ger89], strongly influence the interparticle friction forces. At the lower ambient humidity used in the current study ( $H_r = 16\%$ ), it can be assumed that pendular bonds are not stable and higher interparticle friction is obtained. As a consequence, W GM exhibits poorer packing characteristics expressed through significant

## 4. DISCUSSION

---

reduction of the apparent density. In the case of agglomerates A1 and initial powders P1 and P2, due to the smaller particle sizes, cohesive forces dictate powder properties, and no important effect of the ambient humidity has been detected.

### Angle of repose

The angle of repose is the natural angle of inclination of powder from the horizontal plane when it is poured through a funnel. Carr's classification of powders in terms of the angle of repose is given in (Table 4.1) [Car70]:

**Tab. 4.1** Classification of powders flow characteristics [Car70].

Very free flowing	25-30°
Free flowing	30-38°
Fair to possible flow	38-45°
Cohesive	45-55°
Very cohesive	> 55 up to 70°

According to Carr's classification, both agglomerated powders have been characterised as very free flowing (Fig. 3.2). In contrast, initial powder P1 has properties of fair to possible flow. This feature is attributed to a particle size below  $\sim 10 \mu\text{m}$ , where substantial bonding coming from Van der Waals forces [Vis89] cause the angle of repose to increase. The angle of repose of W powders / agglomerates decreases as particle size increases. The high dispersion of experimental results observed in the case of agglomerates A2 indicates the existence of several initial metastable packing configurations. Due to a large agglomerate size ( $> 100\mu\text{m}$ ) and dominantly repulsive forces between particles, agglomerates A2 exhibit a disordered structure, characteristic of GM. Therefore in the analysis of statics and dynamics of those systems, a statistical approach should be involved.

### **4.2. Compaction dynamics of tungsten bimodal granular media**

The initial idea of this research was to create a continuous graded material starting from size segregation. Size segregation is generally an undesirable effect connected with vibration of granular media. Nevertheless, the effort has been made in taking advantage of this "natural" event for technological processing of continuously formed gradient of porosity in W preform.

Granular compaction is related to both practical and basic scientific problems. For practical purposes the main issue is to obtain efficient packing. On the other hand, compaction is subject

## 4. DISCUSSION

---

of fundamental theories, oriented to describe and predict general properties of GM packing and their dynamics. There are two most important questions addressed in this field. The first question is: which compaction mechanisms are operating when the GM is subjected to mechanical perturbation? The second question is: what is the nature of their relaxation dynamics?

### 4.2.1 *Compaction mechanisms of tungsten granular media*

The results obtained in this study have shown that for low intensity vibration, geometrical segregation is the operative compaction mechanism of bimodal W-W GM. Under the applied experimental conditions ( $a=6g$ ,  $\nu = 600$  Hz), the selected GM segregates in manner that a steady state with graded packing is obtained (see Fig. 3.3). This process is controlled through particle - particle interactions and the packing structure includes highly packed regions generated from slowly collapsed, mature and flatter bridges [Bak92]. During this process large holes have been replaced by smaller isolated holes, and the collective reorganization of particles (and consequently slow reorganization of particle bridges) will lead to the efficient filling of voids. The result is higher packing fraction and minimization of the void space as compared to compaction under higher acceleration. The mechanism of geometrical segregation is discussed in more detail in section 4.2.2.

This work has been motivated by the extensive study of the compaction mechanism of bimodal W, i.e. W-Cu granular media, conducted by Fiscina et al [Fis04]. The experiments in a wide range of frequencies, agglomerate size ratios and accelerations show the existence of different compaction mechanisms. Depending on the excitation level, mechanisms of convection rolls (CR), geometrical segregation / reorganisation (GS) and surface convection (SC) have been observed, as shown in Fig. 4.1 [Fis04]. A function between dimensionless amplitude  $r/d$  and dimensionless velocity  $V_b$  (Eq. 1.10, 1.11) has been used as a tool for quantitative determination of the particular compaction mechanism dominance (see Fig.4.1). Depending on those two parameters, the following compaction mechanisms are identified:

- geometrical segregation occurs within  $r/d < 0.09$ , and  $V_b < 1$
- geometrical segregation aided by convection motion at the surface of GM-bed occurs within  $1 < r/d < 2$ , and  $1 < V_b < 1.9$ .
- convection rolls occur within  $r/d > 2$ , and  $V_b > 2$ .

In the second step, the same group of authors [Fis04] proved the existence of the observed compaction mechanism at constant frequency (600 Hz), but for various vibration intensities ( $a = 18, 12, 6$  g) It has been observed that in all experimental conditions applied, initial contraction ( $-\Delta l$  (mm)) corresponds to percolation, where the smaller agglomerates fill the

## 4. DISCUSSION

openings beneath the larger agglomerates. The appearance of the first larger agglomerate on the bed surface can be followed through the second oscillation on the relaxation curve  $\Delta l$  vs.  $t$  (see arrows in Fig 4.2) and depending on the excitation level ( $a = 18, 12, 6$  g) large particles reach the top position after 0.89, 1.26 and 2.29 ks respectively.

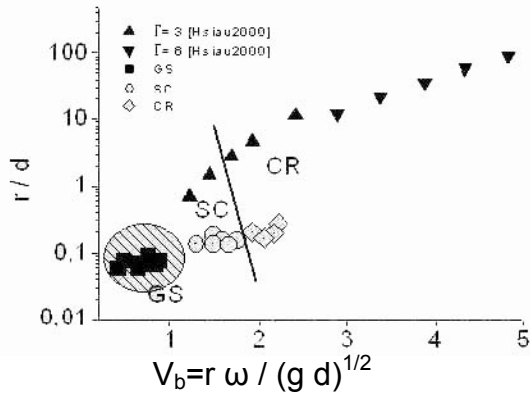


**Fig. 4.1** Segregation mechanisms observed under different experimental conditions. GS-geometrical segregation, SC-surface convection, CR-convection rolls. The experiment of Hsiau and Chen [Hsi00] (points marked with  $\blacktriangledown$  and  $\blacktriangle$ ) was taken as reference [Fis04].

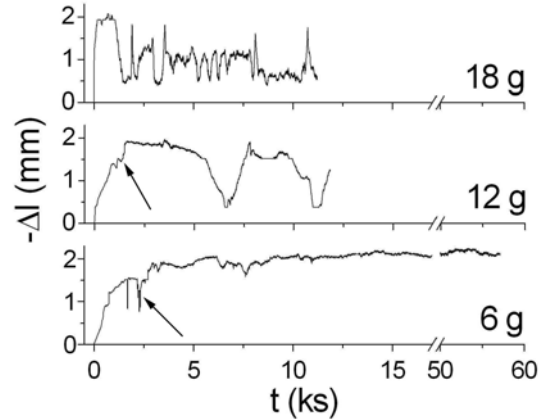


**Fig. 4.2** Time evolution of bed height of a GM formed with  $200 / 250 \mu\text{m}$  W agglomerates and  $45 / 60 \mu\text{m}$  Cu agglomerates.; at 600Hz, for accelerations of  $a = 6, 12$  and  $18$  g. The arrows show occurrence of the first large W agglomerate on the surfaces [Fis04].

Additionally, it has been shown that compaction behaviour under high excitation (Fig. 4.2,  $a = 18$  g) is dominated by a movement of smaller particles through convective rolls (CR). The CR rises at the centre of the container, dragging large particles to the surface, and a ring structure composed of large particles close to the wall is formed [Fis04]. Once on the top of the surface, large particles remain stranded because they cannot follow the small grains in the thin layer of downward convective flow along container walls. The diagram from Fig. 4.1 ( $a = 18$  g) shows that after reaching its maximal contraction (after 0.18 ks), the system rapidly expands to total segregation, manifested by bed expansion (0.94 - 1.46 ks). Convection mixing suffers from the development of mixing barriers, such as islands, that do not interact with surrounding material. Convection in GM is driven by particle-wall interaction, and due to the dominance of defect creation, this process is difficult to control. During high - intensity vibration, cooperative structures such as arches, bridges, and clusters form and disappear readily. The nonsequential and cooperative simulation done by Baker, Mehta [Bak,92], shows that most of a formed bridges are only one or two generations old, with an unfavorable angular shape which causes lower packing efficiency (Fig. 1.4). It was also observed that the high - intensity vibration creates overlapping and connected holes.

## 4. DISCUSSION

---

The mechanism of surface convection has been observed at a lower vibration intensity (Fig.4.2,  $a=12g$ ) and, if the vibration is stopped at a suitable time (1.5 - 5.52 ks), total segregation can be suppressed and a graded packing can be self formed. The SC rolls are localized on the surface and are dominantly controlled through particle-particle interaction [Elp97, Hsi00].

Based on the experimental determination of self-diffusion in a flowing powder depending on excitation intensity, two different diffusive regimes have been observed [Meh93], [Zik92]. At higher excitation intensity, the diffusion coefficient is linearly dependant on vibration amplitude, while a slower regime was observed for lower shaking intensity. This situation can be interpreted in terms of two distinct hopping processes. For large intensity vibration, the major contribution to particle displacement occurs when the particles have broken out of their clusters and are moving independently of each other (hydrodynamic behavior). At lower intensities, self diffusion arises from particle motion within clusters (viscous behavior). The crossover between the two kinds of behavior appears to occur at a value of the vibration amplitude that leads to an expanded packing in which the volume occupied by particles is the same as the volume occupied by voids [Bar93].

### 4.2.1.1 Compaction mechanisms in weakly excited tungsten granular media

Compaction of bimodal W GM under low excitation intensity (Fig. 3.3a,  $a = 6g$ ) has been considered in this work and two distinct compaction stages are observed. The first stage (percolation) occurs under a lower packing density, with a quasi linear  $\Delta l - t$  behavior (see Fig. 4.1,  $a = 6g$ ) i.e.  $\rho - t$  behavior (see Fig. 3.3a). In the framework of Mehta's macroscopic approach [Meh91], this stage corresponds to single particle relaxation (individual motion of smaller particles), which is effective for moderate packing density (for monomodal packing  $\Phi = 0,3-0,4$ ) where instantaneous, inelastic, two - particle collisions dominate. It was demonstrated that in this situation, particles experience a period of free diffusion. In the experimental work of HD`Anna et al. this linear time dependence, typical of standard Brownian diffusive motion [D`An03], [D`An01], [D`An01a] has been recognized. Otherwise in the work of Fiscina et al. [Fis05], a deviation from Brownian motion has been found, and this feature was attributed to a more complex collective aspect of the motion.

In the final compaction stage, a non equilibrium steady state has been obtained which remains also after the longer vibration duration (60ks, Fig. 4.2). In this quasi static stage energy lost through collision are equal to energy added externally and slow collective motion of close packed collections of particles (for monomodal packing,  $\Phi \geq 0,55$ ) is active.

## 4. DISCUSSION

---

Transition from the percolation to the quasi static steady state is followed by the intermediate stage with a diffusive nature, where, according to Mehta's approach, beds locally experience a competition between individual particle motion and collective relaxation. In this stage, vibrated W-GM exhibits dynamics of critical slowdown. This behavior can be compared to the jamming (as glasses freeze when they reach the glass transition) [Liu98], [D'An01]. The similarity of GM with out-of-equilibrium systems, like glasses, is based on the idea that geometry of grains plays a major role, similar to „geometrical frustration „ in thermal glasses. In this stage it can be imagined that a grain can jump into a hole in the packing only if the hole is empty (geometric frustration mechanism). GM, like glasses, can be trapped in a metastable configuration unless an external perturbation is applied. Critical slow down of compaction kinetics prior to the steady state was attributed to the density state, which is close to the density limit of random close packing (0.64%). The high improvement in packing density between initial and final (steady state) bed configurations of the W bimodal GM used ( $\rho_{rip} / \rho_{rcp} = 1.6$ ) (Tab. 3.2) is assumed to be an indication that the weakly excited bimodal GM system progresses towards maximal disorder packing density, probably given by the random close packing density limit.

A simulation of density relaxation in a frustrated lattice gas, performed by Nicodemi et al. [Nic97], reveals a relationship between the diffusion coefficient and the bed density (represented as the particle mean square displacement). In long time behavior, the diffusion coefficient goes to zero when the density reaches the random close packing limit, signaling a localization in which particles are confined in local cages and macroscopic diffusion-like process are suppressed. This phenomenon may also be described in a way that  $\rho_{max}$  represents the density above which it becomes impossible to obtain a macroscopic rearrangement of particles without increasing the system volume. This density limit is associated with the maximal packing fraction and seems to correspond to the Reynold's transition observed in real GM [Rey85, Nic97]. Above the maximal density, a macroscopic shear in the system is impossible without dilatancy.

### - Relaxation behavior of weakly excited tungsten granular media

Compaction dynamics can be understood as the consecutive transitions among the metastable (glassy) configurations. By analogy to the free volume theory, as suggested by Hong et al. [Hay97], it can be assumed that the dominant process involving particle rearrangement is hopping, with the rate dominated by the activation energy.

The compaction behaviour of weakly excited bimodal W GM is fitted with two of the most frequently used relaxation laws used for describing compaction dynamics of a monomodal system: inverse logarithmic law (so called Chicago law) proposed by Knight et al. [Eq 3.2] [Kni95] and stretched exponential law (Kohlrausch-Williams-Watts law) proposed by Philippe

## 4. DISCUSSION

et al. [Eq 3.3] [Phi02, Phi03, Ric05]. In order to prove the validity of the relaxation laws in bimodal W GM, Table 4.2 summarizes experimental conditions of both experiments from the literature conducted at critical accelerations, and experiments applied in the current study. The reverse logarithmic law, proposed by Knight et al., can reasonably well describe the compaction dynamics of studied W GM prior to the steady state (Fig.3.3), but the steady state cannot be predicted. It is proposed that the strong boundary condition explored in the Knight's et al. experiment (aspect ratio  $\sim 47$ , and 10 particles in tube diameter, Tab 4.2) suppressed convection causing a moderate GM packing density and that the system was actually far from the equilibrium state. According to the results from Fig. 4.1, and Tab 4.2 [Fis04], the compaction behavior observed in this experiment can be associated to: 1) geometrical reorganisation for lower acceleration  $a = 1,4$  and  $1,8$  and 2) geometrical reorganisation aided by surface convection caused by high aspect ratio active under higher acceleration.

**Tab. 4.2** Comparison of vibration parameter, dimensionless amplitude ( $r/D$ ), dimensionless velocity ( $V_b$ ), aspect ratio and mechanism of compaction obtained by different research groups.

<i>Experiment</i>	<i>D</i> [ $\mu\text{m}$ ]	<i>a</i> [ $\text{m/s}^2$ ]	<i>Vib.</i> <i>Amplitude</i> [ $\mu\text{m}$ ]	<i>r/D</i>	<i>V<sub>b</sub></i>	<i>Aspect ratio</i>	<i>No. of particles in column diameter</i>	<i>Regime</i>
<i>This work</i> <i>(bimodal W-W GM)</i>	50			0.089	0.016	$\sim 1$		GS
	225	6 g	4	0.016	0.330		870	GS
<i>Knight et. al [Kni95]</i> <i>monomodal</i>	2000	1.4g	386	0.190	0.440	$\sim 47$	10	GR
		1.8g	497	0.240	0.056			GR
		5.5g	1500	0.79	0,86			GR+SC
<i>Phillipe et al. [Phi02]</i> <i>monomodal</i>	1000	1g	276	0.276	0.5	$\sim 1$	100	GR
		5g	1380	1.38	2.6	CR		

\*GR geometrical reorganisation in monomodal GM systems. For bimodal systems, the corresponding process is geometrical segregation.

In the case of technologically more realistic experiments done by Phillipe et al. for the low acceleration ( $a = 1\text{g}$ ), the system is also far from a steady state [Phi02]. Hence with the increase of excitation level ( $a = 5\text{g}$ ), convection dominates the global flow and the system reaches the nonequilibrium steady state. The bed surface shows typical surface instabilities i.e. inclination and flat conical shape.

Mathematically, a more precise insight of the effect of density on relaxation dynamics comes from the theory of automobile parking developed by Ben-Naim, and can be helpful in

## 4. DISCUSSION

---

understanding the difference between the two noted relaxation laws [Kad99,Her03]. The model shows that for high density, the time to park varies exponentially with the available parking space. On the contrary, for lower density, the packing density varies in a logarithmic law involving time. Hence, Chicago's experiment is far away from a steady state and is characterized by moderate packing density with a logarithmic dependence between packing density and time. In the experiment from the Rennes group [Phi02], GM achieves a steady state characterized by the maximal random packing density, and the relaxation dynamics can be well predicted by a stretched exponential law.

There are different approaches to explain the steady state. Depending on the excitation level, the steady state is regarded as: a dynamic balance between convection and compaction [Phi02], the reflection of a balance between the vibration amplitude and gravity [Meh90] or the balance between internal GM force network and segregation.

In the present work, weakly excited W bimodal GM additionally experiences size segregation, mainly controlled through particle reorganization (mechanism of geometrical segregation). In this mechanism, no convection signs occur and the surface of bed remains flat. Furthermore, the system achieves a steady state which remains stable even for large vibration duration (60 ks). Contrary to the Rennes group, the steady state observed in the current work cannot be attributed to the action of convection. Compaction dynamics of Cu-W GM [Fis04] investigated under different excitations reveal that in all cases, GM beds reach almost the same maximal packing density, which remains stable only in the regime of geometrical segregation. It is assumed that particle reorganization in a weakly excited GM bed progresses through hopping of particles toward the minimum of potential energy. In this stage, GM can be used as a macroscopic model system for visualization of the atomistic diffusion process. However, it has been demonstrated that stretched exponential law fits well the experimental data which agree with the proposed theory of automobile parking [Kad99].

Fitting with a stretched exponential law (Eq. 3.3 and Fig. 3.3) reveals the following fitting parameters:  $\tau$  in the range of 1400-2000 s and  $\beta$  in the range of 0.5-0.8 for a constant acceleration of 6g and an ambient humidity from 8 to 10 g/m<sup>3</sup>. The both fitting parameters are sensitive to the variation of ambient humidity. In the framework of Barker and Mehta's model,  $\tau$  can be considered as the characteristic time defining single particle relaxation (quasi linear part of the diagram in Fig 3.3 (b)). The low particle connectivity in such a loose state can be easily broken by vibration, causing predominantly single particle relaxation. Whereas, in long time behavior, packing density increases significantly through collective relaxation and local connectivity is preserved.

## 4. DISCUSSION

---

For the present experimental conditions, the above mentioned variations in parameters  $\tau$  and  $\beta$  are attributed to the intrinsic nature of GM (particle packing preparation history and its disorder structure). The experiments of Josserand et al. demonstrated the existence of a short-time memory effect in vibrated GM [Jos00]. The future evolution of packing depends not only on its initial value but also on the occurrence and relative stability of a large number of metastable configurations.

### Effect of ambient humidity on compaction dynamics

Variation of the ambient humidity in GM systems causes a drastic change in interparticle forces [Ger89]. The dominant interaction between particles in powders are Van der Waals attraction forces. When the experimental environment is gas or liquid, electrostatic and capillary forces are of relevance. In the experimental conditions applied in the current study, W agglomerates are exposed to a wet air, and vapor condensation may take place in the gaps between agglomerates. The amount of water adsorption depends on the relative humidity and the surface curvature. At low vapor pressure the powder surface is uniformly coated with a thin layer of adsorbed water vapor. By increasing vapor pressure, the critical level is reached when the vapor condenses to form capillary bridges localized at the particle contacts.

In the current experimental procedure, the following scenario is possible: At the absolute ambient humidity between 8 and 10 g/m<sup>3</sup>, particles are initially uniformly covered with thin water layers. As the compaction progresses, particles are better packed, and pendular bridges have been built, causing the reduction of friction forces. In this case, a slow relaxation process takes place with collective relaxation as the dominating mechanism. During vibration at the lower ambient humidity (Hr = 28% i.e. Ha = 6-6,4 g/m<sup>3</sup>, Hr = 35% i.e. Ha = 7-7.1 g/ m<sup>3</sup>), the connectivity of packing is destroyed due to repulsive electrostatic forces. This situation leads to more intense initial compaction, followed by the significant decrease of relaxation time ( $\tau$ ) from 2000 s for Hr = 45% to 100 and 400s for the two lower values of the ambient humidity Hr = 28% and 35%, respectively (see Fig 3.4). The strong dependence of compaction dynamics on interparticle forces in this stage is reliable evidence of single particle relaxation as the active process.

### *4.2.2 Geometrical segregation*

Size segregation of polymodal GM (i.e. Brazil Nut Problem, BNP) is a specific case of vibro-compaction, where the collective nature is dominated by the excitation level, particle size and friction forces. Depending on the excitation level, polymodal GM can segregate through convection rolls, geometrical segregation aided by surface convection, and geometrical

## 4. DISCUSSION

---

segregation (see Figs 4.1 and 4.2). Local rearrangement of particles, as one of the origins of segregation, may include shifting or percolation [Ros87] and an arching effect [Dur93]. Another important aspect which should be considered is the collective motion as discussed by Mehta [Meh91].

It was shown that through geometrical segregation (GS) and geometrical segregation aided by surface convection (GS + SC), a graded packing can be formed in vibrated W GM. Due to its better time efficiency (1.5 - 5.52 ks), the regime of GS + SC (Fig 4.1,  $a = 12$  g) has a potential for industrial application. At an acceleration of 6 g the system segregates without convection, and geometrical segregation takes place. The bimodal assembly evolves towards an ordered non equilibrium steady state and even after the long vibration time (60 ks), total segregation does not occur. Hong proposed that these mechanisms correspond to the collective motion of smaller particles, whereas larger particles play the role of an inert phase [Hon01]. Applying Hong's assumption in the current study it can be interpreted that agglomerates of type A1 interact only with themselves while other particles of type A2 are regarded as phantom particles, and vice versa. The idea what opposite particles do not "feel" one another has been proposed in a different context in the Widom Rowlinson model, where the "nonadditivity" of the diameters is known to drive demixing [Hon 01]. The possible existence of an attractive force between two large spherical particles immersed in a sea of smaller particles has been proposed by Duran et al [Dur98]. By analyzing the "effective granular interaction", Mehta et al. have observed that particles of similar size have a tendency to interlock [Meh90a].

The experimental results in the current have revealed that under the low excitation (Fig.3.3,  $a=6$ g) in the regime of GS, tungsten GM exhibits fluidization only in a first layer. This situation can be explained according to Hong's approach as follows:

$$T < T_c(s) < T_c(l), \dots \dots \dots (4.1)$$

where the given temperature  $T_c$  corresponds to the critical temperature of smaller ( $T_c(s)$ ) and larger ( $T_c(l)$ ) particles, below which particles undergo condensation [Fis04]. Above the corresponding critical temperature, the particles are fully fluidized.

It can be seen (Eq. 4.1) that the system temperature ( $T$ ) of W GM is below the critical temperatures of both the smaller and the larger particles. In this situation, larger particles try to condense and fluidization has been observed only in the highest layer of initial particle packing. The current experimental conditions can be explained in the context of Hong's theory as clear indication of two distinct regimes: the solid near the bottom, and the liquid-like on the bed surface, where the particles are dynamically active and change their positions via collisions. Unlike particles

## 4. DISCUSSION

in liquid regime, those particles in the solid state regime are largely confined in cages and fluctuate around fixed positions. Their motion resembles lattice vibration. The formation of the solid at the bottom has been noticed by the appearance of a massively occupied low-energy state due to the volume exclusion principle [Qui00, Hon01]. Manipulating the system temperature, it is possible to control this gravity induced liquid-solid phase transition. The authors pointed out that this transition is an intrinsic transition associated with any system where the excluded volume interaction is dominant. Such systems cannot be compressed indefinitely and must exhibit a unique low energy state.

Due to the non spherical and irregular shape of applied W GM, the tetris model proposed by Herman et al. [Her99] can be useful in understanding geometrical segregation. The tetris model reveals that particle morphology, approximated with different numbers of legs provokes segregation. Particles with more legs (with more irregular structure) will move toward the top. The buoyancy of particles with more legs occurs due to the greater quantity of surrounding voids. Applied to the current study, agglomerates A2 (200-250 $\mu\text{m}$ ) have more legs in the sense of Herman's approach and therefore can move upwards.

The different stages of the geometrical segregation mechanism are presented in Fig. 4.3 A-D.

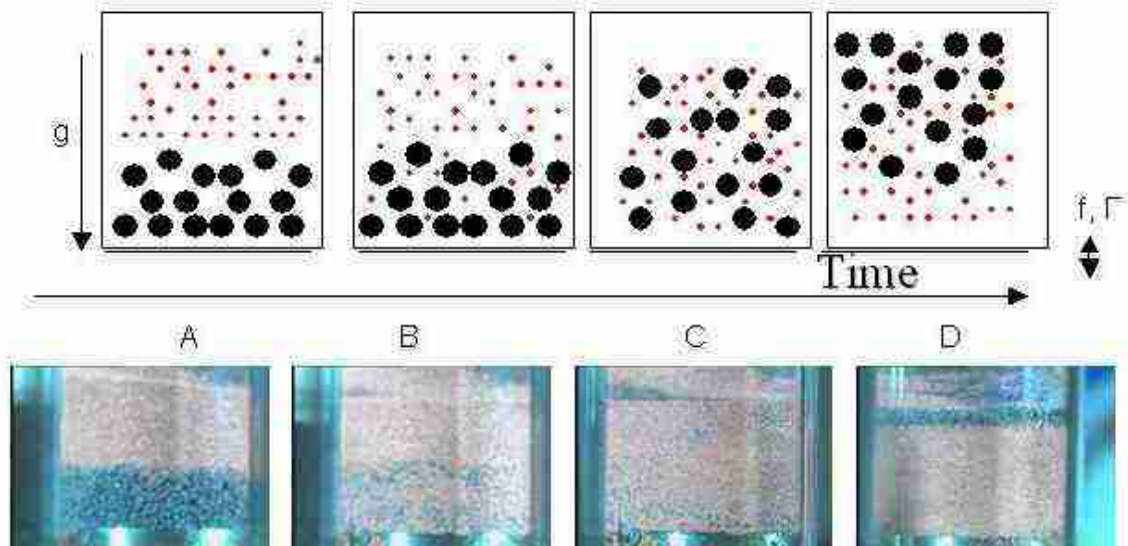


**Fig. 4.3.** Macroscopic view of different segregation stages in Cu-W (Cu agglomerate size 45/60 $\mu\text{m}$ , W agglomerate size 200/250  $\mu\text{m}$ ). Initial position (A), percolation (B), intermediate (C) and final stage with partial / total segregation (D). Cu-W GM was used to better visualise macroscopic development of segregation [Fis04].

I) Firstly, large particles, initially placed on the bottom (Fig.4.3A), start to wiggle around their initial positions. As a result of this motion, gaps are created which allow the smaller particles to percolate and to fill the voids beneath them (Fig.4.3 B). In this stage, percolation overrides

## 4. DISCUSSION

---

condensation. This stage can be monitored through the significant bed contraction ( $(-\Delta l)$ , Fig. 4.1 and Fig. 4.3 (B)).

II) In the next configuration, smaller particles diffuse through hopping, thereby changing their configuration in the potential energy gradient of GM [Fis04]. Dynamics of smaller particles provoke the rearrangement of larger particles, possibly towards the hexagonal close packed structure [Bre03]. In this stage large gaps are additionally create, smaller particles will be free to move down and fill these gaps, and the bed height remains constant. The larger particles act as a inert phase producing a perturbation on the accessible states for the smaller particles (Fig. 4.3 C). This theoretical approach has been proved in the experimental work of Duran et al. [Dur94] in the system containing one single large particle in a sea of  $Al_2O_3$ . Namely, horizontal bed reorganization was directly visualized just above the intruder during its way towards the surface. Once the intruder had left the lower regions, no internal motion was any longer evidenced.

III) In the final stage, a steady state has been reached, which is characterized by the existence of the self formed graded packing (partial segregation Fig.4.3 D). The graded structure represents the most effective random packing model (Tab 3.2). Thermodynamically speaking, this steady state represents a state where the maximum in configurational entropy has been reached [Hay97,Fis05].

### 4.2.2.1 Microstructural characteristics of geometrical segregation mechanism

The mechanism of geometrical segregation has been analyzed through the microstructural characteristics of various sintered structures which were previously subjected to vibration for different times. The percolation, intermediate and non equilibrium steady state stages were revealed by the existence of different final packing structures.

In the percolation stage (Fig.3.5 a and c) small W agglomerates A1 are interconnected and a skeleton structure of smaller particles is formed. In the intermediate stage, this skeleton type turns into a structure with a layer of smaller particles on the bottom and a layer with homogeneously distributed large agglomerates A2 in the form of a skeleton structure (Fig. 3.5e). The fully graded structure, which corresponds to a non-equilibrium steady state, has been self formed after 120 min of vibration (Fig. 3.5g). Quantitative image analysis has shown that the graded structure has higher W contiguity in comparison to the previous skeleton type microstructures (Tab. 3.9), indicating that the large particle rearrangement provokes the increase of the packing density.

### 4.3 Sintering of tungsten granular media

Agglomerates and inhomogeneities in powder / GM, due to non uniformities in their size and shapes, can usually cause hindering of sintering. Furthermore, reproducibility of sintering data is additionally limited by intrinsic properties of GM such as hysteresis, disorder structure and memory effect. All these reasons make a polydisperse powder undesirable in sintering praxis. However, the thermodynamically caused porosity reorganization [Kin67, Lan 83b, Lan89, Kel89, Sla93] opens a possibility to take the advantages of such polymodal structure in the production of material with a gradient in porosity.

The sintering kinetics of various structures obtained in weakly excited W bimodal GM (skeleton and graded types) was a subject of analysis in this work. A first concern with all mixed-powder structures should be the proper understanding of the behavior of each individual powder during sintering. Accordingly, during the sintering of single monomodal W GM, it was observed that simultaneous action of GBD and particle rearrangement process controls global sintering kinetics. Secondly, it was recognized that the sintering of bimodal systems is determined by the type of structures obtained during the vibration route. The sintering of skeleton bimodal structures resembles sintering of the skeleton-forming monomodal GM component. The graded type has a more complex structure with highly non homogeneous particle spatial distributions. As a consequence of the improved packing density, in the graded structure conditions for GBD to be initial sintering mechanism are fulfilled. In order to expand the concentration profile in regions with larger concentration gradients, the evolution of graded structures with sintering temperature has been studied.

#### 4.3.1 Sintering kinetics of small monomodal tungsten agglomerates

It is well established, that at ~1300 K, a densification of tungsten is dominantly initiated by GBD [Kot63, Kot64, Bel91, Las99]. Surface diffusion (SD) dominates sintering at lower temperatures (from 900 to 1300 K) and causes intensive neck growth [Ger76, Ash74, Swi80]. Neck growth by SD does not give densification, but leads to a formation of grain boundaries at the particle contacts. Hence, the combined effects of increased grain boundary area, decreased surface area and higher thermal energy caused by temperature increase, promote GBD to be an operative sintering mechanism. Experimentally measured grain boundary diffusion coefficients [Kre67] and surface diffusion coefficients [Bar60] give the apparent activation energy for GBD and SD:  $E_a = 385$  kJ/mol and  $E_a \sim 300$  kJ/mol, respectively. These results confirm estimations made from sintering measurements [Kot63, Kot64, Ger76, Ash74, Swi80]. Concerning volume diffusivity in W single crystals, responsible

## 4. DISCUSSION

---

for creep behavior [Mud78], the related activation enthalpy for self-diffusion was estimated between 534 and 665 kJ/mol.

The sintering kinetics of monomodal agglomerates A1 show non uniform sintering behavior, strongly sensitive to the configuration of the initial loose packing structure (Fig. 3.7). It should be noted that the differences in sintering behavior between samples (30 and 57) are assigned to variations proper to the individual preparation details (agglomerate processing routes, ambient humidities and the way of filling a die prior to vibration) which significantly affected the initial packing properties. Depending on the initial structure of W GM the intervals of more intense sintering, represented by densification peaks, occur at different temperatures ((1400-1580 K, sample 30); (1700-1800 K, sample 57) Fig. 3.7b). In order to study the kinetics of sintering, Young and Cutler's model for grain boundary diffusion in the initial stage of sintering (Equations 3.4 through 3.6) has been applied [You70]. In the several temperature intervals proposed, the model fits the experimental data well and the apparent energy of 480 kJ/mol has been calculated (Fig. 3.8). The higher value of  $E_a$  than noted in literature ( $E_{a(\text{lit})} = 385$  kJ/mol) is attributed to simultaneous action of an SD-controlled process and GBD. At higher temperature (from 1900 K to 1950 K) (Fig. 3.8), a much higher apparent activation energy of ~800 kJ/mol has been calculated. Such increase of the  $E_a$  with the increase of the sintering temperature could manifest simultaneous activity of GBD, the rearrangement process and SD.

The analysis of isothermal hold densification additionally proved the assumption of GBD to be the controlling mechanism. By applying the power law, firstly proposed by Kingery and Berg [Kin55], a linear relationship between shrinkage and time has been observed (Fig. 3.9). The calculated value for the exponent  $n$  ( $n = 0.32$ ) is very close to the predicted value of 0.3 for GBD as the operative mechanism. The microstructural observation of a sample sintered at 1725 K for 3h reveals clear evidence of necking and particle rounding (Fig. 3.12), supporting the assumption of GBD as the operating sintering mechanism.

There are lot of doubts concerning the power law as a method for indicating mass transport. Rockland and Exner criticized such approaches, based on quantitative description of the sintering behavior of real powder compacts by extrapolating the results derived for two-particle models to multi-particle system, as a relevant method for identifying the dominant sintering mechanism [Roc67, Exn73, Sha89]. Shrinkage equations have been derived in a straightforward way by simply assuming that the relative linear shrinkage,  $\Delta L/L_0$ , is equal to the ratio of centre-to centre approach and particle diameter,  $h/a$ . In this way, rotational and gliding components of motion are neglected. Additionally, the analytical models are based on

## 4. DISCUSSION

---

the assumptions of isotropic surface energy and diffusion coefficient. The second subject of criticism is that usually more than one diffusion process propagate simultaneously. This situation has been considered in the work of Johnson and Rockland [Roc67, Joh69, Hil92, Hau92].

Figure 3.8 shows that the regimes, where GBD model is applied, are disrupted by the regimes with significantly lower slope ( $\sim 220\text{kJ/mol}$ ). It is assumed that a concurrent process to GBD is particle rearrangement. During initial sintering, weak necks are built, predominantly between W particles inside agglomerates. This fact, as well as a lower number of contacts between agglomerates / particles facilitate the rearrangement process. Additionally, during sintering, the spontaneous formation of vacancies, dislocations and possibly other defects can occur in the neck area. Such increased defect concentration in the neck area could strongly increase the creep rate, or decrease the equivalent “viscosity” of that region [Sch92]. These “softened” contact regions can then promote partial rotation of the sintering particles. As a first approximation in order to model this process, Kingery’s model for rearrangement in liquid phase (Eq. 3.8) has been proposed. By applying Kingery’s law, a linear relationship between  $\ln(d[\Delta l(T)/l_0]/dT)$  and the variable  $(1/T(K))$  has been obtained (Fig. 3.10), and from the slope, the apparent energy of  $100\text{ kJ/mol}$  has been calculated (Tab 3.3). The rearrangement process has kinetics which are related to surface diffusion. For both mechanisms it is recognized that increased densification can be achieved by improving the packing factor. The rearrangement process continues until the geometrical factors for repacking, defined by the random close packing density limit, are exhausted. Geometrically speaking, the repacking mechanism offers the most effective way to improve densification [Che97].

Equation 3.8 can be also used to describe densification via viscous flow (Frenkel’s theory [Fre45]. Frenkel’s theory has been adapted for the analysis of CHR data by Cutler [Cut69]. Additionally, the behavior following Eq.3.8 may also be adequate to describe the creep or deformation of certain solids at high temperature, as shown in the work of Benavidez et al. [Ben05]. In such approach the strain rate ( $d\varepsilon/dt$ ) of the crystals by diffusional creep is proportional to the applied stress ( $d\varepsilon/dt \sim \sigma$ )[Cob63].

It can be tentatively summarized that, depending on the initial packing characteristics, two sintering concepts are possible. In the case of initial packing close to the random loose limits, better packing efficiency and higher number of initial contacts allow GBD to progress easily (Fig.3.8, sample 30). On the contrary, with the less effective packing density, particle rearrangement occurs firstly by satisfying conditions for GBD to be later operative (Fig 3.8, sample 57).

## 4. DISCUSSION

---

### 4.3.1.1. Microstructural characteristics of sintered small monomodal tungsten agglomerates (A1)

The sintering behavior of monomodal W GM is strongly affected by the agglomerate structure. The complex agglomerate structure can be simplified visually through a polymodal porosity distribution presented in Figs 1.14 and 1.15, with smaller pores within agglomerates (intradomain / interdomain porosity) and larger pores between agglomerates (interagglomerate porosity). The microstructural development shows that microstructure changes significantly with sintering temperature, although not always in agreement with the measured global macroscopic densification (Tab 3. 4).

More dense units (domains) inside the agglomerates, resulting from earlier sintering, (Fig. 3.11), are observed already at 1373 K. The densification of agglomerates progresses more intensively at ~1723 K, and sintering signs like neck formation and surface smoothing within the agglomerates are evident (Fig. 3.12). Domains within agglomerates range from a few grains strung together as a chain – to a large group with irregular shape. Tendency towards a formation of lineal and ring-like structures [Lan86] is noticeable. Probably, in the case of contact between smaller particles (1 $\mu$ m), some grain growth can take place [Lan89], but most of the particles retain their initial size. At 1973 K, the microstructure changes significantly in spite of the fact that no important macroscopic densification occurs (Fig. 3.13). This micrograph shows the coarsening of the microstructure with clear evidence of densification of domains accompanied by decrease of intradomain porosity. The image analysis revealed that the number of pores was reduced significantly (~20%) (Tab 3.4). Clear separation between nearly dense units, termed fissures, has been observed [Vas70, Rho81], and Exner [Exn75, Exn79] classified this phenomenon as rearrangement. A higher sintering rate, in domains establishes tensile stresses that are continually subject to particle relaxation by viscous flow of surrounding less dense regions. Although some bulk shrinkage can occur, the void space defining the separation grows by “absorbing” smaller interdomain pores. In spite of the fact, that the number of pores has been significantly reduced (Tab. 3.4), the pores surface area is even higher ( 69.17 %) in comparison to the value of 67.30 % determined after sintering at 1373 K. This can be understood through porosity reorganization. From the work of Kingery and Francois [Kin67] it was well established that only pores with coordination number lower than the critical coordination number (concave curvature) are unstable and have a thermodynamical potential to disappear, while pores with higher coordination number (convex curvature) will even grow. Kellet and Lange [Kel89] have shown that for a given grain size, convex pores are expected to obtain an equilibrium size for either shrinkage or growing conditions. Growth of more coordinated pores on account of less coordinated pores leads to porosity reorganization.

## 4. DISCUSSION

---

Important bulk densification does not occur below a temperature of 2123 K. Microstructure of the sample sintered at 2123 K for 1h (Fig. 3.14a) reveals highly dense domains, having smaller interdomain pores and large pores between the agglomerate units. The density increases up to 78% and number of pores, as well as pore surface, decrease significantly (Table 3.4). In spite of the small number of measurements, it was observed that the average pore diameter decreases from 2.66  $\mu\text{m}$  at 1973 K to 2.37  $\mu\text{m}$  at 2123 K. All these microstructural parameters demonstrate intensive densification of the domains dominantly through GBD. Densification of the domains is completed after sintering for 3h at 2123 K (Fig. 3.14b). The pores change morphology into more circular forms, with a mainly concave curvature. The pore surface area is significantly reduced and bulk density increases up to 83% (Tab. 3.4). In a similar manner, the elimination of interagglomerate porosity at higher sintering temperature should be expected.

### *4.3.2 Sintering kinetics of large monomodal tungsten agglomerates*

The effect of the rearrangement process on the general sintering behavior of agglomerates A2 will be pointed out. The two typical sintering behaviors, presented in Fig. 3.15a and b, show non uniform sintering with two distinct densification processes, similar to sintering of small agglomerates (A1). That is, the initial GM structures for agglomerates A2 depend strongly on the preparation conditions, as noted above for the smaller agglomerates A2.

In order to study a low temperature behavior (the first densification peak), Kingery's model for rearrangement process in LPS [Kin55] has been applied. The Kingery's law covers sintering data in the wide temperature range (sample 48), suggesting rearrangement as the controlling mechanism (Fig. 3.16). As the microstructure of samples sintered at 1723 K (Fig. 3.18 a-c) reveals no sintering signs, the afore mentioned observation proved the assumption that the principal densification mechanism can be particle rearrangement, with an apparent activation energy between 70 and 80 kJ/mol (Tab. 3.5). The isothermal sintering behavior did not obey the power law, which can be an indication of more simultaneously active mass transport mechanisms (rearrangement and GBD). The lower apparent activation energy for the rearrangement process in agglomerates A2 compared to the values obtained for small agglomerates A1 ( $E_a \sim 100\text{kJ/mol}$ ) can be explained through the better initial packing properties of smaller agglomerates. Later, as sintering progresses, the neck formation and higher connected network in the smaller particle system hinder the rearrangement process. The rearrangement process itself, provides the necessary condition for GBD to be later on more active.

## 4. DISCUSSION

Fitting the experimental results with Young and Cutler's model for GBD in the temperature range between 1814 and 1940 K (Fig. 3.17) revealed the apparent activation energy of 670 kJ/mol. This value indicates that GBD and rearrangement process are the controlling diffusion mechanisms.

### 4.3.3 Effect of agglomerate size on sintering kinetics

Sintering of fine agglomerates A0 (agglomerate size 10-20 $\mu\text{m}$ , initial powder size 1-5 $\mu\text{m}$ (P1)) have been analyzed, additionally to the sintering of the monomodal agglomerates A1 and A2, in order to study the effect of agglomerate size on sintering kinetics. Fig. 4.4 summarizes shrinkage (Fig. 4.4a) and shrinkage rate (Fig. 4.4b) as a function of temperature for the investigated agglomerates. The maximal linear dimensional changes after the constant heating rate dilatometric run up to 1970 K are also summarized in Table 4.3. Evidently, shrinkage is strongly related to the agglomerate size, and the smaller the agglomerates, the higher is the shrinkage because of larger driving force.

**Tab 4.3** Relative shrinkage of agglomerates A0, A1, and A2 after constant heating rate up to 1970K

Agglomerates	Relative shrinkage %
<b>A0</b> agglomerate size 10-20 $\mu\text{m}$ (initial powder size 1-5 $\mu\text{m}$ )	6.1
<b>A1</b> agglomerate size 45-60 $\mu\text{m}$ (initial powder size 1-5 $\mu\text{m}$ )	4.1
<b>A2</b> agglomerate size 200-250 $\mu\text{m}$ (initial powder size 45-75 $\mu\text{m}$ )	1.65

\*Measurement accuracy was 0.1%

In order to compare the sintering behaviors of investigated powders, Young and Cutler's model for GBD and Kingery's model for the rearrangement process in liquid phase sintering have been applied (Fig. 4.5a and b). In the lower temperature range (between 1400 and 1700 K) GBD with apparent activation energy  $E_a=486$  kJ/mol controlled the sintering of powders A1 and A0. (Fig. 4.5a).

## 4. DISCUSSION

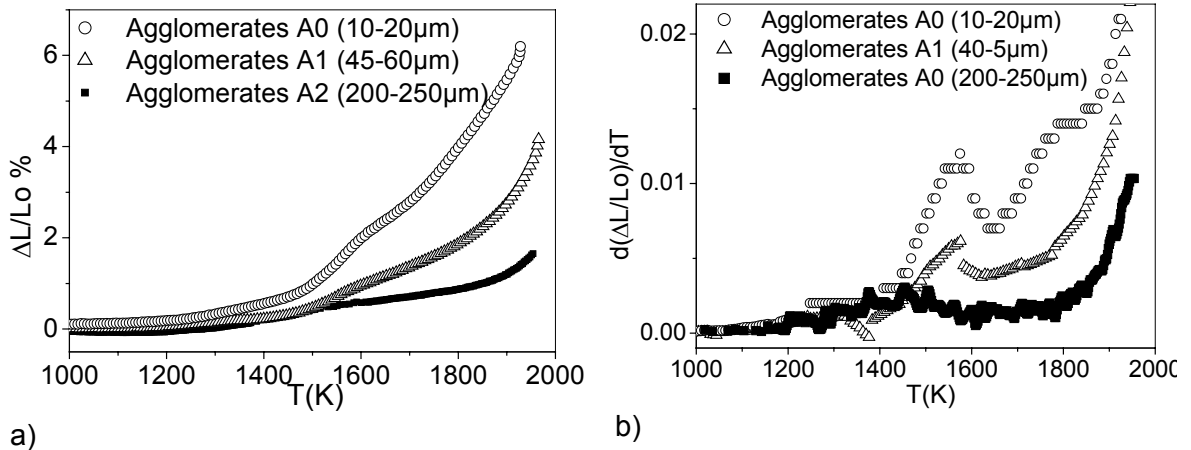


Fig. 4.4 Summarized dilatometric runs for agglomerates A0,A1 and A2, as: (a) shrinkage vs temperature and (b) shrinkage rate vs. temperature.

In spite of the fine particle size of A0, the calculated apparent activation energies for GBD ( $E_a = 486 \text{ kJ/mol}$ ) are even though higher than reported in the literature. Such a sintering behavior of fine power A0 is attributed to the still bimodal pore distribution, and sintering progresses through densification of domains mainly via GBD with significant contribution from SD-controlled processes. The larger agglomerates A2 show very high apparent activation energy ( $E_a = 760 \text{ kJ/mol}$ ) for GBD to be accepted as the densification mechanism. Because of this it was proposed that for the large agglomerates, in this temperature range, rearrangement is the controlling process. These results agree with the results of Kothari, which noticed that GBD at low temperature is favored by smaller agglomerates, which seems the opposite of what is expected from the higher surface area [Kot64].

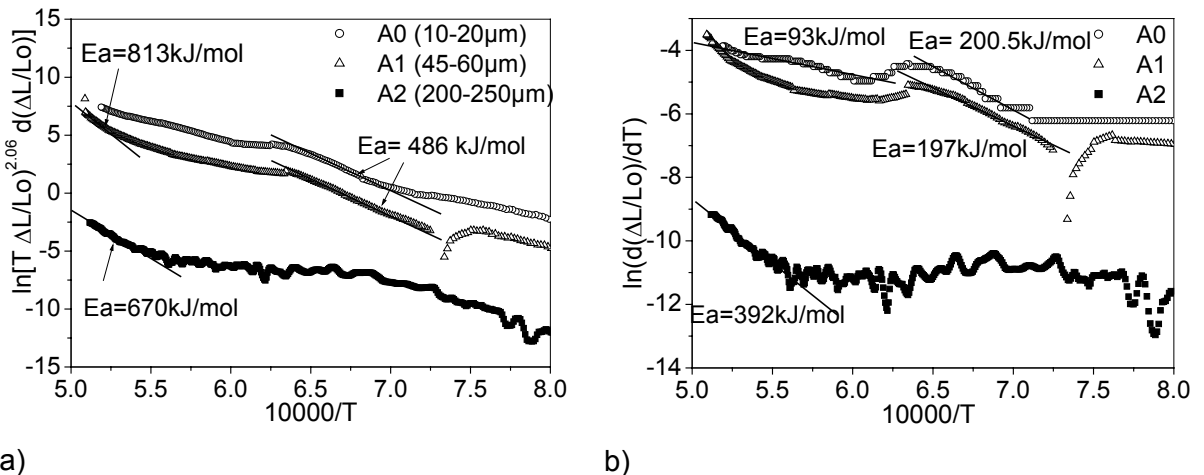


Fig. 4.5 Fitting curves according to : (a) Young and Cutler's model for GBD in the initial stage of solid state sintering and (b) Kingery's model for rearrangement process in liquid phase sintering.

By applying Young and Cutler's model at higher temperatures (1800-1950 K) the activation energies of 813 kJ/mol for agglomerates A1 and 670 kJ/mol for A2 have been calculated. Such

## 4. DISCUSSION

---

high apparent activation energies can be explained through simultaneous action of GBD, SD, and rearrangement process. The activation energy of GBD ( $E_a = 320 \text{ kJ/mol}$ ) for sample A0 calculated in the temperature range 1633-1940K is lower than the values reported in the literature ( $E_a = 385 \text{ kJ/mol}$ ) [Ger94]. On the other hand, fitting with Kingery's law in the same temperature range revealed an apparent activation energy for the rearrangement process of  $E_a = 93 \text{ kJ/mol}$ , similar to those for the rearrangement process in A1 (Fig.4.5 b). This result, at first sight unexpected indicates that the high density domains, densified dominantly through GBD (Fig.4.5a), undergo spatial reorganization at higher T probably through viscous flow or creep.

### 4.3.4 *Effect of vibration on sintering kinetics*

The effect of vibration on sintering behavior has been studied by vibration of monomodal agglomerates A1 and A2 for 2h at a frequency of 600 Hz, an acceleration of 6g and under 45 % relative humidity. It was expected that powder vibration prior to pressing would lead to better packing density of powder and later contribute to more uniform sintering. However, under the applied experimental conditions, the starting assumption did not turn out as realistic and no difference between sintering of vibrated and non vibrated powder was detected. It is known that packing density is strongly related to vibration frequency [Aye65], powder properties, and ambient condition. It was assessed that the applied excitation conditions were not appropriate to induce an improvement in the monomodal particle packing. However, important contribution from vibration was obtained in the bimodal system (agglomerates A1 + A2) and its sintering kinetics will be discussed in the next section.

### 4.3.5 *Sintering kinetics of vibrated bimodal tungsten granular media in percolation and diffusion stages*

It was recognized that depending on vibration duration, different structures occur in W GM: skeleton of small particles (percolation stage), skeleton of large particles (intermediate or diffusion stage), and graded structure (stationary state). Each of those self formed structure exhibits characteristic sintering behaviour. Sintering kinetics of a homogeneous bimodal W GM mixture have been additionally considered, and similarities with sintering of the graded structure have been observed.

#### Percolation stage

The microstructure in the percolation stage has been characterized by interconnected smaller agglomerates A1 in the form of a skeleton (Fig. 3.5 a and c). This skeleton type of microstructure governs the sintering kinetics of global bimodal W GM. The analysis of dilatometric

## 4. DISCUSSION

---

measurements demonstrate a non uniform sintering (Fig.3.19a,b). Similar to sintering of the monomodal powders, regions of more intensive densification occur on different temperatures and this behavior is attributed to the effect of initial packing characteristics varying of. In accordance with to the sintering of monomodal GM in the percolation stage, bulk densification is caused mainly through the sintering of domains within small agglomerates A1.

Additionally, global skeleton structure in the percolation stage can be imagined as a matrix composed of smaller particles, with the larger particles as the dispersed phase. A large difference in sintering rates between matrix and disperse particles induces compressive stresses in the matrix and tension in the region where disperse particles are placed. The complex bimodal structure induces differential sintering rates which in turn produce transient, and sometimes residual, stresses within the sample [Jon86, Eva82, Hsu86]. These stresses influence particle rearrangement, resulting in the development and enlargement of void space. They may also influence creep processes within the porous sintering sample and induce creep damage by generation of crack-like voids. In accordance with the very high activation energy calculated from GBD model ( $\sim 700$  kJ/mol, see Tab.3.6) it is proposed that particle rearrangement is operating with the apparent activation energy of  $E_a \sim 100$  kJ/mol. Furthermore, a similar activation energy was observed for the sintering of monomodal agglomerates A1. For this reason it is proposed that the structure in the percolation stage resembles the sintering behavior of the network forming component (agglomerates A1).

### Diffusion stage

As vibration time increases, diffusion stage occurs with a particle structure that is significantly changed. In this stage, the skeleton of smaller particles turns into a new form: homogeneously distributed larger particles in the form of a skeleton (Fig. 3.6b). The sample vibrated for 100 min exhibits the following microstructure: layer of smaller particles on the bottom and upper layer with homogeneously distributed large particles. The structure has been characterized by a higher interconnectivity between larger particles demonstrated by the higher contiguity parameter (Tab. 3.9). This structure remains stable until the coordination number is below the percolation limits for larger particles [Leu99].

The sintering kinetics in this stage are also similar to sintering in the percolation stage. Compared to the shrinkage in the percolation stage the diffusion or intermediate stage is characterized by slightly lower shrinkage. This can be correlated to the higher interconnectivity of smaller particles in the percolation stage, which are the main contributors to global shrinkage.

## 4. DISCUSSION

---

Due to a large difference in sintering rates between the matrix (large particles) and the disperse phase (small particles), generated stresses cause particle rearrangement. The calculated activation energy for this process ( $E_a = 80\text{kJ/mol}$ ) is similar to the calculated value for rearrangement in monomodal large agglomerates A2. For this reason, it is proposed that the global sintering, in the diffusion stage, is governed by sintering behavior of the skeleton-forming GM component (agglomerates A2, Tab.3.5).

### *4.3.6 Sintering kinetics of a bimodal tungsten granular media: homogeneous mixture*

In the self formed skeleton type structures, the particles are mainly interconnected in such a way that contacts between the particles of a same particle assembly (A1 - A1, A2 - A2) dominate. On the contrary, the homogeneous mixture has been characterized by contacts between particles from the different agglomerate assembly (A1 - A2). Such a strong asymmetry in initial particle contacts acts as a driving force for the rearrangement process. In this situation, clear evidence of a rearrangement process should be expected. To confirm this assumption, three successive dilatometric runs (Fig. 3.20) have been carried out. This analysis has revealed the existence of two temperature dependant sintering processes. The first process is active up to 1770 K and shows a irreversible nature. After two repeated dilatometric runs, this process evidently slows down. A slightly noticeable densification that occurs in this stage is attributed to the rearrangement process ( $E_a = 65\text{-}80\text{ kJ/mol}$ , Tab. 3.7).

As temperature increases, stable interparticle bonds prompt the second process (GBD) to be more active and dominant densification of domains within smaller agglomerates A1 takes place. In the temperature range from 1745 to 1860 K, the apparent activation energy for GBD has a value of  $\sim 800\text{ kJ/mol}$ , indicating competition between GBD, SD and rearrangement starts. The important difference compared to sintering in percolation and diffusion stages comes from the absence of the densification peaks in the lower temperature range.

### *4.3.7 Sintering kinetics of bimodal tungsten granular media in stationary state - graded structure*

In the regime of geometrical segregation, W GM segregates in a manner that a gradient in packing is self formed. During the sintering process, such graded packing structure turns into a W preform with a gradient in porosity. Figure 3. 23a reveals the microstructure of the sample sintered at 1723 K. The complex graded structure is composed of two parts. In the lower part of the sample, a highly dense W layer built from small particles (agglomerates A1) is founded. Graded distribution of the large particles in the upper part is finished with the

## 4. DISCUSSION

---

upper layer being composed exclusively of large particles. Interpreted through a porosity spatial distribution, the smaller pores ( $< 10\mu\text{m}$ ) are located in the lower part, hence, in the upper volume part, the number of the larger pores continuously increases. The corresponding concentration profile of a W graded preform, subsequently infiltrated with Cu, is shown in Fig. 3.23 b.

It is observed that sintering of the graded structure shows strong similarities with the sintering of the homogeneous mixture. In accordance with this, the absence of a low temperature densification peak (Fig. 3.22) is attributed to the formed graded structure which does not manifest skeletal character. In the temperature range between 1600-1800 K, the averaged apparent energy of 413kJ/mol for GBD has been calculated. On the contrary to the homogeneous mixture, the sintering data of graded structure does not obey Kingery's model for the rearrangement. This feature can be explained through the improved packing density achieved during vibro compaction and formation of more sintering necks. As a consequence of that, GBD should be the primary transport mechanism in graded sample which causes the global densification of about 3% predominantly through the densification of domains in W high density layer.

### 4.3.7.1 Development of graded profile with sintering temperature

In order to produce a mechanically stable W porous preform, the self formed graded packing of W agglomerates has been sintered at the high temperature ( $T = 2123\text{ K}$ ). The sintering behavior of such a structure is strongly influenced by: spatial particle size distribution, characteristics of porosity, and nature of particle contacts. All mentioned factors make it difficult for the gradient to develop and preserve during sintering. In solid state sintering, the diffusion lengths are usually small enough to fulfill this condition. On the contrary, for liquid phase sintering, macroscopic flow of liquid can easily occur (in fact, it depends strongly on the particular system) and could destroy the initial graded structure [Kie03].

However, it is demonstrated that by taking the advantage of a thermodynamically driven porosity reorganization, where larger pores grow on account of smaller ones to reduce the surface area, a graded structure can be retained after high temperature sintering. The development of microstructures and corresponding concentration profiles of self-formed W skeletons have been presented in Fig. 3. 23a-f. With the increase in sintering temperature and time, the concentration profile spreads in the direction of a steeper gradient. It was observed that at 1723 K the concentration gradient is in the range from 100 to 70 vol. % of W. At the higher sintering temperature ( $T = 2123\text{ K}$ ), the profile expands: firstly to the

## 4. DISCUSSION

---

concentration range from 100 to 30 Vol.% after 1 h of sintering time, and secondly, after 3 h of sintering, to the concentration range from 100 to 15 Vol.% of W (Fig. 3.23 d and f). The quantitative microscopic analysis shows that after prolonged sintering time at 2123 K (from 1 to 3h), the number of smaller pores decreases by ~ 4 % and the number of larger pores increases proportionally (Tab 3.8). The global effect is an improvement of bulk density (5%) dominantly through the densification of domains within smaller agglomerates (agglomerates A1) and correspondingly through the elimination of intradomain porosity. The critical point during high temperature sintering of W graded preform could come from a dimensional distortion caused by different sintering rates along the gradient. In any case, the sintered preform should be injected still having the holder used for sintering, and after the metal intrusion is completed this holder can be removed or machined.

### 4.4. Characteristics of copper - tungsten materials

The aim of the current work was to produce Cu-W graded material with satisfactory interface quality and mechanical properties. This objective has been achieved by subsequent infiltration with molten copper of self formed W preforms, having controlled porosity profiles.

W-Cu materials are used as contact materials under extreme environmental conditions (high thermal flux, neutron flux) and therefore the superior conductive properties of Cu should be supported by the mechanical stability and wear resistance of W. For this reason, electrical and elastic properties of produced material have been investigated.

#### 4.4.1 *Electrical resistivity*

A good prediction of thermal and electrical conductivity of composite materials can be achieved by applying an effective media theory, a percolation theory and a general effective media equation [McL90,Web03]. For the modeling of the effective composite properties, knowledge of the microstructural arrangement of the constitutive phases is necessary. A much more complex case is present in graded materials, where the microstructural field cannot be assumed to be homogeneous, and models and approximations used for traditional composites are not directly applicable. Due to large experimental errors associated with the experimental determination of thermal conductivity (and the complexities involved in such measurements) in the current work, electrical resistivity ( $\rho$ ) enables the comparison of the electrical properties of produced Cu-W materials. Applying the Wiedemann - Franz-Lorenz's law [Sma99], electrical resistivity can be related with thermal conductivity for pure metals. There are several factors influencing electrical conductivity: Some of them are: composition,

## 4. DISCUSSION

---

residual porosity, residual stresses (due to difference in CTE), microstructural parameters (dehedral angle, connectivity of phases, spatial phase distribution), impurities, number and quality of interfaces. The effects of microstructure on electrical conductivity are difficult to measure, since the changes in other variables may mask the influence of the microstructure.

In order to correlate material properties of produced Cu-W materials with microstructural parameters, the dependence between electrical resistivity and the W contiguity for different vibration durations are shown in Fig. 3.24. It was observed that both W contiguity and electrical resistivity increase with increasing vibration time. Microstructural analysis of the sintering at 1723 K for 3 h revealed significant neck growth between smaller W particles (see Fig. 3.12). This interconnected W network, with larger W particles dispersed within, facilitates a complicated current path through the composite structures. The lowest resistivity was obtained for a vibration duration of 60 min., where the skeleton of smaller particles has been formed (Fig.3.5 a and c). Two features can be used to explain this experimental observation. Generally, the main current path is through the highly conductive Cu-phase and, consequently, the samples with higher Cu contents will exhibit lower resistances to current flow. Additionally to the effect of composition, the lower contiguity of the W phase observed in this structure limits the contribution of current path through the less conductive W phase (Tab.3.9).

In the structure with the skeleton of large agglomerates (100 min. of vibration, Fig. 3.5e) the W contiguity is higher (Cu content is smaller), causing higher effective resistivity. The highest electrical resistivity was obtained for the graded structure (Fig. 3.5g) compared to both of the skeleton types. Quantitative microstructural analysis revealed that the graded structure is characterized by the highest W contiguity and the lowest Cu content. In this case, the electrical properties of the graded structure can be assigned to the larger contribution of a complicated current path through the W phase. Additionally, the microstructures of the graded sample and the sample with skeleton of larger particles show an occurrence of an individual, highly dense W layer. The new interface between this layer and the upper region with graded / homogeneous particle distribution, represent an additional obstacle for current flow.

Effects of particle size and particle size distribution on the electrical resistivity of W-Cu and Mo-Cu composites have been studied by Wang et al. [Wan98] and Scorey [Sco94]. Wang pointed out that in samples with a different initial particle size (but with the same density), resistivity increases as particle size decreases. This effect has been explained through a higher W contiguity, due to more efficient packing (and later on improved sintering) obtained in the system

## 4. DISCUSSION

with smaller particle size. In the case of Mo coated with Cu, the composite structure consisting of a copper matrix with dispersed Mo powder has shown to be a better conductor [Sco94]. In both studies, the maximal conductivity was obtained in the structure where W or Mo particles were isolated in the Cu phase (zero contiguity).

The effect of the contiguity of the W phase on electrical resistivity can be properly visualized through connectivity patterns, i.e. “building blocks model” [McL90]. The concept of “building blocks model” exhibits two extremes of the resistivity for Cu-W composites: the maximum resistivity occurs when the Cu-W layers are in series to the current direction (Fig. 4.6a), and the minimum, when the layers are in parallel to the current (Fig. 4.6b). In the real practice, instead of these two extreme distributions, the distribution of Cu and W phase is more homogeneous and isotropic (Figs.4.6c-d). The pattern shown in Fig. 4.6 c is designated as 3-0 pattern, with the first number indicating that the Cu phase is 3-D interconnected, and the second number indicating that the W phase is isolated. This pattern represents the case of an infiltrated green compact in which most W particles are dispersed in Cu matrix. Since the highly conductive phase is interconnected, resistivity is lower. In contrast, both W and Cu phase are interconnected as illustrated in Fig 4.6d, and this 3-3 pattern represents the structure of a sintered compact after Cu infiltration which gives higher resistivity. Applied to the current research, in all of three self formed structures, the Cu phase is 3-D connected, but the degree of W interconnectivity varies. The highest packing efficiency and correspondingly higher W contiguity in the graded structure (see Tab.3.9), gives poorer electrical networking for current transport in comparison with the other two skeleton type structures.

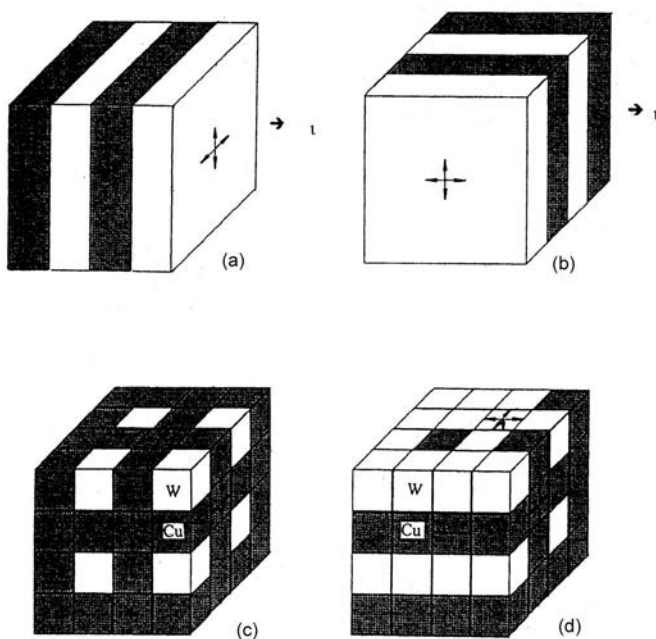


**Fig 4.6** Connectivity patterns of a Cu-W composite: (a) each phase has a two - dimensional conducting path perpendicular to the current flow; (b) conducting path is parallel to current direction; (c) W phase is not interconnected while Cu has a 3-D conducting path (3-0 pattern); and (d) both W and Cu have interconnecting conducting paths (3-3 pattern – percolation limit) [Wan98].

## 4. DISCUSSION

---

The study of the temperature dependence of the electrical resistivity of Cu-W structures (Fig. 3.25) shows a nearly linear increase of electrical resistivity with temperature increase. The Cu-W structures exhibit a behavior which is between those for pure Cu and pure W. Furthermore, the Cu-W structures show similar behavior below 673 K. The difference in electrical resistivity occurring at higher temperatures could be attributed to different factors: microstructural effects, but also to the quality of the contact points. It is important to note that pure Cu and Cu-W systems are characterized by similar slopes (at least for  $T < 673$  K), which indicates electron-phonon interaction as the main effect controlling electrical resistivity.

### 4.4.2 Elastic properties

A strong relationship between the microstructure of produced Cu-W materials and their elastic properties has been demonstrated by experimental determination of effective E-modulus and position dependant E-modulus. Both testing methods show that the graded structure has superior elastic characteristics compared to the skeleton structures. This characteristic can be attributed to the more efficient packing density obtained in the graded structure, which is indicated by the higher W content and higher W contiguity. The graded structure has almost 10% higher density compared to the structure in percolation stage (Tab. 3.9;  $\rho_t$ ). Another factor that explains the higher E-modulus is connected with the reduction of residual stresses caused by the graded structure itself. Sintering of W skeleton at 2073 K shows an important improvement in its elastic constant, which is related to the stronger sinter bonds between W particles. The results of E-modulus measurement presented in Tab.3.9 show good agreement with commercially available homogeneous Cu-W composites, where E-modulus is in the range of 250-280 GPa [Gra06].

Despite the complex and highly disperse structure of produced Cu-W materials, B scan method was found to be useful for determination of E-modulus profile. It has been shown that the E-modulus profiles (Fig. 3.26 a,b,c) correspond well to the concentration profiles (clearly seen for a sample vibrated for 60 min, percolation stage, Fig.3.5 d,f,h). Additionally, strong sensibility to microstructural characteristics (porosity, interfaces) has been observed. The more uniform E-modulus profile observed for the sample vibrated for longer time (diffusion stage (100 min, Fig.3.26b) and stationary stage (120 min, Fig. 3.26c)), where large W particles are more interconnected, can be the result of stress reduction due to structural changes. Implementation of such non destructive, ultrasonic techniques in the characterization of graded materials, can be helpful for future commercial applications of these materials.

### 5. CONCLUSIONS

The objective of the present work was to produce continuously formed Cu-W functionally graded materials (FGMs) with adequate mechanical and electrical characteristics for application in extreme environmental conditions. For that purpose, a novel process based on size segregation of bimodal granular media (GM) has been applied. The fundamental study of GM compaction and related relaxation behavior, was demonstrated; under weak excitation and under controlled ambient condition vibrated bimodal W-W GM segregates in a manner that a gradient in packing is self formed. During sintering, such graded packing structure turns into a W perform with a gradient in porosity. Studied W GM fulfills both critical demands, i.e. size segregation and effective sintering process. The final Cu-W FGM has been produced by subsequent infiltration of molten Cu into the W graded perform. The produced Cu-W composite / graded materials have been characterized by measurements of electrical resistivity and E-modulus.

#### 5.1 Compaction dynamics of weakly excited bimodal tungsten granular media

Compaction dynamics are dominantly affected by vibration amplitude and, depending on the excitation intensity, compaction of studied granular media can be driven by: convection rolls, geometrical reorganisation aided by surface convection or *solely geometrical reorganisation*.

Weakly excited GM ( $\nu = 600\text{Hz}$ ,  $a = 6g$ ) shows two distinguished behaviours. The first quasi linear time regime is attributed to percolation, where smaller particles fall into openings between larger particles. This process is controlled by individual particle relaxation where inelastic collision between particles dominates and it is effective to achieve a moderate packing density. Through a transient stage, where critical slow down occurs, the system attains a steady state. The steady state is driven by the collective relaxation of close packed particle clusters, where interparticle forces are of primary importance. Compaction dynamics of the studied W GM were well predicted by the stretched exponential law (KWW's law). The validity of this relaxation law has also been experimentally proved in polydisperse system (bimodal agglomerate sizes). From the KWW's relaxation law, relaxation time ( $\tau$ ) as a free parameter has been calculated. Applying Mehta's macroscopic approach the  $\tau$  is attributed to the characteristic time of the single particle relaxation. A strong dependence of  $\tau$  on ambient humidity has been observed. By changing the ambient humidity from 28 to 45 %, the interparticle forces change their nature from electrostatic repulsive forces to cohesive capillary forces, causing a significant change in the relaxation time from 400 to 2000 seconds, respectively.

## 5. CONCLUSIONS

---

### 5.1.1 Size segregation

When bimodal W-W GM (large agglomerates A1 + small agglomerates A2) is subjected to vertical vibration, size segregation occurs and can lead to de-mixing. In the regime of geometrical segregation and geometrical segregation aided by convection motion a gradient in packing has been self formed. Each of these regimes corresponds to the collective motion of smaller agglomerates, whereas the larger agglomerates play the role of an inert phase. It was shown that the gradient of packing represents the most effective random packing model. After sintering the graded structure shows compared to the percolation structure a density increase of 10%.

Geometrical segregation progresses through various steps. In the initial position, larger agglomerates have a lower potential energy position, while smaller agglomerates are at a higher potential energy position. As vibration starts, the first percolation effect occurs, which is monitored by a contraction of the bed height. The second stage corresponds to an intermediate stage where the bed height remains unchanged. This stage exhibits a diffusive nature which progresses through hopping of the smaller agglomerates, and due to a configurational change of the smaller agglomerates, the larger agglomerates rearrange themselves, reaching an uniform distribution in volume. Finally, in the steady state the graded structure has been formed.

## 5.2 Sintering

Sintering kinetics of W GM (monomodal and bimodal) are strongly dependant on inhomogeneities in size and shape of initial agglomerates and the disordered structure of GM. As a consequence, studied GM exhibits non uniform sintering with a statistical nature of reproducibility.

### 5.2.1 Sintering of monomodal tungsten granular media

The sintering of monomodal W GM is strongly influenced by the initial agglomerate size and structure. The initial agglomerate structure is composed of more dense regions (domains) and results in a polymodal porosity distribution. Low temperature sintering of W GM is controlled by the simultaneous action of a rearrangement process and grain boundary diffusion (GBD). A dominance of one of the processes is determined by the initial agglomerate size. Particle contact asymmetry and therefore induced transient / residual stresses cause the rearrangement or softening process. The analogy with rearrangement in liquid phase sintering was drawn and both

## 5. CONCLUSIONS

---

mechanisms recognize that enhancement of densification can be achieved by improving the packing factor. The rearrangement process continues until the geometrical factor defined by the random close packing density limit is exhausted, and makes a condition for GBD to occur later.

During sintering of small particles (agglomerates A1), the rearrangement process and GBD occur simultaneously. The sintering of large agglomerates (agglomerates A2) is strongly related to their rearrangement, thus the main diffusive process has been interrupted due to packing structure, coordination number and irregularity of agglomerate shape. The rearrangement process in the system with the large agglomerates requires a lower activation energy ( $E_a \sim 80$  kJ/mol) compared to the rearrangement process operating in the system with small agglomerates ( $E_a \sim 100$  kJ/mol). In both monomodal agglomerates with different agglomerate sizes, GBD as the single densification mechanism starts at temperatures above 1850K. Densification in this stage occurs dominantly through the reduction of interdomain porosity.

### *5.2.2 Sintering of bimodal tungsten granular media*

Sintering kinetics of bimodal W GM are strongly influenced by the packing structure obtained during vibration. This packing structure evolves through three stages: 1) skeleton of smaller particles (percolation stage); 2) skeleton of larger particles (diffusion stage); and 3) graded structure (steady state). The self formed skeleton and graded structures exhibit different sintering behaviors. Sintering kinetics of the skeleton type structure resemble the behavior of skeleton-forming powder, and the global sintering is controlled by the competition between rearrangement and GBD. Sintering of the graded structure shows strong similarities with the sintering of the homogeneous mixture. In accordance with this, the absence of a low temperature densification peak is attributed to the formed graded structure which does not manifest skeletal character. Due to improved packing density achieved during vibro compaction and formation of more sintering necks, sintering of the graded structure is dominantly controlled by GBD. By applying the appropriate sintering cycles, it is possible to enlarge the gradient in concentration, taking advantage of the thermodynamically favorable porosity redistribution. After sintering, the graded structure shows density increase of 10% compared to the percolation structure.

### ***5.3 Properties of graded copper tungsten materials***

Properties like electrical resistivity and effective E-Modulus of the final Cu-W FGMs are generally very dependant on the self formed packing structures of W GM obtained during vibration. The current flow on elevated temperature is also influenced by this structure.

#### ***5.3.1 Electrical resistivity***

Cu content and W-W contiguity are two features which determine the resistance for current flow in the studied materials. Tungsten networks in the final materials make complicated current paths, resulting in the increase of electrical resistivity. Due to higher Cu content and lower W-W contiguity, the structure in the percolation stage (skeleton of smaller particles) exhibits a more efficient current path. On the contrary, the higher W packing density in graded structure and correspondingly lower Cu content lead to a poorer current flow. The electrical resistivity of investigated Cu-W materials is between those of pure W and Cu, indicating the improvement coming from the concept of a composite / graded structure.

The electrical resistivity increases nearly linearly with the temperature. Different resistivities obtained for a temperature higher than 673 K could be attributed to the microstructural effects and the quality of the contact-points. It is important to note that both pure Cu and Cu-W FGM are characterized by similar temperature dependence of electrical resistivity (up to  $T = 673$  K), indicating electron-phonon interaction as the main effect controlling the electrical resistivity.

#### ***5.3.2 E-Modulus***

E-modulus of the Cu-W FGMs is also strongly affected by composition and W-W contiguity. The graded structure has a higher E-modulus compared to the skeleton structure. The superior characteristics of graded structure are attributed to its better packing efficiency and higher W-W contiguity. The position dependant E-modulus profile corresponds well to the concentration profile.

## **6. FINAL REMARKS AND SUGGESTIONS FOR FURTHER RESEARCH**

The literature review and results presented in this work pointed out the specifics of Cu-W FGM produced by the novel method based on size segregation of W bimodal granular media. Five main steps are of relevance in this work: (i) agglomeration of W, (ii) vibration of bimodal W granular media aimed to facilitate self-formation of a gradient in packing / porosity, (iii) sintering into a strong preform, (iv) metal infiltration into the porous W preform and (v) measurements of physico-chemical properties of the final Cu-W composites.

(i) The process of agglomeration can require special dispersion methods to be applied to each type of particle and agglomerate size, like when the binding polymer is added in different solution forms to optimize such methods of agglomeration. Also, wettability of the W particles by different polymers should be analyzed. Additionally, the development of a process route directed towards their production of spherical agglomerates is of great interest in both, vibrational compaction and sintering studies.

(ii) The fabrication of graded structures applied in this work could be improved if the ambient conditions during vibrational compaction (humidity and electrostatic forces) are strictly controlled. In that way, it can be realistic to expand segregation experiments to systems composed of finer particles.

(iii) Through vibrational compaction of selected W GM and subsequent sintering, sufficiently strong preforms with a gradient in pore distribution were obtained. By detailed analysis of densification kinetics applied to CHR dilatometric data of priorly vibrated pellets, GBD and rearrangement (softening) mechanisms were suggested to act during partial sintering of such structures. The contribution of rearrangement stages in solid state sintering of W can be clarified if the external load on the sample in the dilatometer is systematically changed. In this way, the obtained CHR sintering curves should span a reasonable range of variation in the sintering regimes (and temperature) and application of kinetics laws (like the ones for the rearrangement stage or high temperature creep) should provide a better framework for suggesting the most probable densification mechanisms. Another relevant aspect of the conducted sintering study relates to the very clear effect of isothermal densification at 2123 K between 1 and 3 h, whereby very interesting gradients were obtained for the final preforms. It would certainly be of basic interest to have densification-time data at constant temperature, describing the 5% increase in pallet-density with time elapsing between 1 and 3 h. Such theoretical analysis can be very useful to elucidate the densification mechanisms and to

## 6. FINAL REMARKS AND SUGGESTIONS FOR FURTHER RESEARCH

correlate them to the CHR analysis. Also, further effort should concern the correlation between compaction dynamics and particular sintering behavior of vibrated specimens.

(iv) For a potential industrial application of Cu-W materials it would be of interest to conduct a study of the infiltration with molten Cu on much larger samples of graded W structures. Applying an external axial load may be needed to rapidly inject the porous specimens. The threshold pressure ( $P_0$ ) and the spatial metal pressure gradient ( $\Delta P/\Delta z$ ) should be measured at constant injection temperature and gas flow or vacuum conditions.

(v) For the intended application of the produced Cu-W composites (in the first wall and divertor structure in fusion reactors), properties like neutron-flux damage, high temperature creep resistance, and measurement of thermal conductivity should be specified.

## 7. REFERENCES

- [Ahm73] Ahmad K., Salley.I.J, Pow.Tech.Vol.8,p.69 (1973).
- [Ash05] Ashammakhi N., Veirato M., Niemela S-M., Tiainen J., Leinonen S., Suokas E., Törmälä P., Mater.Sci. Forum Vols 492-493, p.195 (2005).
- [Ash74] Ashby M.F., Acta Metallurgica, Vol.22, p.275 (1974).
- [Aye65] Ayer J.E., Soppet F.E.,J.Am.Ceram.Soc, Vol. 48, No.4,p.180 (1965).
- [Bar51] Bardeen J., Herring C., "Atom Movements", Amer.Soc. for Metals, p.87-111 (1951).
- [Bar60] Barbour J.P.,Charbonnier F.M., Dalan W.W.,Dyke W.P., Martin E.E., Trolan J.K.Phys.Rew., Vol. 117,No6, p.1452 (1960).
- [Bar92], Barker G.C., Mehta A., Phys.Rew A,Vol. 45,No 6 ,p.3435 (1992).
- [Bar93] Barker G.C., Mehta A., Phys.Rew A,Vol. 47,p.184(1993).
- [Bee76] Beere W.,Metal.Sci J., Vol.10, p.294 (1976).
- [Bel91] Belhadjhamida A., German R.M., Tungsten and Tungsten Alloys-Recent Advances Ed: A.Crowson, E.S.Chen, The Minerals, Metals &Materials Society, p. 3-19 (1991).
- [Ben05] Benavidez E. R.,J.Mat..Sci.,Vol.40,p.3749 (2005).
- [Bir99] Birth U., Joensson M., Kieback B., Science Forum Vols.308-311,p.766 (1999).
- [Bok99] Bokuchava G., Schreiber J., Shamsutdinov N., Stalder M., Materials Science Forum Vols. 308-311, p.1020 (1999).
- [Bou94] Bourell D.L., Kaysser W.A., Metallurg. and Materials Trans A,Vol.25A,p.677 (1994).
- [Bre03] Breu A.P.J.,Ensner H-M.,Kreulle C.A., Rehberg I., Phys. Rev. Lett.,Vol.90, No1, p.014402-1 (2003).
- [Bri85] Bridgwater J.,Foo W.S., Pow. Tech.Vol.41,p.147 (1985).
- [Cah88] Chan J.W., Sintering of Adv Ceram., Vol p.185 (1988)
- [Can02] Canul-Chay, Belmont P.A.,Nahmad-Molinar Y.,Ruiz-Suarez J.C., Phys. Rev. Lett., Vol.89,No18,p.189601-1 (2002).
- [Car] Carr R.L., Brit. Chem. Eng, Vol.15,(12),p.1541(1970).
- [Car91] Caram H.,Hong D. C.,Phys.Rev.Lett, Vol67,p.828 (1991).
- [Che97] Chen P-L., Chen I-W., J Am. Ceram. Soc., Vol. 80(3), p.637 (1997).
- [Cle91] Clement E., Rajchenbach J., Europhys. Lett., Vol.16, p.133 (1991).
- [Cle92] Clement E.,Duran J., Rajchenbach J.,Phys. Rew. Lett, Vol.69,p.1189 (1992).
- [Cob58] Coble R. L., J. Amer. Ceram. Soc, Vol.41, p.55 (1958).
- [Cob61] Coble R. L.,J. of Appl. Physic, Vol.32,No5,p.787 (1961).
- [Cob61a] Coble R. L.,J. of Appl. Physic, Vol.32,No5,p.793 (1961).
- [Cob63] Coble R. L.,J. of Appl. Physic, Vol.34,p.1673 (1963).
- [Cut69] Cutler i.B.,J. Am. Ceram. Soc.,Vol.52,0.14 (1969).
- [D'An01] D'Anna G.,Gremaud G., Nature, Vol. 413,p.407 (27Sep.2001).
- [D'An01a] D'Anna G.,Gremaud G., Europhys. Lett. Vol.54(5),p.599 (2001).
- [D'An03] D'Anna G., Mayor P., Barrat A., Loreto V., Nori F., Nature, Vol. 424, p.909 (21Aug 2003).
- [Dud84] Dudrova E., Rudnayova E., Leitner G.,Powder Metall. Int., vo.16,(6),p.255 (1984).
- [Dur93] Duran J.,Rajchenbach J.,Clemente.,Phys. Rev. Lett., Vol. 70,No16,p.2431 (1993).
- [Dur94] Duran J., Mazozi T., Clement E.,Rajchenbach J., Phys. Rev. E, Vol. 50, p.5138 (1994).
- [Dur98] Duran J., Jullien R., Phys. Rev. Lett., Vol.80, No16, p.3547 (1998).
- [Edw89] Edwards S.F., in Proceedings of the Int.School of Physics:Enrico Fermi Course 106,Chiarotti, Fumi F.,Tosi M.P.,Eds.(North-Holland,New York), p.849 (1990)
- [Elp97] Elperin T.,Golshtein E.,Physica A 247,p.67 (1997).

- [Erd95] Erdogan F., MRS Bulletin Vol. XX N01,p.43, January (1995).
- [Eva82] Evans A.G., J. Am. Ceram. Soc., Vol.65,No10, p.497 (1982).
- [Exn73] Exner H.E., Petzow G.,Wellner P., In: Sintering and related Phenomena Ed. G. C. Kuczynski, New York, Plenum Press,p.351 (1973).
- [Exn75] Exner H.E., Petzow G.,in Sintering and Catalysis, Ed. G. C. Kuczynski, New York, Plenum Press,p.27 (1975).
- [Exn79] Exner H.,Rev. Powder Metall. And Phys. Ceram.,Vol.1,p.7 (1979).
- [Exn96] Exner H.E., Arzt E., Physical Metallurgy; forth, revised and enhanced edition, Ed. R. W. Cahn, P. Haasen, Elsevier Science BV, 2629-2662,(1996).
- [Fan05] Fano L., Fano V., Ma W. Y., Wang X.G., Mater. Sci. Forum Vols 492-493, p. 183 (2005).
- [Far31] Faraday, M.,Phil. Trans. R. Soc. London, Vol.52, p.299 (1831).
- [Fer45] Frenkel J.,J.of Physics, Vol.IX,No5,p.385 (1945).
- [Fis04] Fiscina J. E.,Jankovic Ilic D.,Mücklich F.,Granular Matter, Vol.5, p.207 (2004).
- [Fis05] Fiscina J. E. ,Caceres M. O., Physical Review Letters, Vol.95,p.108003, (2005).
- [Fle89] Fleischer R.L., Gilmore R.E., Zabala R.J.,Acta Metal., Vol.37/10, pp.2801 (1989).
- [Gal92] Galas J.A.C., Herrmann H.,J., Sokolowski S., Phys. Rev. Lett.,Vol.69,No9, p.1371 (1992)
- [Gas03] Gasik M.,Mat. Sci Forum, Vols. 423-425, p.11(2003).
- [Gas05] Gasik M., Mater. Sci. Forum Vols. 423-425,p.17 (2005).
- [Gas05] Gasik M., Mater. Sci. Forum Vols 423-425,p.17(2005).
- [Gas99] Gasik M., Ueda S., Materials Science Forum Vols. 308-311, p.603 (1999).
- [Ge03] Ge C-C., Zhou Z-J., Ling Y-H., Mater. Sci. Forum, Vol. 423-425, p. 11 (2003).
- [Ger76] German R.M., Munir Z.A., Metallurgical Transaction A, Vol7A,p.1873 (December 1976).
- [Ger96] German R., Sintering theory and practice, John Wiley Sons,INC (1996).
- [Ger89] German R., Particle Packing Characteristic, Metal Powder Industries Federation, Princeton, N.J.(1989).
- [Ger94] German R. M., Powder Metallurgy Science, Metal Powder Industries Federation, Princeton, N. J.(1994).
- [Ger99] Gerk Ch., Willerr-Porada M., Mater. Sci. Forum Vols. 308-311, p.806 (1999).
- [Gra06] [www.graphiccorp.com](http://www.graphiccorp.com), www. mkt-intl.com (Tungsten-Copper Alloys)
- [Haf86] Haff P. K., Werker E. T., Pow. Tech. Vol.48, p.239 (1986)
- [Han92] Hansen J. D., Rusin R. P., Teng M-H, Johnson D. L., J. Am. Ceram. Soc.,Vol.75 (5) p.1129 (1992).
- [Hay97] Hayakawa H.,Hong D. C., Phys. Rev. Lett., Vol78, No14, p.2764 (1997).
- [Her03] Herrmann H. J., Mahmoodi Baram R.,Wackenhut M.,Braz.J of Physics, Vol.33, No 3,p.591 (2003).
- [Her50] Herring C., J. of Applied Physics, Vol.21, p.301 (1950).
- [Her51] Herring C., "The Physics of Powder Metallurgy", McGraw-Hill Book Co, New York,p.143, (1951).
- [Her95] Herrmann H. J., Chaos, Solitons and Fractals, Vol.6 p.203 (1995).
- [Her99] Herrmann H. J., Physica A Vol.263, p.51 (1999).
- [Hil92] Hillman S. H., German R. M., J. of Mater. Sci. Vol. 27,p.2641 (1992).
- [Hir95] Hirano T., Wakashima K., MRS Bulletin Vol. XX, N01,p.40 January (1995).
- [Hon01] Hong D. C.,Quinn P. V., Phys. Rev. Lett. Vol. 86, No15, p.3423 (2001).
- [Hsi00] Hsiao S. S.,Chen C. H.,Powder Technology, Vol.111,p.210 (2000).
- [Hsu86] Hsueh C-H Evans A. G., McMeeking M. M., J. Am. Ceram. Soc., Vol.69, No4,P.C-64 (1986).
- [Hsu86a] Hsueh C-H., Evans A.G.,McMeeking M., J.Am.Ceram.Soc.,Vol. 69, No4, p.C-64 (1986).
- [Ils99] Ilschner B., Gasik M., Mater. Sci. Forum Vols 308-311, p.3-10 (1999).
- [Ite06] www.ITER. Org
- [Jae89] Jaeger, H. M.,S. R.Nagel, Phys. Rev. Lett. Vol.62, p.40 (1989).

- [Jae92] Jaeger H. E., Nagel S. R., *Science*, Vol.255,p.1523 (1992).
- [Jae96] Jaeger H. E., S. R. Nagel, R. P. Behringer, *Rev. Mod. Phys*, Vol. 68, No 4, p.(Oct 1996).
- [Jed96] Jedamzik R., Neubrand A., Rödel J., *Proceedings FGM 1996* p.239 (1996).
- [Jed00] Jedamzik R., Neubrand A., Rödel J.,*J.of Materials Science*,Vol. 35, p.477(2000).
- [Jen02] Jenkins J. T., Yoon D.,K.,*Phys.Rev.Lett.*,Vol.88, No19,p. 194301-1 (2002).
- [Joh64] Johnson D. L., Clarke T. M., *Acta Metall.*, Vol12, p.1173, (1964).
- [Joh69] Johnson D. L., *J. of Appl. Physic*, Vol.40,No1,p.192 (1969).
- [Joh69] Johnson L. D.,*J. of Appl. Physics*, Vol.40,No1,p.192 (1969).
- [Joh80] Johnson D.L., In *Sintering Processes*, Ed. G.C.Kuczynski, Plenum, p.97 (1980).
- [Jon86] Jonghe L. C., Rahman M. N., Hsueh C.H., *Acta Metall.* Vol. 34, no7, p.1467 (1986).
- [Jos00] Josserand C.,Tkachenko A. V. ,Mueth D. M., Jaeger H. M., *Phys. Rev. Lett.*,Vol.85,p.3632 (2000).
- [Jul92] Jillien R., Meakin P., Pavlovotch., *Phys. Rev. Lett.*,Vol69, No4, p.640(1992).
- [Kad99] Kadanoff L. P., *Rev. Mod. Phys* Vol. 71, No1,p. 435(1999).
- [Kel89] Kellett B. J, Lange F. F., *Am. Ceram. Soc*, Vol. 72,No5, p.725 (1989).
- [Kie03] Kieback B., Neubrand A., Riedel H., *Materials Science and Engineering A* 362 p.81 (2003).
- [Kin55] Kingery W. D., Berg M., *J.of Applied Physics* Vol.26,No.10, p.1205 (1955).
- [Kin60] Kingery W.D., *J.of Applied Physics*, Vol. 31, No5, p.833 (1960).
- [Kin67] Kingery W. D., Francois B., in *Sintering and Related Phenomena*, Ed.by G. C. Kuczynski, H. A. Hooten, and G. N. Gilbon,p.471, Gordon and Breach, New York, (1967).
- [Kir05] Kirihara S., Takeda M. W., Sakoda K., Honda K., Miyamoto Y., *Mater. Sci. Forum* Vols. 492-493, pp.719, (2005).
- [Kis05] Kisara K., Niino M., *Mater.Sci. Forum* Vols 492-493, p.761 (2005).
- [Kni95] Knight J., Fandrich C. G., Lau C. N., Jaeger H., Nagel S., *Phys. Rev. E*, Vol. 51,p.3957 (1995).
- [Kni95] Knight J.B, Fandrich C.G., C.N.Liu, H.M.Jaeger, S.R. Nagel, *Phys.Rev E* Vol.51, p.3957 (1995).
- [Kno00] Knorr P., Nam J. G., Lee J. S. , *Metallurg. and Materials Trans A*, Vol.31A,p.503 (2000).
- [Koi95] Koizumi M., Niino M., *MRS Bull.* Vol. 20(1),p.19 (1995).
- [Koi95] Koizumi M., Niino M., *MRS Bulletin* Vol.1 p.19 (1995).
- [Kot63] Kothari N. C.,*J. Less-Common Metals*, Vol.5,p.140 (1963).
- [Kot64] Kothari N. C., *Powder Metallurgy*,Vol.7, No14, p. 250(1964).
- [Kre67] Kreider K. G., Bruggemann G., *Transactions of the Metallurgical Society of AIME*,Vol.239., p.1222(1967).
- [Kre99] Krell T., Schulz U., Peters M., Kaysser W.A., *Mater. Sci. Forum* Vols 308-311,p.396 (1999).
- [Kuz49] Kuczynski G. C., *Metals Transactions*, p.169Feb. (1949).
- [Lan 83b] Lange F. F., *J. Am. Ceram. Soc*, Vol. 67,(2),p.83 (1983).
- [Lan83] Lange F. F., Metcalf M., *J. Am. Ceram. Soc*, Vol. 66,(6), p.398 (1983).
- [Lan83a] Lange F. F.,Davis B. I., *J. Am. Ceram. Soc*, Vol. 66,(6), p.405 (1983).
- [Lan84] Lange F. F., *J. Am. Ceram. Soc*, Vol. 67, p.83 (1984).
- [Lan86] Lange F. F., *J.de Physique*, Vol.47,p.205 (1986).
- [Lan89] Lange F. F.,Kellett B., *J. Am. Ceram. Soc*, Vol 72,No5, p.735 (1989).
- [Las03] Lasagni A., private communication.
- [Las99] Lassner E.,Schubert W-D.,*Tungsten:properties, chemistry, technology oh the element,alloys and chemical compounds*, Kluwer Academic, N,Y,p.235(1999).
- [Lee95] Lee J.S., Kim T.H., *Nano Structured Materials*, Vol.6, p.691 (1995).
- [Leu99] Leuenberger H., *Advanced Powder Technology*, Vol.10 84),p.323 (1999).
- [Lez87] Lezanski J., Rutowski W., *Pow. Metall. Int* Vol. 19,No2,p. 29 (1987).

- [Lin03] Ling Y., Bai X., Ge C., Mater. Sci. Forum Vols. 423-425, p.49 (2003).
- [Liu98] Liu A.J., Nagel S.R., Nature, Vol.,p. 396,(5 Nov 1998).
- [Lud99] Luding S.,Herrmann H.J.,Cond-mat/9910089 v1,p.1 (1990).
- [Luk05] Lukas P., Vrana M., Saroun J., Ryukhtin V., Vleugles J., Anne G., Van der Biest O., Gasik M., Mater. Sci. Forum Vols 492-493, p.201 (2005).
- [McL90] McLachlan D. S., Blaszkiewicz M., Newnam R. E., J. Am. Ceram. Soc., Vol.73 (8),p.2187 (1990).
- [Meh89] Mehta A., Edwards S. F.,Phys. A Vol.157, p.1091 (1989).
- [Meh90] Mehta A.,Edwards S. F., Physica A Vol. 168,p.714 (1990).
- [Meh90a] Mehta A., "Correlations and Connectivity" Ed. Stanley H. E.,Ostrowsky N., Kluwer Academic Publishers,p.88 (1990).
- [Meh91] Mehta A., Barker G. C., Phys. Rev. Lett.,Vol.67, No3,p.394 (1991).
- [Meh93] Mehta A.,Granular Matter An Interdisciplinary Approach,Springer-Verlag (1993).
- [Mit77] Mitkov M., "Anisotropie der Linearen Schrumpfung beim Sintern metallischer Pulver" Doktorarbeit, Universität Stuttgart (1977).
- [Miy05] Miyamoto Y., Kirihara S., Takeda M. W., Honda K., Sakoda K., Mater.Sci. Forum Vols. 492-493, p.77 (2005).
- [Müc97] Mücklich F., Lorinser M., Hartmann S., Beinstigel S., Linke J., Rödiger M.,Proc 3<sup>rd</sup> IEA workshop on Be Technology for Fusion, Ed. by Kawamura, H., Okamoto M., Mito City, Japan, P. 102 Oct (1997).
- [Müc99] Mücklich F., Beinstigel S., S., Arnold W., Proceedings of FGM, Materials Science Forum, Vols 308-311,p. 25 (1999)
- [Miy99] Miyamoto Y., Kaysser W. A., Rabin B. H., Kawasaki A., Ford R.G., "Functionally Graded Materials", Kluwer Academic Publishers,Boston, (1999).
- [Mül03] Müller E., Drasar C., Schulz J., Kaysser W. A., Mater. Sci. and Eng A362 p. 17 (2003).
- [Mül99] Müller E., Schackenberg K., Schilz J., Kaysser W. A., Mater. Sci. Forum Vols 308-311,p.681-686 (1999).
- [Neu97] Neubrand A., Rödel J., Z.Metallkd. 88 (1997).
- [Nic97] Nicodemi M., Coniglio A., Herrmann, H.J., Phys.Rev. E,Vol.55(4), p3965 (1997).
- [Oto95] Oto K., MRS Bulletin Vol. XX N01,p.48 January (1995).
- [Pet76] Petzow G., Exner H. E., Z. Metallkunde, Vol. 67, p.611 (1976).
- [Pet76] Petzow G.,Exner H. E.,Z. Metallkunde, Vol.67, p.611,(1976).
- [Phi02] Philippe. P.,Bideau D.,Europhys. Let., Vol.60,p.677 (2002).
- [Phi03] Philippe. P.,Bideau D., Phys. Rev. Let., Vol 91, no10, p.104302 (1993).
- [Phi98] Philips V., Pospieszczyk A., Huber A., Kirschner A., Rapp J., Schweer B., Wienhold P., van Oost G., Sergienko G., Tanabe T., Ohya K., Wada M., Ohgo T., Rubel M., J of Nuc.Mater. Vols.258-263,p. 858 (1998).
- [Qui00] Quinn P. V., Hong D. C., Phys. Rev. E, Vol.62,p.8295 (2000).
- [Rey85] Reynolds O., Philos. Mag. Vol.20, p.469 (1885).
- [Rho81] Rhodes W. H., J. Am. Ceram. Soc.,Vol. 64 (1) p.19 (1981).
- [Ric05] Richard P., Nicodemi M., Delanny R., Ribiere P., Bideau D., Nature Materials, Vol. 4,p.121 (Feb 2005).
- [Roc67] Rockland J. G. R, Acta Metall., Vol 15, p.277(Feb1967).
- [Roc67] Rockland J. G. R., Acta Met. Vol.14,p.277 (1967).
- [Roc67a] Rockland J. G. R., Z. Metallkunde, Vol.58,p.477 (1967).
- [Roc67b] Rockland J. G. R., Z. Metallkunde, Vol.58,p.564 (1967).
- [Ros86] Rosato A., Prinz F., Pow. Tech.,Vol.49,p.59 (1986).
- [Ros87] Rosato A., Strandburg K. J., Prinz F., Swendsen R. H., Phys. Rev. Lett., Vol. 58, No10,p.1038 (1987).
- [Ryu02] Ryu S. S., Kim Y. D., Moon I.H., J. of Alloys and Compounds Vol. 335, p.233 (2002).
- [Sch03] Schulze U., Peters M., Bach Fr.-W., Tegeder G., Mat. Sci. and Eng. A362, p.61 (2003).
- [Sch92] Schatt W., Sinternvorgänge, VDI-Verl., 1992.

- [Sch99] Schilz J., Müller E., Helmers L., Kang Y.S., Noda Y., Niino M., Mater. Sci. Forum Vols. 308-311, p.647 (1999).
- [Sco94] Scorey C. U.S.Patent5,292,478,Mar.8 (1994).
- [Sha89] Shaw N. J., Pow. Metall. International, Vol. 21 (3) p.16 (1989).
- [Shi01] Shinbrot T., Wassgren C. R., Phys. Rev. Lett.,Vol.87,No8,p.084302-1 (2001).
- [Shi98] Shinbrot T., Muzzio F.J., Phys.Rev.Lett.,Vol.81, No.20,p.4365 (1998).
- [Sla93] Slamovich E. B., Lange F. F., Am. Ceram.Soc, Vol 76,No6, p.1584 (1993).
- [Sma99] Smallman R. E., Bishop R. J.,"Modern Physical Metallurgy & Materials Engineering" Butterworth-Heinemann, Oxford, 6<sup>th</sup> Ed, p.181 (1999)
- [Smi98] Smid I., Akiba M., Vieider G., Plöchl L., J. of Nuc. Materials, Vols.258-263. p.160 (1998).
- [Str97] Stromberger F., Jedamzik R., Neubrand A., Rödel J., in Proceedings of the 14<sup>th</sup> International Plansee Seminar, Eds. G. Kneringer, P. Rödhammer, P. Wilhartitz, Metallwerk Plansee, Reute Vol 1,p.1 (1997).
- [Str99] Stromberger F., Jedamzik R., Neubrand A., Rödel J., Mater.Sci Forum ,Vols. 308-311, p. 163 (1999).
- [Sur98] Suresh S., Mortensen A., "Fundamentals of Functionally Graded Materials", IOM Communications Ltd, London (1998).
- [Swi80] Swinkels F. B., Ashby M. F., Acta Metallurgica, Vol.29, p.259 (1980).
- [Tak90] Takahashi M., Itoh Y., Kashiwaya H., Proceedings: The first International Symposium , FGM Sendai, p.129 (1990).
- [Tak93] Takahashi M., Itoh Y., Miyazaki M., in Proceedings of the 13<sup>th</sup> international Plansee Seminar, Eds. H.Bildstein, R. Eck, Metallwerk Plansee, Reute, Vol.4, p.17(1993).
- [The93] Theunissen A. M., Winnubst A. J. A., Burggraaf A. J., J of the European Ceram Soc., 0955-2219, p.315 (1993).
- [Thu93] Thümmler F., Oberacker R., "An Introduction to Powder Metallurgy", The Institute of Materials, 1 Carlton House Terrace, London (1993).
- [Tok05] Tokita M., Mater. Sci. Forum Vols 492-493, p.711 (2005).
- [Vas64] Vasilos T., Smith J. T., J. Appl .Phys, Vol. 35, No 1, p.215 (1964).
- [Vas70] Vasilos T., Rhodes W., in Ultrafine-Grain Ceramics, Ed.J.J.Burke, N.L.Reed, and W. Weiss, Syracuse University, Syracuse , New York, p.137 (1970)
- [Vis89] Visser J., Pow.Tech.,Vol58,p.1 (1989).
- [Wan98] Wang W.S., Hwang K.S., Metallurgical and Materials Transactions A, Vol. 29A, p.1509 (May 1998).
- [Wat95] Watanabe R., MRS Bulletin Vol. XX , N01,p.32 January (1995).
- [Kaw97] Kawasaki A., Watanabe R., Ceram. Int Vol.23, p.73 (1997).
- [Web03] Weber L., Dorn J., Mortensen A., Acta Mater., Vol. 51,p.3199 (2003).
- [Wil76] Williams J.C., Powder . Technology Vol.15, p.245 (1976).
- [Yos99] Yoshida N., J of Nuclear Materials Vols.266-269,p. 197 (1999).
- [You70] Young W.S., Cutler I.B., J. Am. Ceram. Soc., Vol. 58, No12, p.659 (1970).
- [Zik92] Zik O., Stavans J., Rabin Y., Europhys. Lett.Vol.17 849p.315 (1992).
- [Zou05] Zouai S., Mezahi F., Achour S., Harabi A., Mater.Sci. Forum Vols 492-493, p.235 (2005).